



U.S. Department of
Transportation

**Federal Railroad
Administration**

Laboratory Study of the Failure Characteristics of Fouled Ballast: Phase II

Office of Research,
Development
and Technology
Washington, DC 20590



NOTICE

This document is disseminated under the sponsorship of the Department of Transportation in the interest of information exchange. The United States Government assumes no liability for its contents or use thereof. Any opinions, findings and conclusions, or recommendations expressed in this material do not necessarily reflect the views or policies of the United States Government, nor does mention of trade names, commercial products, or organizations imply endorsement by the United States Government. The United States Government assumes no liability for the content or use of the material contained in this document.

NOTICE

The United States Government does not endorse products or manufacturers. Trade or manufacturers' names appear herein solely because they are considered essential to the objective of this report.

REPORT DOCUMENTATION PAGE*Form Approved*
OMB No. 0704-0188

Public reporting burden for this collection of information is estimated to average 1 hour per response, including the time for reviewing instructions, searching existing data sources, gathering and maintaining the data needed, and completing and reviewing the collection of information. Send comments regarding this burden estimate or any other aspect of this collection of information, including suggestions for reducing this burden, to Washington Headquarters Services, Directorate for Information Operations and Reports, 1215 Jefferson Davis Highway, Suite 1204, Arlington, VA 22202-4302, and to the Office of Management and Budget, Paperwork Reduction Project (0704-0188), Washington, DC 20503.

| | | | | | |
|--|--|---|----------------------------|--|--|
| 1. AGENCY USE ONLY (Leave blank) | | 2. REPORT DATE February 2020 | | 3. REPORT TYPE AND DATES COVERED Technical Report, May 2017–December 2018 | |
| 4. TITLE AND SUBTITLE Laboratory Study of the Failure Characteristics of Fouled Ballast: Phase II | | | | 5. FUNDING NUMBERS DTFR531GC00020 FR16RPD31000000026 | |
| 6. AUTHOR(S) Andrew K. Rohrman, Carlton L. Ho, Hamed F. Kashani, and James P. Hyslip | | | | | |
| 7. PERFORMING ORGANIZATION NAME(S) AND ADDRESS(ES) University of Massachusetts Amherst Hyground/LORAM Maintenance of Way, Inc. 140 Natural Resources Way P.O. Box 324 Amherst, MA 01003 Williamsburg, MA 01096 | | | | 8. PERFORMING ORGANIZATION REPORT NUMBER | |
| 9. SPONSORING/MONITORING AGENCY NAME(S) AND ADDRESS(ES) U.S. Department of Transportation Federal Railroad Administration Office of Railroad Policy and Development Office of Research, Development and Technology Washington, DC 20590 | | | | 10. SPONSORING/MONITORING AGENCY REPORT NUMBER DOT/FRA/ORD-20/04 | |
| 11. SUPPLEMENTARY NOTES COR: Hugh Thompson | | | | | |
| 12a. DISTRIBUTION/AVAILABILITY STATEMENT This document is available to the public through the FRA website . | | | | 12b. DISTRIBUTION CODE | |
| 13. ABSTRACT (Maximum 200 words) This report presents the results of a series of triaxial tests and modified box tests performed on abraded ballast at the University of Massachusetts Amherst. While Phase I involved the same tests performed on highly angular ballast, this phase is broken into two parts: Phase IIa and IIb. Both parts use ballast taken from a rail line in Shelburne Falls, MA, which were abraded and fouled from years of service in-track. Phase IIa used the natural fouling material, and Phase IIb mixed the natural fouling material with a kaolinite clay. The tests in each phase were prepared to comparable moisture contents and fouling conditions. This allows for a better understanding of the influence of ballast particle shape and fouling types on the strength properties and deformation of ballast. The results show that the angular and abraded ballasts have similar strength properties, but that the abraded ballast experiences higher amounts of deformation and settlement. The addition of fouling containing plastic fines results in losses in strength for the abraded ballast, as well as increased susceptibility to deformations. | | | | | |
| 14. SUBJECT TERMS Railroad, track, substructure, ballast, fouling, water content, loading, laboratory test, box test, triaxial test, box test | | | | 15. NUMBER OF PAGES 93 | |
| | | | | 16. PRICE CODE | |
| 17. SECURITY CLASSIFICATION OF REPORT Unclassified | 18. SECURITY CLASSIFICATION OF THIS PAGE Unclassified | 19. SECURITY CLASSIFICATION OF ABSTRACT Unclassified | 20. LIMITATION OF ABSTRACT | | |

NSN 7540-01-280-5500

Standard Form 298 (Rev. 2-89)
Prescribed by
ANSI Std. Z39-18
298-102

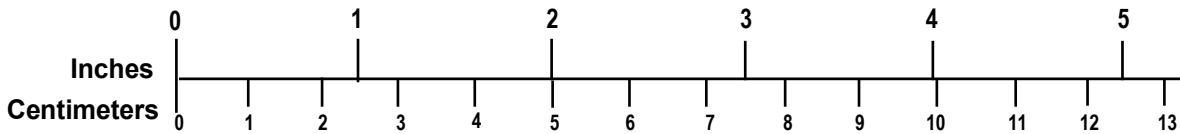
METRIC/ENGLISH CONVERSION FACTORS

ENGLISH TO METRIC

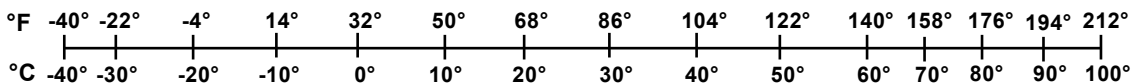
METRIC TO ENGLISH

| | |
|---|---|
| <p style="text-align: center;">LENGTH (APPROXIMATE)</p> <p>1 inch (in) = 2.5 centimeters (cm) 1 foot (ft) = 30 centimeters (cm) 1 yard (yd) = 0.9 meter (m) 1 mile (mi) = 1.6 kilometers (km)</p> | <p style="text-align: center;">LENGTH (APPROXIMATE)</p> <p>1 millimeter (mm) = 0.04 inch (in) 1 centimeter (cm) = 0.4 inch (in) 1 meter (m) = 3.3 feet (ft) 1 meter (m) = 1.1 yards (yd) 1 kilometer (km) = 0.6 mile (mi)</p> |
| <p style="text-align: center;">AREA (APPROXIMATE)</p> <p>1 square inch (sq in, in²) = 6.5 square centimeters (cm²) 1 square foot (sq ft, ft²) = 0.09 square meter (m²) 1 square yard (sq yd, yd²) = 0.8 square meter (m²) 1 square mile (sq mi, mi²) = 2.6 square kilometers (km²) 1 acre = 0.4 hectare (he) = 4,000 square meters (m²)</p> | <p style="text-align: center;">AREA (APPROXIMATE)</p> <p>1 square centimeter (cm²) = 0.16 square inch (sq in, in²) 1 square meter (m²) = 1.2 square yards (sq yd, yd²) 1 square kilometer (km²) = 0.4 square mile (sq mi, mi²) 10,000 square meters (m²) = 1 hectare (ha) = 2.5 acres</p> |
| <p style="text-align: center;">MASS - WEIGHT (APPROXIMATE)</p> <p>1 ounce (oz) = 28 grams (gm) 1 pound (lb) = 0.45 kilogram (kg) 1 short ton = 2,000 pounds (lb) = 0.9 tonne (t)</p> | <p style="text-align: center;">MASS - WEIGHT (APPROXIMATE)</p> <p>1 gram (gm) = 0.036 ounce (oz) 1 kilogram (kg) = 2.2 pounds (lb) 1 tonne (t) = 1,000 kilograms (kg) = 1.1 short tons</p> |
| <p style="text-align: center;">VOLUME (APPROXIMATE)</p> <p>1 teaspoon (tsp) = 5 milliliters (ml) 1 tablespoon (tbsp) = 15 milliliters (ml) 1 fluid ounce (fl oz) = 30 milliliters (ml) 1 cup (c) = 0.24 liter (l) 1 pint (pt) = 0.47 liter (l) 1 quart (qt) = 0.96 liter (l) 1 gallon (gal) = 3.8 liters (l) 1 cubic foot (cu ft, ft³) = 0.03 cubic meter (m³) 1 cubic yard (cu yd, yd³) = 0.76 cubic meter (m³)</p> | <p style="text-align: center;">VOLUME (APPROXIMATE)</p> <p>1 milliliter (ml) = 0.03 fluid ounce (fl oz) 1 liter (l) = 2.1 pints (pt) 1 liter (l) = 1.06 quarts (qt) 1 liter (l) = 0.26 gallon (gal) 1 cubic meter (m³) = 36 cubic feet (cu ft, ft³) 1 cubic meter (m³) = 1.3 cubic yards (cu yd, yd³)</p> |
| <p style="text-align: center;">TEMPERATURE (EXACT)</p> <p style="text-align: center;">[(x-32)(5/9)] °F = y °C</p> | <p style="text-align: center;">TEMPERATURE (EXACT)</p> <p style="text-align: center;">[(9/5) y + 32] °C = x °F</p> |

QUICK INCH - CENTIMETER LENGTH CONVERSION



QUICK FAHRENHEIT - CELSIUS TEMPERATURE CONVERSION



For more exact and or other conversion factors, see NIST Miscellaneous Publication 286, Units of Weights and Measures. Price \$2.50 SD Catalog No. C13 10286

Updated 6/17/98

Acknowledgements

The authors would like to acknowledge the Federal Railroad Administration's Program Manager Hugh Thompson and former Chief of the Track Division Gary Carr, and Ted Sussmann of the Volpe National Transportation Systems Center for their support, advice and assistance during this project. The authors would also like to acknowledge and thank Pan Am Railways for supplying the ballast, Shelburne Falls Trolley Museum for allowing access to the site, and DMO Construction for providing the equipment to collect and transport testing materials back to the lab.

Contents

| | |
|--|----|
| Executive Summary | 1 |
| 1. Introduction | 2 |
| 1.1 Background | 2 |
| 1.2 Objectives | 3 |
| 1.3 Overall Approach | 3 |
| 1.4 Scope | 3 |
| 1.5 Organization of the Report | 3 |
| 2. Methods of Investigation | 4 |
| 2.1 Quantification of Fouling | 5 |
| 2.2 Triaxial Tests | 5 |
| 2.3 Box Tests | 8 |
| 3. Presentation of Results and Discussion | 12 |
| 3.1 Triaxial Tests | 12 |
| 3.2 Box Tests | 19 |
| 4. Conclusion | 27 |
| 5. References | 29 |
| Appendix A. Additional Figures for Triaxial Tests | 31 |
| Appendix B. Box Test Settlement and Settlement Rate Curves | 63 |
| Abbreviations and Acronyms | 83 |

Illustrations

| | |
|--|----|
| Figure 1 – View of spent ballast on site in Shelburne Falls, MA. Material was collected from the site on April 12, 2017..... | 4 |
| Figure 2 – Triaxial test setup in load frame. Instron control panel is shown to the left; the cell pressure control panel is shown to the right..... | 7 |
| Figure 3 – Top-down view of the empty box in the frame with wooden boards attached | 8 |
| Figure 4 – Completed box test setup showing LVDT placement and plastic covering to prevent moisture loss | 9 |
| Figure 5 – Typical stress-strain curves | 13 |
| Figure 6 – 30 percent fouled triaxial tests at half of field capacity..... | 14 |
| Figure 7 – Poisson's Ratio vs axial strain at which maximum contraction occurs | 16 |
| Figure 8 – Plastic and total cumulative settlement curves for angular ballast and naturally abraded ballast in clean box tests..... | 20 |
| Figure 9 – Test modulus measured for all box tests, with a smoothing function applied for clarity | 21 |
| Figure 10 – Plastic and total cumulative settlement curves for 15 percent fouled box tests. Results from previous tests on granite ballast and current tests on abraded ballast with natural fouling and Prestige clay fouling mixture are included..... | 22 |
| Figure 11 – Plastic and total cumulative settlement curves for 30 percent fouled box tests. Results from previous tests on granite ballast and current tests on abraded ballast with natural fouling and Prestige clay fouling mixture are included..... | 23 |
| Figure 12 – Tie rotation after failure in the 30 percent fouled box test with abraded ballast and natural fouling..... | 24 |
| Figure 13 – Cumulative plastic settlement measurements for all 15 and 30 percent fouled box tests | 25 |
| Figure 14 – 50 percent strength secant modulus for Connecticut granite ballast with breakdown fouling..... | 32 |
| Figure 15 – 50 percent strength secant modulus for abraded ballast with natural fouling | 33 |
| Figure 16 – 50 percent strength secant modulus for abraded ballast with Prestige mix fouling .. | 34 |
| Figure 17 – Clean, dry, 5 psi confining | 36 |
| Figure 18 – Clean, dry, 10 psi confining | 37 |
| Figure 19 – Clean, dry, 15 psi confining | 38 |
| Figure 20 – Clean, 50 percent field capacity, 5 psi confining | 39 |
| Figure 21 – Clean, 50 percent field capacity, 10 psi confining | 40 |
| Figure 22 – Clean, 50 percent field capacity, 15 psi confining | 41 |

| | |
|--|----|
| Figure 23 – Clean, field capacity, 5 psi confining | 42 |
| Figure 24 – Clean, field capacity, 10 psi confining | 43 |
| Figure 25 – Clean, field capacity, 15 psi confining | 44 |
| Figure 26 – 15 percent fouled, dry, 5 psi confining..... | 45 |
| Figure 27 – 15 percent fouled, dry, 10 psi confining..... | 46 |
| Figure 28 – 15 percent fouled, dry, 15 psi confining..... | 47 |
| Figure 29 - 15 percent fouled, 50 percent field capacity, 5 psi confining | 48 |
| Figure 30 – 15 percent fouled, 50 percent field capacity, 10 psi confining..... | 49 |
| Figure 31 – 15 percent fouled, 50 percent field capacity, 15 psi confining..... | 50 |
| Figure 32 – 15 percent fouled, field capacity, 5 psi confining | 51 |
| Figure 33 – 15 percent fouled, field capacity, 10 psi confining | 52 |
| Figure 34 – 15 percent fouled, field capacity, 15 psi confining | 53 |
| Figure 35 – 30 percent fouled, dry, 5 psi confining..... | 54 |
| Figure 36 – 30 percent fouled, dry, 10 psi confining..... | 55 |
| Figure 37 – 30 percent fouled, dry, 15 psi confining..... | 56 |
| Figure 38 – 30 percent fouled, 50 percent field capacity, 5 psi confining..... | 57 |
| Figure 39 – 30 percent fouled, 50 percent field capacity, 10 psi confining..... | 58 |
| Figure 40 – 30 percent fouled, 50 percent field capacity, 15 psi confining..... | 59 |
| Figure 41 – 30 percent fouled, field capacity, 5 psi confining | 60 |
| Figure 42 – 30 percent fouled, field capacity, 10 psi confining | 61 |
| Figure 43 – 30 percent fouled, field capacity, 15 psi confining | 62 |
| Figure 44 – Clean box tests, dry phase | 64 |
| Figure 45 – Clean box tests, field capacity phase..... | 65 |
| Figure 46 – Clean box tests, saturated phase | 66 |
| Figure 47 – 15 percent fouled box tests, dry phase..... | 67 |
| Figure 48 – 15 percent fouled box tests, 1/3 field capacity phase | 68 |
| Figure 49 – 15 percent fouled box tests, 2/3 field capacity phase | 69 |
| Figure 50 – 15 percent fouled box tests, field capacity phase | 70 |
| Figure 51 – 15 percent fouled box tests, saturated phase, 15.6 kip loading | 71 |
| Figure 52 – 15 percent fouled box tests, saturated phase, 19.5 kip loading | 72 |
| Figure 53 – 15 percent fouled box tests, saturated phase, 23.4 kip loading | 73 |
| Figure 54 – 15 percent fouled box tests, saturated phase, 27.3 kip loading | 74 |
| Figure 55 – 30 percent fouled tests, dry phase..... | 75 |

| | |
|--|----|
| Figure 56 – 30 percent fouled tests, 1/3 field capacity phase | 76 |
| Figure 57 – 30 percent fouled tests, 2/3 field capacity phase | 77 |
| Figure 58 – 30 percent fouled tests, field capacity phase | 78 |
| Figure 59 – 30 percent fouled tests, saturated phase, 15.6 kip loading | 79 |
| Figure 60 – 30 percent fouled tests, saturated phase, 19.5 kip loading | 80 |
| Figure 61 – 30 percent fouled tests, saturated phase, 23.4 kip loading | 81 |
| Figure 62 – 30 percent fouled tests, saturated phase, 27.3 kip loading | 82 |

Tables

| | |
|--|----|
| Table 1 - Values of % fouling and corresponding PVC values for each fouling material | 5 |
| Table 2 – Loading schedule for box tests | 10 |
| Table 3 – Friction angles and ultimate strengths for all triaxial tests | 17 |
| Table 4 – 50% secant modulus for all triaxial tests | 19 |

Executive Summary

The Federal Railroad Administration funded the University of Massachusetts, Amherst's performance of triaxial tests and modified box tests on abraded ballast from May 2017 through December 2018. The ballast was sourced from a track in Shelburne Falls, MA, which closely resembled American Railway Engineering and Maintenance-of-Way Association (AREMA) #4 gradation. Samples were prepared clean and to fouling contents of 15 and 30 percent, and tested at different moisture contents. The testing performed in Phase II was divided into two parts: Phase IIa and IIb. Both phases involved the same set of tests and used the same ballast, but with different fouling materials. Phase IIa used the natural fouling material taken from the same track as the ballast. Phase IIb used a mixture of the natural fouling and Prestige™ clay to create a plastic behaving fouling material.

Triaxial tests were prepared by building 2.5-inch (6.4 cm) layers of ballast. Fouling was added to each layer as necessary and mixed before tamping. Each test was prepared to the same ballast density, with changing amounts of fouling. The triaxial tests consisted of draining and loading at a constant rate of strain. These tests assessed Mohr-Coulomb strength properties, modulus, and volumetric strain behavior of the ballast.

The modified box tests were also prepared in lifts comprised of three layers that are 2.5 inches (6.4 cm) in thickness. A quarter length of a wood and concrete railroad tie was placed on top of a total of 16.5 inches (41.9 cm) of ballast and buried with a tapered layer of ballast which extended half way up the tie, providing lateral confinement. The box tests were loaded dynamically, using an equivalent 39.4-ton (350.5 kN) static axle load. Each specimen was subjected to up to 2.5 million cycles. Each test starts in the dry condition followed by phases of increasing water content. After loading in the saturated phase, the load was increased by 25, 50, and 75 percent of the equivalent axle load. These tests assessed settlement of the track. Both plastic and elastic settlements were evaluated, as well as settlement rate.

The tests performed as part of Phase II are all comparable to the tests completed in Phase I, which used a freshly quarried Connecticut granite, which meets AREMA #4 gradation. Additional figures are provided within this report and in [Appendix A](#) and [Appendix B](#) using data from both phases to assess the influence of ballast abrasion and fouling material on the properties and behavior of ballast. The results show that while the abraded ballast achieves similar strengths to the angular granite, it is much more susceptible to deformations and settlement, particularly at higher fouling contents with water introduced. The fouling containing plastic fines tends to further increase this susceptibility. This testing also resulted in the first known basal failure in a box test, showing that heavy fouling can cause localized failures.

1. Introduction

The results of the University of Massachusetts, Amherst's triaxial tests and modified box tests are presented in this report. The Federal Railroad Administration (FRA) funded a series of two tests that were sampled from track located in Shelburne Falls, MA, one using natural fouling material, and the other using a mix of natural material with Prestige clay to achieve a plastic fouling material. These tests were performed from May 2017 through December 2018 at the University of Massachusetts, Amherst. In addition, this report includes a comparison of test results from Phase I of this project, which were performed using freshly quarried granite meeting American Railway Engineering and Maintenance-of-Way Association (AREMA) #4 ballast gradation.

The triaxial and box test specimens in both phases were compacted to the same ballast density typical of railroad track found in North America. Fouling was added to this material as appropriate for the condition desired in each test. Triaxial tests were performed drained and statically loaded at a constant rate of strain. Each test was prepared to a different fouling content, water content, and confining pressure. Box tests were loaded dynamically with an equivalent axle load of 60 tons (534 kN) per cycle. Each test began dry and the water content was increased in several stages after a predetermined number of cycles was reached. The results from the triaxial tests were used to determine the strength and deformation properties of ballast at different fouling conditions and water contents. The box tests were used to evaluate the influence of fouling and water content on track settlement. Comparisons to the previous testing phase are made to determine the effects of abrasion on the performance of ballast.

This report provides a summary of the work completed in Phase II. The objectives, background, and methods of investigation are first given, followed by a presentation and discussion of the results.

1.1 Background

Railway ballast is an important component of the track which plays a role in resisting loading forces, distributing stress to reduce pressure on the subgrade, maintaining track position, draining water away from the track, and providing large voids for the storage and movement of fouling material [8] [14]. Over time, traffic loading results in the breakdown of ballast. Additionally, fouling material enters the track either by abrasion of the ballast itself or by infiltration from outside the track. The introduction of fouling into the ballast has overall unfavorable effects on ballast performance, particularly when in a wet condition. Studies have found that fouling and moisture increases track settlement and decreases ballast strength [4] [10]. Regular maintenance of the track can be performed to remove fouling, through methods such as stone-blowing and tamping [8]. Critical fouling and moisture conditions have not been entirely defined, so maintenance decisions are often made by railroad engineers without fully assessing the ballast condition. This could lead to increased safety risks or unnecessary maintenance costs if sections of track with significant problems go unnoticed.

Past research was performed to evaluate the mechanical properties of ballast in a laboratory setting [2] [6] [7] [10] [11] [12] [15] [16]. Many of these studies utilize new angular ballast and manufactured fouling. In the cases where ballast abrasion is considered, new rock is abraded by methods such as Los Angeles (LA) Abrasion or Mill Abrasion [13]. While these methods allow

for specific levels of abrasion to be compared, they may not be representative of the actual wear that occurs in track. Limited studies, such as one by Indraratna et al. (2013) have included clay fouling [9]. This study showed that introduction of fines into the ballast decreases both peak and post-peak strengths. Additionally, small amounts of clay fouling were shown to act as a lubricant between ballast particles, increasing the compression. In some cases, dilation was reduced, but the benefits were negated due to the loss of strength.

Much of the research conducted on ballast strength properties and deformation have shown the negative effects of fouling and moisture on ballast performance in the laboratory. However, many of these studies use manufactured materials that may not be representative of ballast that has been in serviceable track for many years. This study makes use of naturally abraded ballast and fouling taken from a track that is properly representative of worn ballast. There is also limited understanding of the influence of clay fouling. This study uses a mixture of clay and natural fouling, rather than just clay to create a more representative material while still achieving the plastic behavior of clay. Triaxial tests and box tests are conducted on the abraded ballast with both the natural fouling and the clay fouling mixture to determine strength properties, deformation characteristics, and settlement behavior. The testing procedures and results are presented in the following sections.

1.2 Objectives

This research program aims to increase understanding of the influence of fouling content, moisture content, ballast abrasion, and fouling plasticity on the behavior of ballast approaching failure. The information enclosed will improve the understanding of some aspects of predicting the safety of track systems that have evidence of fouling, and in what conditions those problems become significant.

1.3 Overall Approach

Laboratory tests were performed, followed by analysis of the results. These results were then compared directly with those of the previous Phase I of this project.

1.4 Scope

This work is comprised of 45 triaxial tests and 5 modified box tests performed on railroad ballast. This work focuses on freight rail applications and does not consider passenger rail.

1.5 Organization of the Report

This report gives information on the source of the materials tested in [Section 1](#), while a detailed account of the testing methodology is provided in [Section 2](#). [Section 3](#) presents the results from all the laboratory tests are presented and conclusions are drawn based on these data in [Section 4](#). See [Appendix A](#) for additional figures and [Appendix B](#) provides figures regarding the box test settlement and settlement rate curves.

2. Methods of Investigation

One of the objectives of the research outlined in this report is to better understand differences in ballast behavior based on abrasion. The previous work done in Phase I was performed on an angular granite ballast, freshly quarried in Connecticut. The fouling used in this phase was granitic stone dust taken from the same quarry. This was representative of fouling generated from ballast abrasion. To build on the previous work, the testing in Phase II instead uses an abraded ballast of basaltic origin. This ballast was taken from a track in Shelburne Falls, MA, after a full replacement of ballast was done by the owner of the line. An image of the site, in [Figure 1](#), shows the darker spent ballast adjacent to the newly placed ballast below the track. Both the ballast and fouling from this site were used for all tests in Phase IIa. These tests are representative of a ballast abraded by real train loading conditions, and the resulting fouling conditions in the field, consisting of fouling from abrasion as well as material entering the ballast from other sources. Phase IIb uses this same material, but with Prestige clay mixed into the fouling. Prestige clay is an industrial grade kaolinite clay. After a series of Atterberg limit tests on different fouling mixtures, a mix of 45 percent Prestige clay to 55 percent natural fouling, by mass, was used for testing. This mix provided a sufficient plastic response with as little clay as possible, creating a reasonably realistic mix that could happen in the field given the right conditions.

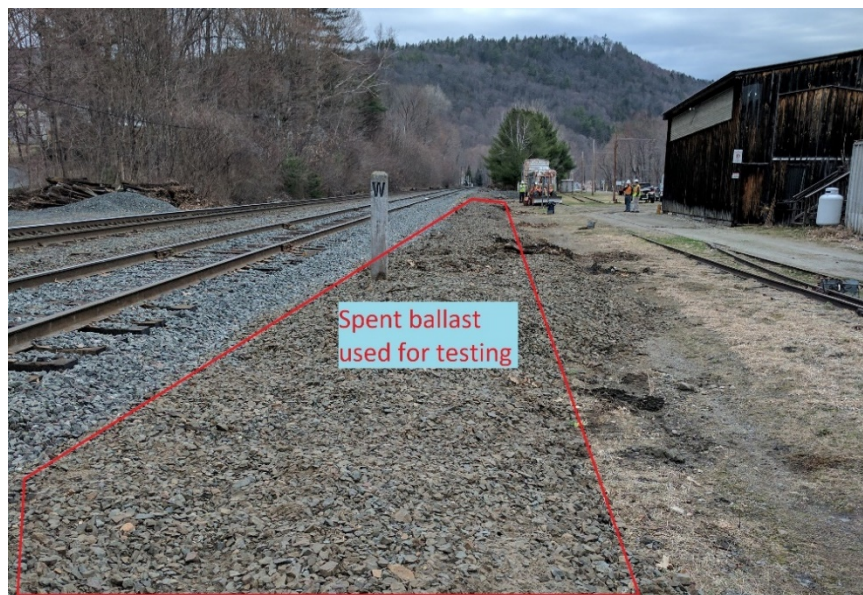


Figure 1 – View of spent ballast on site in Shelburne Falls, MA. Material was collected from the site on April 12, 2017

The two ballasts and three fouling materials used in Phase I and Phase II allow for two important comparisons to be made. The first is the effect of ballast particle shape or abrasion level on ballast performance. The second is the influence of the fouling material on ballast performance. The fouling materials range from predominantly sand to silt sized grains to predominantly clay sized grains. A comparison of tests in similar fouling conditions but with differing fouling material will provide insight to the effects of not just the amount of fouling, but the makeup of it as well.

2.1 Quantification of Fouling

In the United States, fouling is most commonly measured by the percentage fouling index, which is given by the mass of fouling over the total mass of the sample. Phase I of this study used this measure to determine fouling conditions. Both box tests and triaxial tests were performed at 0, 15, and 30 percent fouling. For the abraded ballast and natural fouling used in Phase IIa, this method of measuring ballast was continued. However, the clay mixture used in Phase IIb made apparent some issues with this methodology.

The clay fouling mixture has twice the volume of the natural fouling alone. This is due to the very low unit weight of the clay. When building 30 percent fouled triaxial specimens, the volume of fouling exceeded the volume of the voids in the ballast, so the samples physically could not be built to the proper percent fouling. After some consideration, it was decided that these specimens should be prepared to have the same *volume* of fouling rather than the same mass. This would allow for the results to still be comparable to previous tests. This methodology has been considered before. Feldman and Nissen [5] noted that the percentage fouling index did not account well for situations in which the fouling material and ballast had significantly different specific gravities. They proposed a different measure called percentage void contamination, given by

$$PVC = V_2/V_1$$

in which V_1 is the void volume of compacted ballast and V_2 is the volume of compacted fouling material.

The Percent Void Contamination (PVC) measure was adopted for the tests with the clay fouling mixture. It was found that the naturally abraded ballast at 15 and 30 percent fouling have equivalent PVCs of 35.6 and 86.3 percent, respectively, so the Prestige mixture fouling tests were prepared to this PVC. Because of the reduced mass, these tests have lower percentage fouling values as shown in Table 1. For clarity in this report, the tests with Prestige mixture fouling will still be referred to as 15 and 30 percent fouled since they are compared directly to the other tests.

Table 1 - Values of % fouling and corresponding PVC values for each fouling material

| Fouling Type | 0% | | 15% | | 30% | |
|------------------------------------|-----------|-----|-----------|------|-----------|------|
| | % Fouling | PVC | % Fouling | PVC | % Fouling | PVC |
| Granitic Stone Dust | 0 | 0 | 15 | 35.6 | 30 | 86.3 |
| Natural Fouling | 0 | 0 | 15 | 35.6 | 30 | 86.3 |
| Prestige & Natural Fouling Mixture | - | - | 8.1 | 35.6 | 17.6 | 86.3 |

2.2 Triaxial Tests

Consolidated drained triaxial tests were conducted on reconstituted ballast samples to determine strength properties and deformation behavior of worn ballast under different fouling and moisture conditions. The following sections detail the specimen preparation, including determination of fouling and water content, and the testing procedures.

2.2.1 Specimen Preparation

Consolidated Isotropic Drained Compression Triaxial Tests (CIDC) were performed in general accordance with American Society for Testing Materials' (ASTM) D7181-11 [1]. Ten-inch (25.4 cm) diameter specimens were prepared in eight lifts, each with a thickness of 2.5 inches (6.35 cm). In each lift, the ballast was placed first, followed by the appropriate amount of fouling. The material is then tamped to promote mixing and to achieve the proper density. It is important to note that the quantity of ballast is the same in every test, with only the amount of fouling changing. As a result, the ballast density remains the same while the total sample density increases with increasing fouling.

Once the specimen is prepared and the testing cell is fully assembled, the moisture content can be considered. To simulate field conditions, the water contents are based on field capacity, which is the maximum amount of water that is held by the material in a free draining condition. The field capacity is determined by preparing a sample of ballast and fouling in a bucket with drain holes. The specimen is covered in water, allowed to drain, and the water content is taken. Based on these results, triaxial specimens are tested in the dry condition, at half of field capacity, and at field capacity. Water is added to the top of the sample and a minimum of 16 hours is allowed to pass so that the water has sufficient time to fully penetrate into the sample. A low cell pressure of 2–3 psi (13.8–20.7 kPa) is used to maintain the specimen shape until the time of testing.

Since the tests are performed in undersaturated conditions, the volume change of specimens cannot be directly measured by the flow of water in and out of the sample. Instead, three string potentiometers are placed circumferentially on the mid-point and quarter points of the specimen. The measurements taken are used to calculate radial strain, which in turn are used to estimate volume change, which is discussed further in the next section. [Figure 2](#) shows an example of the triaxial test set up.

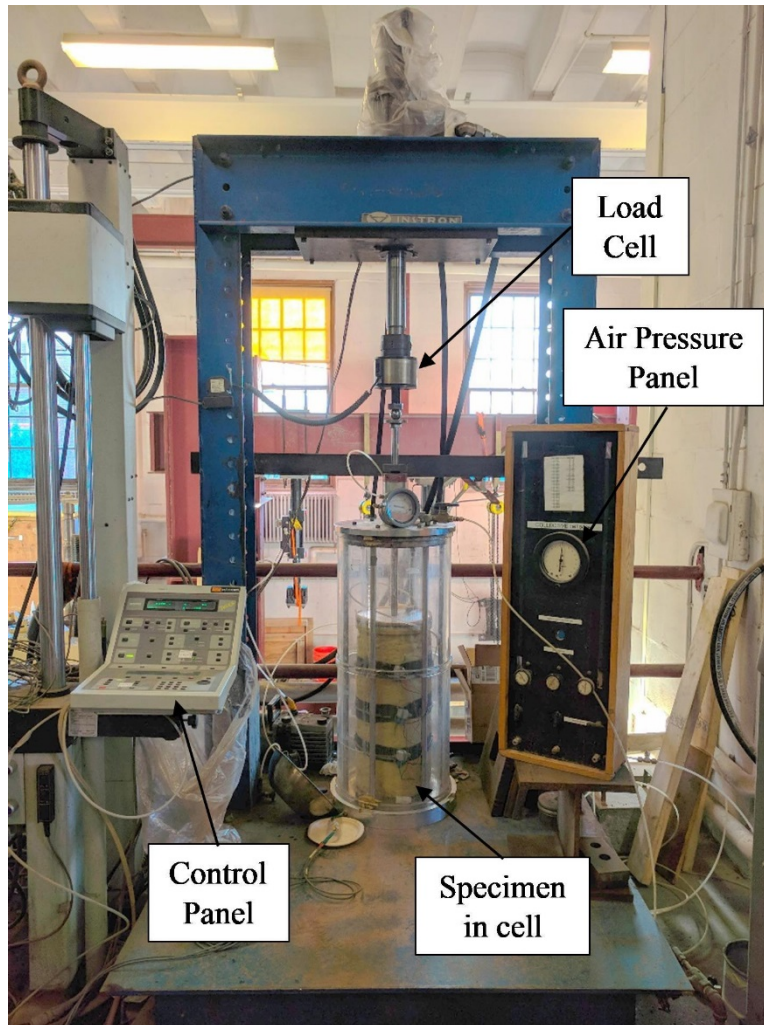


Figure 2 – Triaxial test setup in load frame. Instron control panel is shown to the left; the cell pressure control panel is shown to the right

2.2.2 Testing Procedure

The triaxial test specimens are loaded using a 22.5-kip (100 kN) static capacity actuator operated by an Instron 8501 controller. The test parameters used are taken from a study by Aursudkij et al. 2009, which found that specimens loaded past 12 percent strain had reached and sustained peak strength [2]. This study used the same strain rate of 0.04 inches/min (1 mm/min). Tests were run up to 12 percent strain or were stopped when the bulging specimen risked touching the sides of and damaging the testing cell. Confining pressures of 5, 10, and 15 psi (34.5, 69.0, and 103.4 kPa) were applied to replicate the characteristically low confining pressures of railroad track. All data are collected using a DATAQ Instruments DI-710 data acquisition box and WinDAQ software. Data was recorded at a rate of four readings per second per channel.

2.3 Box Tests

Modified box tests were performed on reconstituted worn ballast samples with both natural and clay mixture fouling to evaluate track settlement in different conditions. The same box developed for Phase I of this project was used in this series of tests. The box is made of half inch steel plate with internal dimensions of 4.3 ft. (1.32 m) x 2.75 ft. (0.82 m) x 1.125 ft. (0.34 m). Wooden boards are attached directly to the upper portion of the box with bolts to increase the height by an additional 6 inches (15.42 cm). All the seams, joints, and bolt holes are sealed with silicone caulk to ensure that the box remains water tight. There is a drainage outlet at the bottom of the box to allow for the addition of water as well as discharge.



Figure 3 – Top-down view of the empty box in the frame with wooden boards attached

2.3.1 Specimen Preparation

Three specimens are prepared for the abraded ballast with natural fouling. Like the triaxial tests, fouling conditions of 0, 15, and 30 percent are used. Because the same ballast is used with the clay mixture fouling, an additional clean test was not needed, so only the equivalent 15 and 30 percent fouling specimens are prepared.

Each specimen is prepared in density-controlled lifts. The first three lifts are 3 inches (7.62 cm) followed by an additional three lifts of 2.5 inches (6.35 cm). As with the triaxial tests, when the lifts are prepared, the ballast is added first, followed by the required amount of fouling. The layer is tamped to promote mixing and achieve the appropriate bulk density. The first six layers provide a ballast depth of 16 inches. The quarter length of concrete tie with length of 27-3/4 inches (70.5 cm), width of 10-1/8 inches (25.7 cm), and height of 9-11/16 inches (24.6 cm) is centered on top of this material. A 9 inch (22.9-cm) length of rail with section designation 13225 is placed atop the tie and a small load is applied to ensure that the rail is level and properly seated in the ballast. A final 4-inch (10.2-cm) layer of ballast and fouling is placed around the tie, completing the specimen. A linear voltage displacement transducer (LVDT) is oriented vertically over the tie. Because of flexure in the self-reacting frame, the LVDT is held in place by a metal frame which is attached directly to the box. This ensures accurate measurement of settlement alone, and not frame movement. Finally, a plastic sheet is placed over the material in the box to

prevent loss of water from the specimen over the duration of testing. Figure 4 shows the completed test setup.



Figure 4 – Completed box test setup showing LVDT placement and plastic covering to prevent moisture loss

2.3.2 Testing Procedure

Each box is built in a self-reacting load frame which is equipped with a 110 kip (500 kN) MTS hydraulic actuator. Cyclic loading is applied sinusoidally at a frequency of 1 Hz. A minimum seating load of 0.2 kips (0.9 kN) is applied to prevent the actuator from lifting off the rail, which would create impact loads. The maximum load applied in each cycle is 15.6 kips (69.4 kN) which is equivalent to a static load of 39.4 tons (350.5 kN) and a dynamic axle load of 60 tons (533.8 kN). The loading was determined using GEOTRACK, a three-dimensional model, which accounts for substructure stress-dependent properties to determine track response [3]. The modeling was done as part of Phase I.

Each test starts in the dry phase and the moisture content is increased in steps. Each test has five different water conditions in which it is tested: dry, 1/3 field capacity, 2/3 field capacity, field capacity, and saturated. After reaching the desired number of loading cycles for each these iterations, the test is stopped and water is added. For the 1/3 and 2/3 field capacity phases, the water is added from the top of the specimen by distributing evenly over the surface with a scoop. The water is allowed to sit for 16 hours so that the water has time to fully penetrate the sample, in accordance with procedures for reconstituted samples in ASTM D7181. Field capacity is achieved by filling the box from the bottom until the material is completely covered, to ensure initial saturation, and then the excess water is immediately drained, taking about half an hour to empty. Saturation is achieved by filling the box with water, covering the box with plastic and preventing water from flowing out of the bottom of the box.

The dynamic loading of rail typically does not exceed 10–20 percent of the static load, but defects in the wheel or rail can cause higher peak loads [14]. To simulate this, higher loads are applied in the saturated phase. After applying sufficient cycles of the 60-ton (533.8 kN) equivalent load to the saturated specimen, the test is stopped, and additional saturated phases are performed with 25, 50, and 75 percent increased load factors. The maximum loads applied are 19.5, 23.4, and 27.3 kips (86.7, 104.1, and 121.4 kN), which are equivalent to static axle loads of 49.3, 59.1, and 69.0 tons (439, 526, and 614 kN) which gives dynamic axle loads of 75, 90, and 105 tons (667, 801, and 934 kN).

Table 2 provides the full loading schedule of each test along with equivalent load and million gross tons (MGT) for each test. The MGT is based on the equivalent static axle loads. Note that the clean box test does not have 1/3 and 2/3 field capacity phases. This is because clean ballast has such a low field capacity that there is no practical difference between the intermittent water contents, so they are not used. Similarly, the clean test is not subjected to higher loading when saturated. Without the presence of fouling, contact between the ballast particles is maintained, even when saturated, so the presence of water has less effect on the ballast performance. This also saves significant time when performing tests.

Table 2 – Loading schedule for box tests

| Fouling Condition | Water Content Phase | Load Applied (kips) | Equivalent Axle Load (tons) | Cycles | MGT | MGT (Cumulative) |
|-------------------|---------------------|---------------------|-----------------------------|---------|-------|------------------|
| 0% | Dry | 15.6 | 39.4 | 121,900 | 9.6 | 9.6 |
| | FC | 15.6 | 39.4 | 225,500 | 17.8 | 27.4 |
| | Saturated | 15.6 | 39.4 | 200,000 | 15.8 | 43.1 |
| 15% | Dry | 15.6 | 39.4 | 200,000 | 15.8 | 15.8 |
| | 1/3 FC | 15.6 | 39.4 | 202,000 | 15.9 | 31.7 |
| | 2/3 FC | 15.6 | 39.4 | 204,500 | 16.1 | 47.8 |
| | FC | 15.6 | 39.4 | 427,500 | 33.7 | 81.5 |
| | Saturated | 15.6 | 39.4 | 422,000 | 33.3 | 114.7 |
| | | 19.5 | 49.3 | 255,000 | 25.1 | 139.9 |
| | | 23.4 | 59.1 | 501,000 | 59.2 | 199.1 |
| 27.3 | | 69.0 | 327,000 | 45.1 | 244.2 | |
| 30% | Dry | 15.6 | 39.4 | 200,000 | 15.8 | 15.8 |
| | 1/3 FC | 15.6 | 39.4 | 200,000 | 15.8 | 31.5 |
| | 2/3 FC | 15.6 | 39.4 | 200,000 | 15.8 | 47.3 |
| | FC | 15.6 | 39.4 | 415,000 | 32.7 | 80.0 |
| | Saturated | 15.6 | 39.4 | 441,300 | 34.8 | 114.8 |
| | | 19.5 | 49.3 | 283,300 | 27.9 | 142.7 |
| | | 23.4 | 59.1 | 500,200 | 59.1 | 201.8 |
| 27.3 | | 69.0 | 350,350 | 48.3 | 250.2 | |

Like the triaxial tests, the box test data is collected using a DATAQ Instruments DI-710 data acquisition box and WinDAQ software. The LVDT data is collected and processed to determine

elastic and total settlements of the tie and, by extension, the ballast. These data, along with load data from the actuator, can also be used to determine rate of settlement and test modulus.

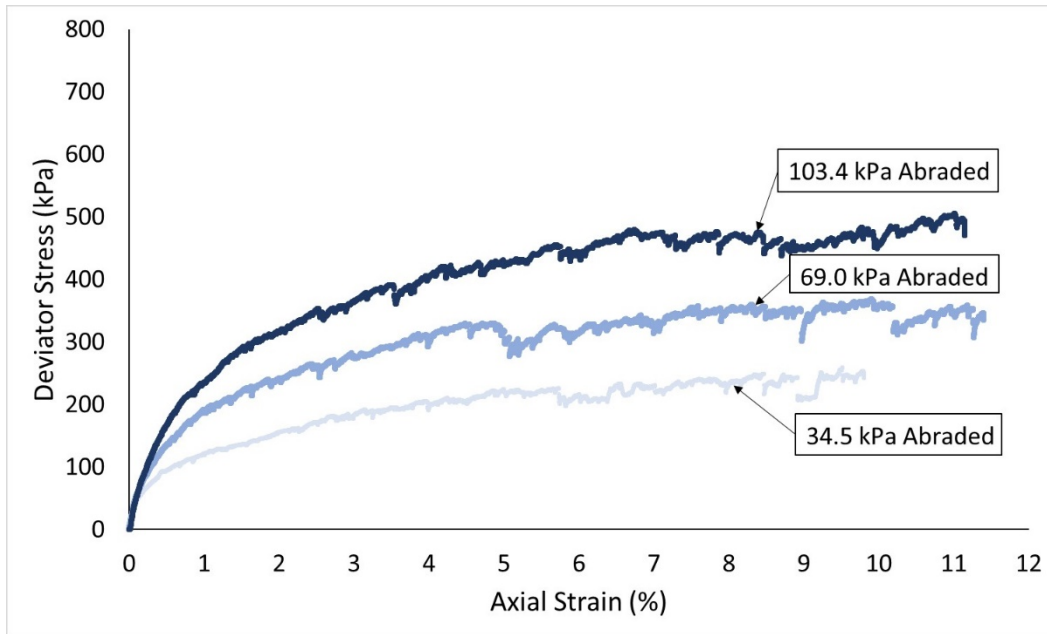
3. Presentation of Results and Discussion

3.1 Triaxial Tests

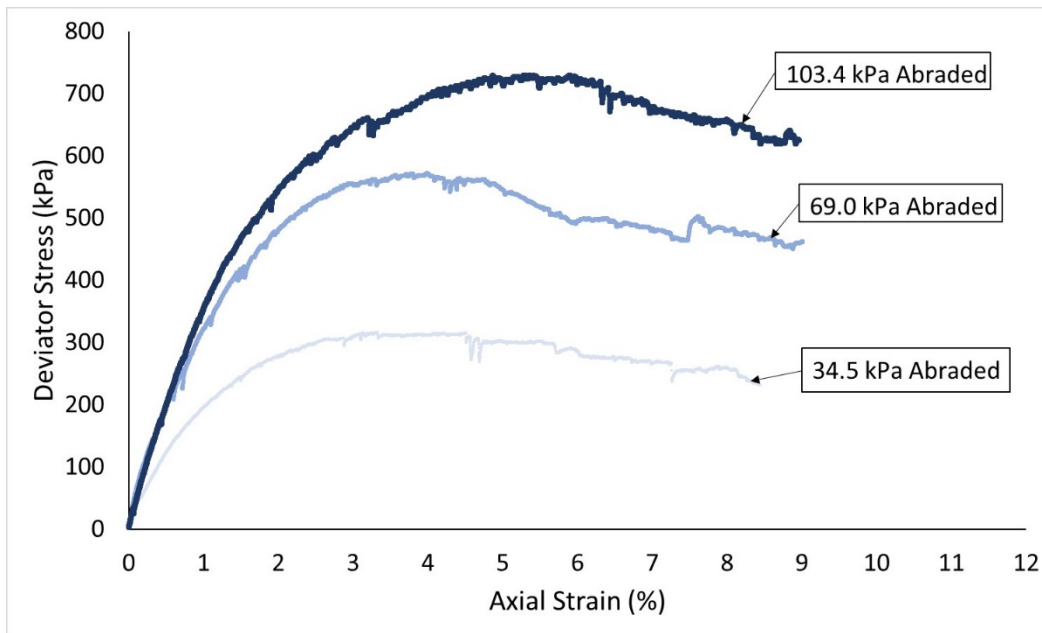
3.1.1 *Stress-Strain and Volumetric Strain Behavior*

The ballast stress-strain curves indicate two distinct behaviors, which are controlled by the fouling content. Most tests have behavior typical of loose sand, as shown in [Figure 5a](#). In the heavily fouled conditions, both the granite ballast and abraded ballast with natural fouling behave similarly to dense sand. [Figure 5b](#) shows curves typical of this behavior. It should be noted that the difference in peak stress and residual stress decreases with the addition of water. While the heavily fouled Connecticut granite maintains this behavior to some extent in all water conditions, the natural ballast and fouling behavior reverts to that of loose sand when water is added.

The stress-strain and volumetric strain of each ballast and fouling combination can be compared to draw further comparisons between their behaviors. [Figure 6](#) shows the stress-strain curves and the volumetric strain curves for all triaxial tests performed at 30 percent fouling at half of field capacity. These tests were chosen as an example for discussion because they provide a good representation of behavior across most of the tests. For further information, [Appendix A](#) contains the stress-strain and volumetric strain curves for all tests performed.



a) Typical stress-strain behavior for clean and moderately fouled ballast. Example curves taken from clean tests in the dry condition



b) Typical stress-strain behavior for heavily fouled ballast. Example curves taken from 30 percent fouled tests in the dry condition

Figure 5 – Typical stress-strain curves

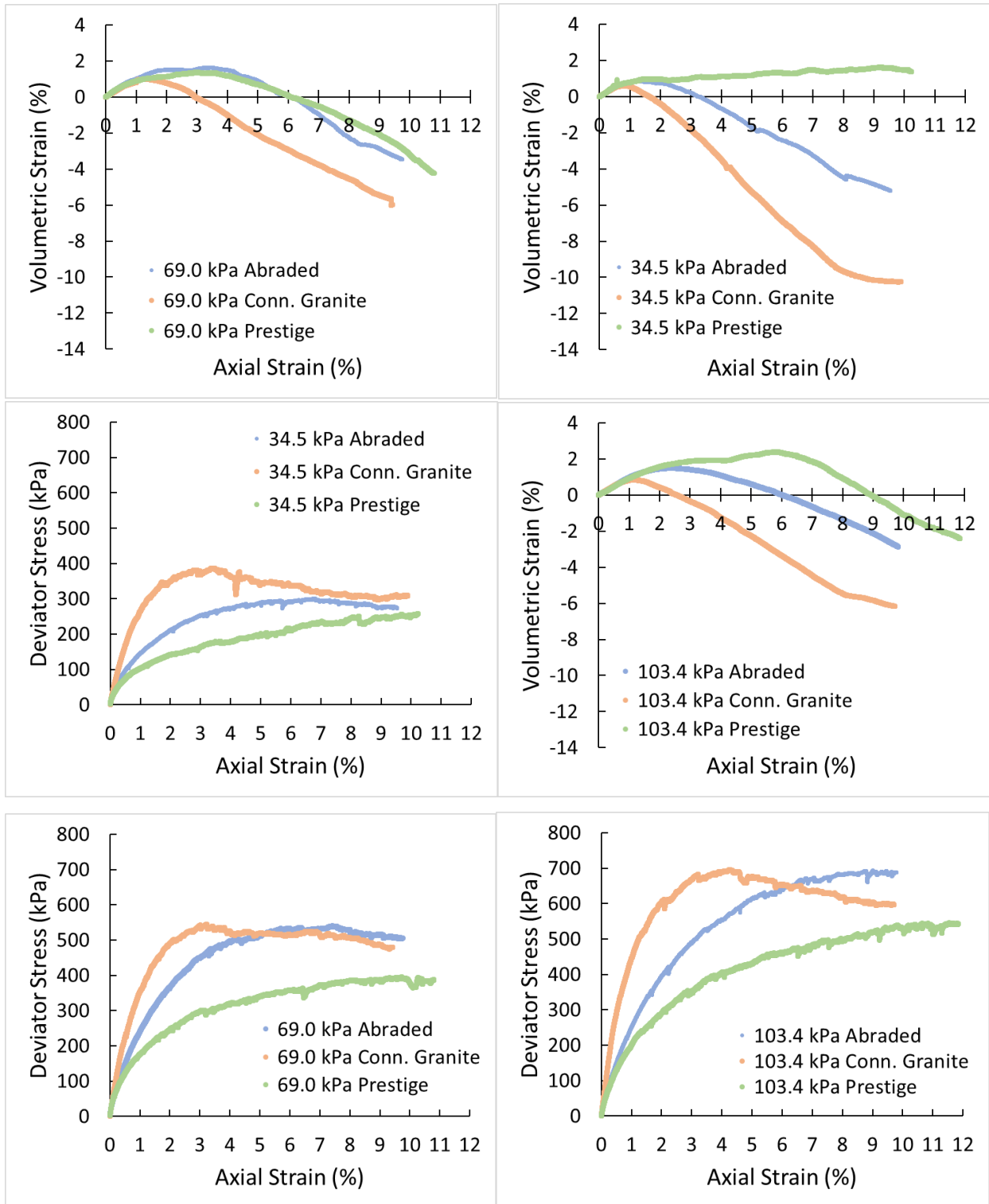
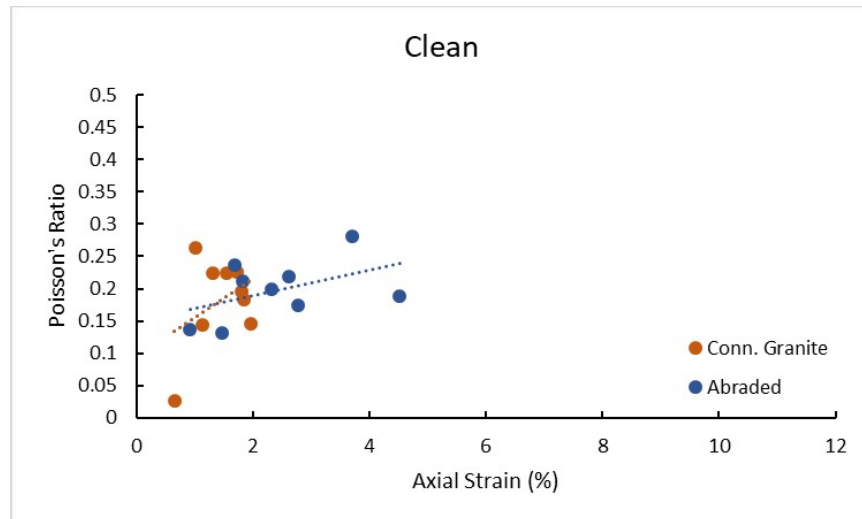


**Figure 6 – 30 percent fouled triaxial tests at half of field capacity
(Larger versions of these plots are available in [Appendix A](#))**

From the example curves, it can first be observed that the granite ballast achieves a peak strength, followed by strain softening. The abraded ballast with natural fouling does not have a strong peak with the addition of water, but the strengths reached are like that of the granite. The addition of Prestige to the fouling with the abraded ballast leads to a drop in strength across all tests. Additionally, observation of the stress strain curves show that the modulus of the abraded ballast is lower than that of the granite. The modulus drops further when the abraded ballast is fouled with the Prestige mixture. Quantification of the modulus and methods of measurement for each test is provided in the following section.

The volumetric strain curves show behavior typical of ballast. The plots use geotechnical conventions, meaning positive strains indicate compression while negative strains indicate dilation. It can be seen that each test undergoes an initial contraction, which is typically followed by a much larger dilation. The abraded ballast undergoes higher levels of contraction than the granite ballast. The addition of Prestige to the fouling causes the abraded ballast to contract more, though in some cases the level of contraction is similar to the abraded ballast with natural fouling only. It can be observed that with increasing confining pressure, the amount of contraction generally increases, as does the point at which contraction ends and dilation begins. In some rare cases, such as the 5-psi (34.5 kPa) test with Prestige mix fouling, the specimen never reaches dilation.

The Poisson's ratio was calculated for each test at the point of maximum contraction. [Figure 7](#) shows that the two ballasts have similar Poisson's ratios in the clean condition, though it takes longer for the abraded ballast to reach maximum contraction. With the addition of fouling, the Poisson's ratio of the granite drops slightly, while it increases slightly for the abraded ballast. It can also be seen that the Prestige mixture fouling further increases the Poisson's ratio of the ballast and fouling matrix. These plots also further demonstrate how the addition of Prestige to the fouling material contributes to a prolonged period of initial contraction in the tests.



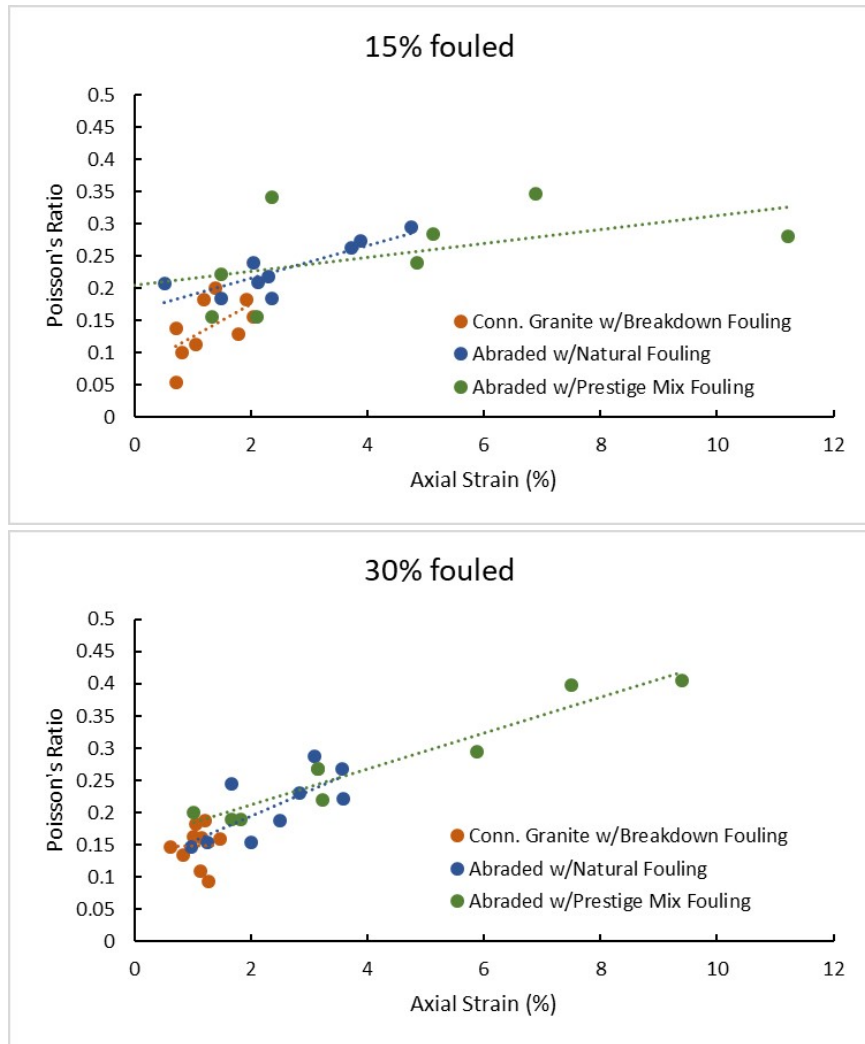


Figure 7 – Poisson's Ratio vs axial strain at which maximum contraction occurs

Table 3 – Friction angles and ultimate strengths for all triaxial tests

| Water Condition | Confining Pressure | 0% Fouling | | | | 15% Fouling | | | | | | 30% Fouling | | | | | |
|-----------------|--------------------|---------------|---------------|-------------------|---------------|---------------|---------------|-------------------|---------------|----------|---------------|---------------|---------------|-------------------|---------------|----------|---------------|
| | | Conn. Granite | | Naturally Abraded | | Conn. Granite | | Naturally Abraded | | Prestige | | Conn. Granite | | Naturally Abraded | | Prestige | |
| | | ϕ' | ult. strength | ϕ' | ult. strength | ϕ' | ult. strength | ϕ' | ult. strength | ϕ' | ult. strength | ϕ' | ult. strength | ϕ' | ult. strength | ϕ' | ult. strength |
| | kPa | degrees | kPa | degrees | kPa | degrees | kPa | degrees | kPa | degrees | kPa | degrees | kPa | degrees | kPa | degrees | kPa |
| Dry | 34.5 | | 243 | | 259 | | 268 | | 253 | | 210 | | 393 | | 316 | | 260 |
| | 69.0 | 47.4 | 418 | 46.5 | 369 | 48.0 | 450 | 48.5 | 433 | 46.7 | 387 | 52.2 | 561 | 52.4 | 572 | 49.9 | 508 |
| | 103.4 | | 528 | | 506 | | 529 | | 581 | | 529 | | 673 | | 729 | | 610 |
| 50FC | 34.5 | | 239 | | 244 | | 263 | | 289 | | 229 | | 387 | | 300 | | 258 |
| | 69.0 | 45.1 | 334 | 47.7 | 393 | 47.8 | 420 | 50.7 | 511 | 47.2 | 382 | 52.2 | 544 | 51.5 | 541 | 47.5 | 395 |
| | 103.4 | | 473 | | 566 | | 542 | | 654 | | 552 | | 696 | | 692 | | 546 |
| FC | 34.5 | | 209 | | 230 | | 239 | | 221 | | 171 | | 346 | | 285 | | 174 |
| | 69.0 | 43.4 | 366 | 46.6 | 404 | 45.8 | 373 | 47.5 | 382 | 45.0 | 315 | 49.9 | 452 | 50.4 | 471 | 44.1 | 395 |
| | 103.4 | | 438 | | 547 | | 478 | | 575 | | 509 | | 610 | | 671 | | 399 |

3.1.2 Strength Properties

The Mohr-Coulomb strength properties can be obtained from the triaxial tests. Ultimate strengths are determined by the maximum deviator stress measured during the test. Each fouling and water condition combination was tested at three confining pressures, allowing for the determination of a friction angle. It was assumed that there is no cohesion in these tests. [Table 3](#) presents the friction angles and ultimate strengths.

Both the Connecticut granite and abraded ballast with natural fouling see increased friction angles with increasing fouling content, regardless of water condition. The abraded ballast with Prestige mixture fouling sees this same trend in the dry state, but increased fouling contents do not increase the friction angle when water is added. For any material at a given fouling content, the addition of water generally reduces the friction angle. In some cases, however, the specimens show an increase in friction angle from dry to 50 percent field capacity, followed by a decrease from 50 percent field capacity to field capacity. Typically, the friction angle of the granite and the abraded ballast are comparable, with the abraded ballast often showing higher values. However, the addition of Prestige clay causes a drop in the friction angle. At 15 percent fouling, Prestige mix fouling results in friction angles that are 1.8–3.5 degrees lower than their counterparts with natural fouling alone, and the 30 percent fouled tests have friction angles that are 2.5–6.8 degrees lower. All the friction angle trends described herein are also reflected by the ultimate strengths.

Stress-strain curves of soils typically exhibit an initial linear-elastic portion, which are useful to determine the initial tangent modulus, or elastic modulus. However, observe that the test results presented in this report have minimal or no linear portion to the curve, which makes the tangent modulus difficult to determine. The 50 percent secant modulus resolved this by determining the secant from the origin to the point where 50 percent of the ultimate strength reached. This method allows for more consistent and accurate measurement of the modulus. [Table 4](#) presents the results. [Figure 15](#) through [Figure 17](#) presents these data found in [Appendix A](#). For both the angular Connecticut granite and the abraded ballast with natural fouling, there is a general trend of increasing strength with increasing fouling at a constant confining pressure. The addition of water at any given fouling condition generally lowers the strength. The abraded ballast with Prestige mix fouling shows increasing strength with increasing fouling, but only in the dry condition. The addition of water causes the strength to generally decrease with increased fouling, further demonstrating the problematic nature of fouling containing plastic fines.

Table 4 – 50% secant modulus for all triaxial tests

| Water Condition | Confining Pressure | Secant Modulus at 1% Axial Strain | | | | | | | |
|--------------------|--------------------|-----------------------------------|-------------------|---------------|-------------------|----------|---------------|-------------------|----------|
| | | 0% Fouled | | 15% Fouled | | | 30% Fouled | | |
| | | Conn. Granite | Naturally Abraded | Conn. Granite | Naturally Abraded | Prestige | Conn. Granite | Naturally Abraded | Prestige |
| | kPa | MPa | MPa | MPa | MPa | MPa | MPa | MPa | MPa |
| Dry | 34.5 | 17.1 | 12.0 | 20.2 | 13.7 | 11.3 | 29.9 | 19.4 | 16.0 |
| | 69.0 | 28.5 | 18.9 | 27.0 | 19.0 | 17.5 | 41.1 | 32.2 | 23.9 |
| | 103.4 | 34.8 | 23.5 | 34.9 | 26.2 | 18.6 | 41.9 | 35.3 | 27.7 |
| 50% Field Capacity | 34.5 | 15.7 | 13.9 | 18.6 | 12.9 | 9.7 | 26.4 | 14.3 | 9.5 |
| | 69.0 | 24.3 | 16.8 | 24.4 | 20.4 | 15.5 | 35.3 | 24.0 | 16.6 |
| | 103.4 | 0.0 | 27.8 | 31.6 | 22.5 | 19.2 | 44.5 | 24.7 | 19.2 |
| Field Capacity | 34.5 | 15.0 | 11.2 | 17.8 | 10.4 | 7.8 | 24.8 | 12.6 | 8.3 |
| | 69.0 | 20.6 | 18.7 | 24.4 | 17.3 | 13.5 | 25.5 | 19.7 | 16.6 |
| | 103.4 | 28.8 | 25.9 | 29.2 | 22.2 | 18.0 | 35.2 | 24.6 | 14.0 |

3.2 Box Tests

3.2.1 Plastic, Elastic, and Total Ballast Settlement

The cumulative settlement curves for the clean box tests, shown in [Figure 7](#), provide a good baseline of the ballast settlement behavior. The labeled vertical lines indicate the beginning of new phases after the addition of water. The previously tested granite experiences an initial settlement at the beginning of each water content phase, with the settlement curve mostly flattening out after approximately 10,000 cycles. The abraded ballast has similar higher initial settlement, but the rate of settlement does not slow to the same extent as the granite. This is particularly pronounced in the dry phase, which has plastic settlements nearly four times as large as the granite at the end of the phase. The larger settlement from the abraded ballast may be due to increased rearrangement of particles facilitated by the more rounded particle shapes. An additional note from these results is the elastic settlement represented by the difference in the plastic and total settlement. The elastic settlement is consistent throughout the duration of the test. The granite ballast has an average elastic settlement of 0.02 inches (0.5 mm) while the abraded ballast has a higher elastic settlement of 0.07 inches (1.8 mm). Further, this difference is reflected by the higher test moduli of the granite ballast box tests versus the abraded ballast box tests, as seen in the first plot of [Figure 9](#). Interestingly, the abraded ballast modulus is consistent throughout the test, while the angular granite ballast experiences two distinct increases, which occurred at the beginning of each new phase. This is likely the result of additional compaction occurring after the addition of water to the specimen. The second two plots show the modulus of the 15 and 30 percent fouled tests. From reading to reading, the modulus varied widely, so the use of smoothing could comprehend an overall trend. Observe that the modulus generally increases. Smaller areas of increase or decrease can be accounted for by the overall varied nature of the results and smoothing and are not necessarily indicative of changes occurring in the material during testing.

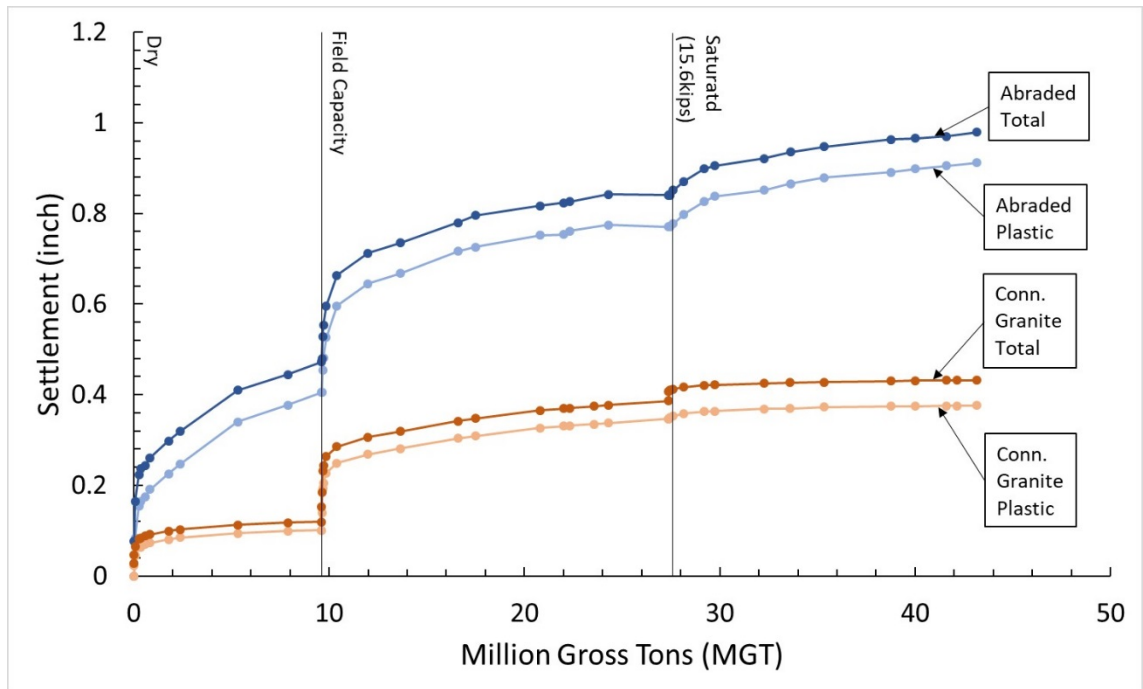


Figure 8 – Plastic and total cumulative settlement curves for angular ballast and naturally abraded ballast in clean box tests

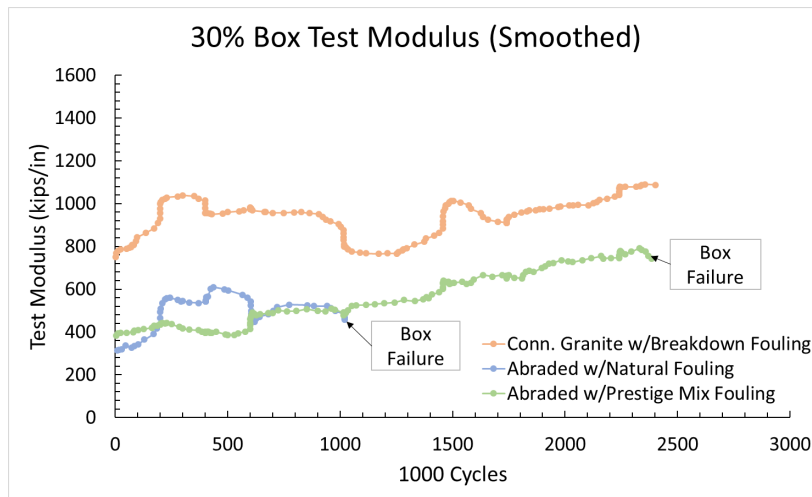
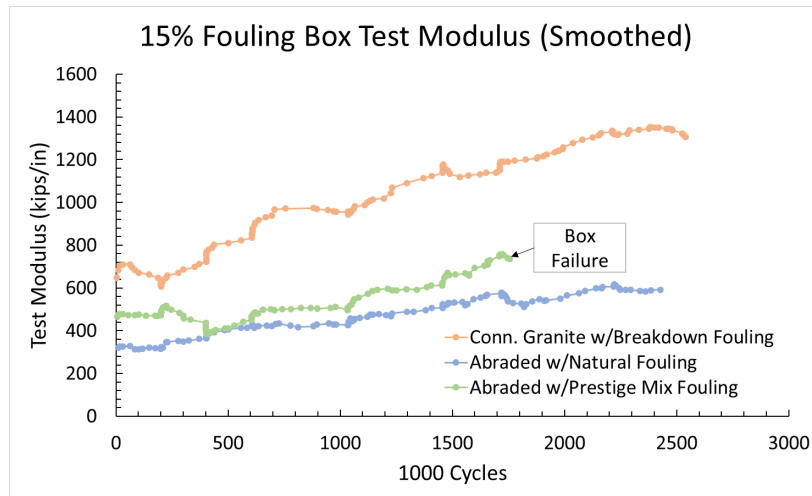
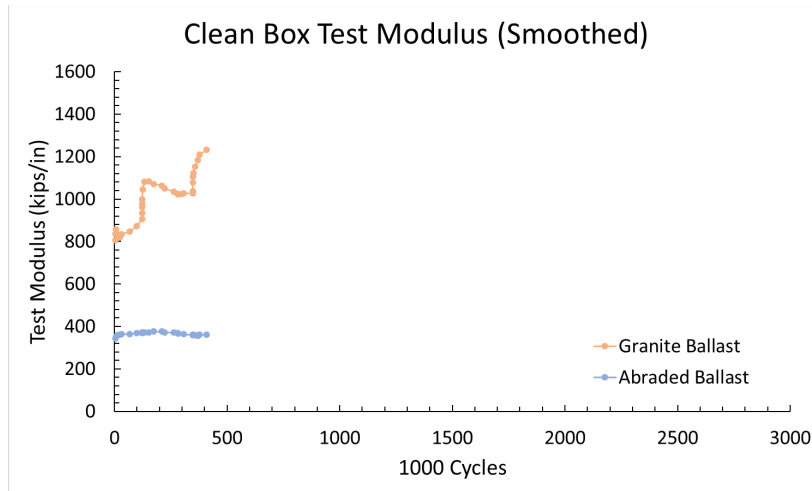


Figure 9 – Test modulus measured for all box tests, with a smoothing function applied for clarity

The introduction of fouling to the ballast leads to some changes in the ballast settlement behavior. Figure 10 and Figure 11 show the results of the 15 percent fouled and 30 percent fouled box tests, respectively. As with the clean tests, each addition of water generally produces a larger initial settlement at the beginning of the phase. First, observe that the addition of fouling increases the overall settlement of both ballasts in the 15 percent tests. The abraded ballast again has higher settlements than the granite ballast, particularly in the dry and partially saturated phases. Interestingly, the settlement curves in the saturated phases, including those with increased loading, are very similar.

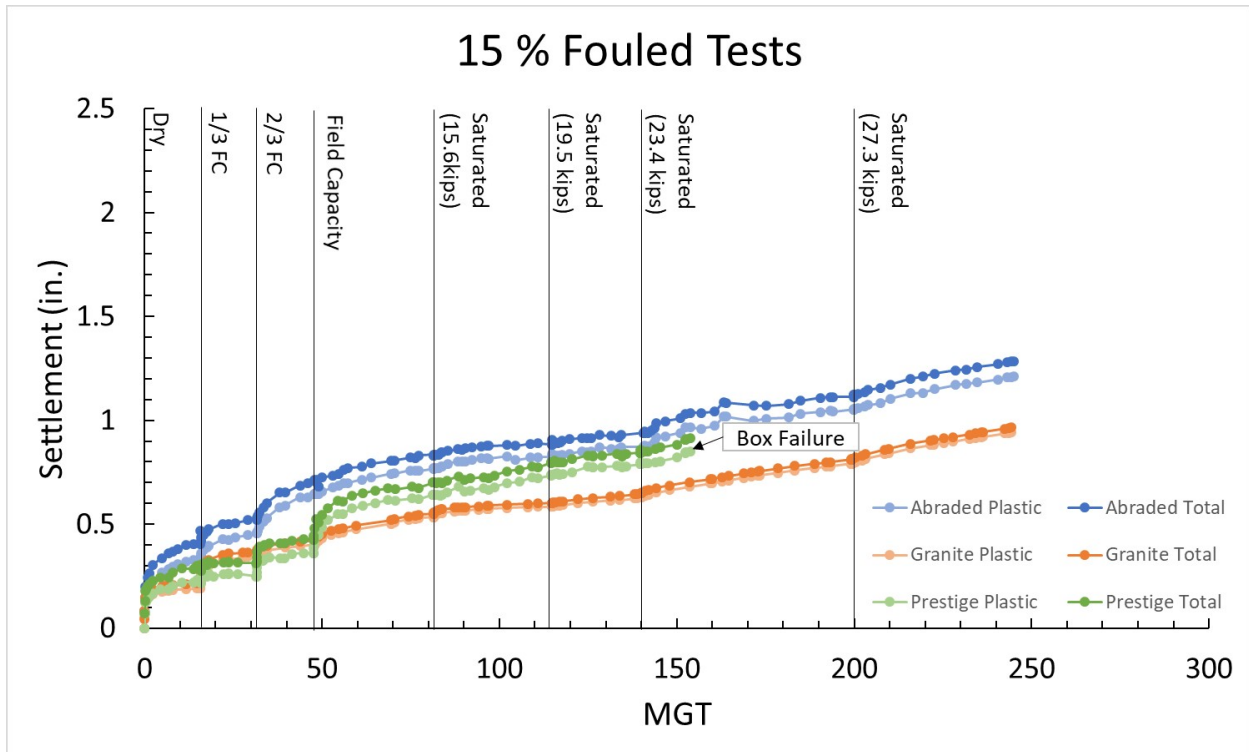


Figure 10 – Plastic and total cumulative settlement curves for 15 percent fouled box tests. Results from previous tests on granite ballast and current tests on abraded ballast with natural fouling and Prestige clay fouling mixture are included

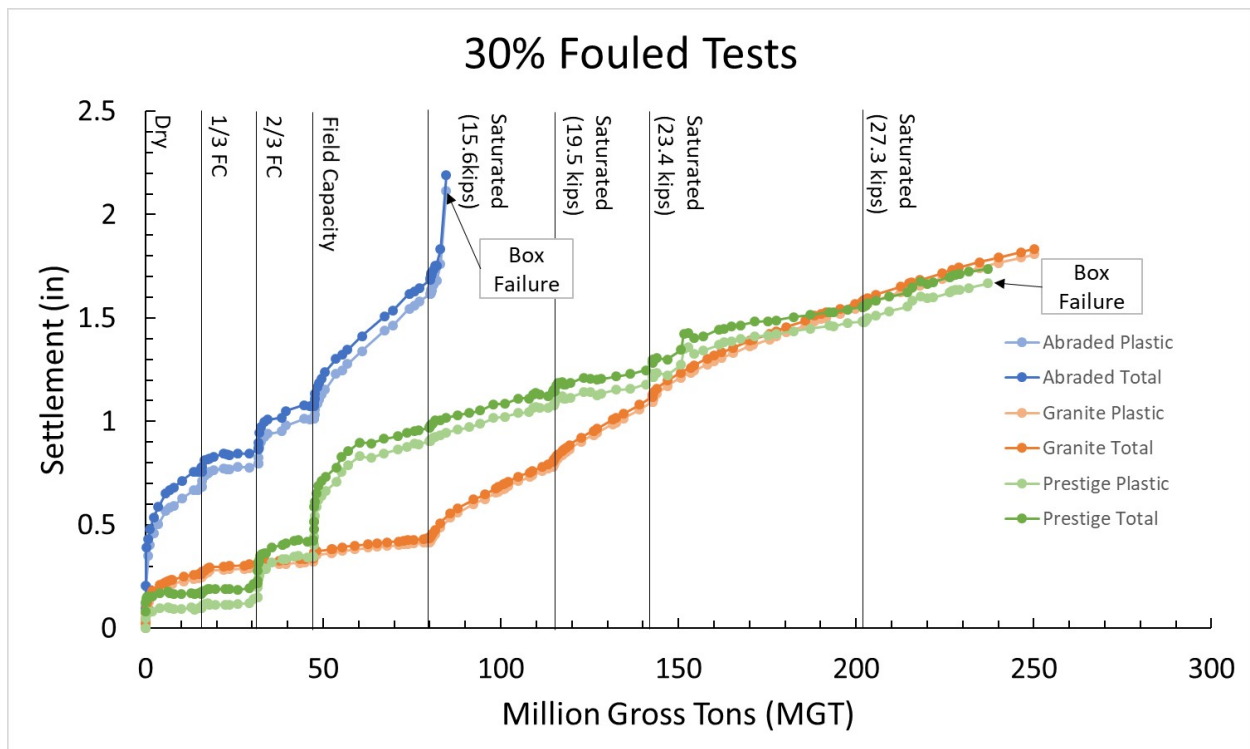


Figure 11 – Plastic and total cumulative settlement curves for 30 percent fouled box tests. Results from previous tests on granite ballast and current tests on abraded ballast with natural fouling and Prestige clay fouling mixture are included

The addition of clay into the fouling mixture leads to more variable settlement behavior. In the phases with water contents less than field capacity, the Prestige mix fouled ballast settles less than the natural fouling alone. By contrast, during the field capacity phase, the Prestige mix fouled ballast underwent a settlement more than double that of the abraded ballast with natural fouling. The settlements in the saturated phases are similar to each other. However, after increasing the loading to the equivalent axle load of 90 tons (801 kN), the ballast with Prestige mix fouling experienced a lateral failure, which caused a sliding of the tie, as well as movement of the entire box within the frame.

One possible explanation for this behavioral shift in the ballast-fouling mixture is the behavior of the Prestige clay itself. Prestige has a very low unit weight and is not easily compacted in the dry condition. Because it is a kaolin, the clay contracts with the addition of water. This contraction may have actually increased ballast particle contact during the 1/3 and 2/3 field capacity phases, increasing the overall strength of the material, resulting in lower settlements. Once field capacity is reached, a larger settlement occurs, which may indicate that the clay had fully contracted by this point. It should be noted that this explanation is based solely on experience working with the material and assumptions drawn about the behavior of the material. Confirming this hypothesis would require further research to confirm.

Despite some differences in behavior, the 15 percent fouled settlement curves are overall very similar regardless of the ballast type or fouling material. However, the 30 percent fouled tests show different behaviors from one another. The granite ballast settlement in the undersaturated phases is not much larger than the same material with 15 percent fouling. However, once

saturated, settlements occur at much higher rates, which continues with higher loading. The naturally abraded ballast test with 30 percent natural fouling settles more than twice as much as the granite in the dry phase. Settlements are again higher, but more moderate, in the 1/3 and 2/3 field capacity phases. In the field capacity phase, settlement of the natural ballast is more than six times larger than the granite. During the saturated phase, somewhere between 2.8 and 4.4 MGT of loading, the natural ballast experiences a basal failure made evident by a large settlement as well of a rotation of the tie, which is in [Figure 12](#). Together, this evidence indicates a complete loss of support below the tie.



Figure 12 – Tie rotation after failure in the 30 percent fouled box test with abraded ballast and natural fouling

The 30 percent fouled test with the Prestige clay fouling mixture has initial settlements lower than the granite ballast in the early phases, similar to the 15 percent fouled tests. The amount of settlement increases moderately at 2/3 field capacity, but there is a drastic increase upon reaching field capacity. Like the abraded ballast with natural fouling, the overall settlement in this phase is six times higher than the granite. However, it can be seen that the settlement with the Prestige mix fouling begins to level off. This settlement rate continues into the saturated phase. This test undergoes a lateral failure similar to the 15 percent fouled test with the Prestige fouling mixture, but it does not occur until much later in the test when the 105-ton (934 kN) equivalent axle load is reached.

The results between the 15 and 30 percent tests can also be compared directly for a better understanding of the effects of fouling. Figure 13 provides the cumulative plastic settlements from all the 15 and 30 percent fouled box tests. Appendix B provides additional plots that compare settlement rates at different water contents and fouling conditions. The angular granite ballast exhibits similar settlement rates in the undersaturated phases of the test. Once saturation is reached, increased fouling increases the settlement rates by more than double.

The abraded ballast sees immediate negative effects from the addition of natural fouling. The settlement in the dry phase for this material more than doubles when fouling is increased from 15 to 30 percent. In the field capacity phase, the settlement is more than 5 times greater with this increase in fouling. Increased settlement rates persist throughout the 30% fouled test until failure is reached in the saturated phase.

The abraded ballast with Prestige mix fouling has lower settlement rates in the dry and 1/3 field capacity phases when the fouling is increased from 15 to 30 percent. During the 2/3 field capacity and field capacity phases, the settlement rate is much higher for the 30 percent test. However, the settlement rate slows in the field capacity phase, and this rate continues through the saturated phases. The rate of settlement is only slightly larger than the comparable 15 percent test.

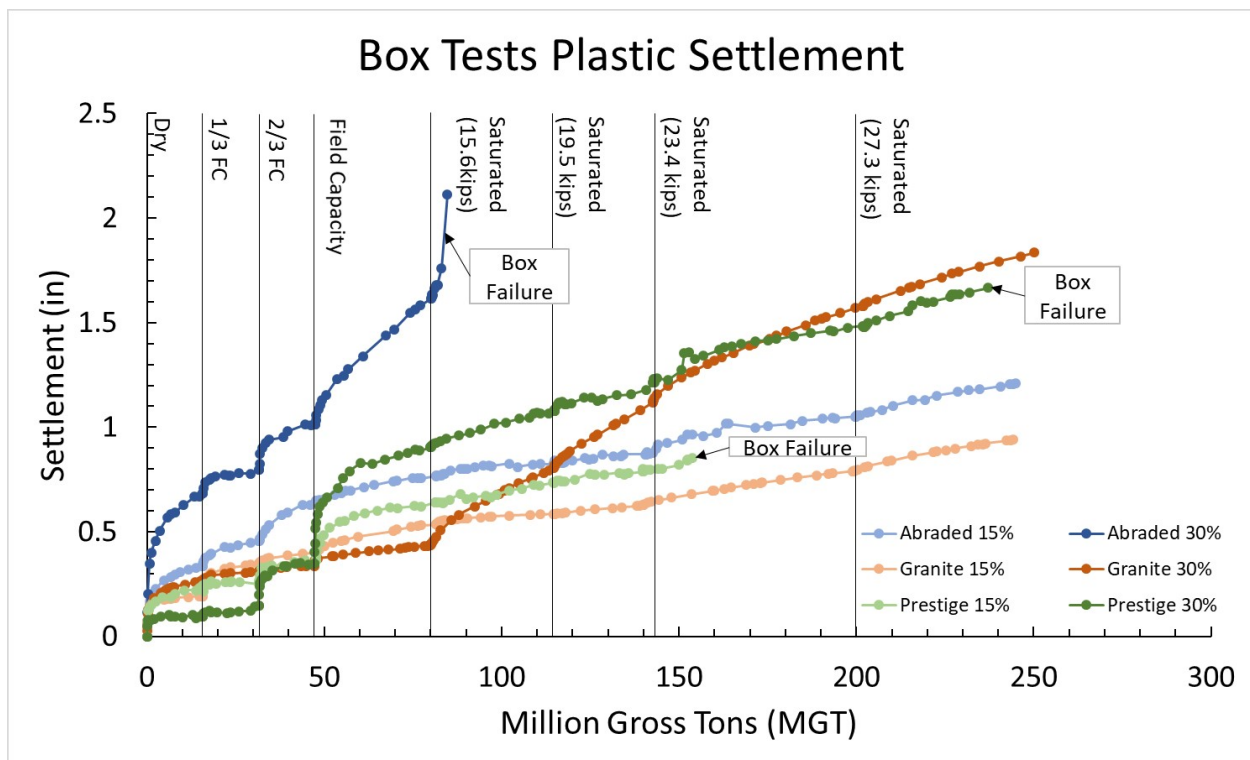


Figure 13 – Cumulative plastic settlement measurements for all 15 and 30 percent fouled box tests

Based on the box results from Phase I and II of testing, the addition of fouling material increased overall settlements for each ballast-fouling combination. At the 15 percent fouled condition, the largely similar behavior between the three tests seems to indicate that the ballast particles still dominate the overall behavior of the specimen. Once fouling is increased to 30 percent, however, the behavior of the three tests varies more, indicating that the different fouling materials are

beginning to have a larger effect on the behavior of each specimen. It is likely that further increases to fouling would result in more variation in the settlement behavior.

3.2.2 Failure Mechanisms in the Box

Two different failure mechanisms occurred during box testing in Phase II of this project. The failure that occurred in the 30 percent fouled test with abraded ballast and natural fouling was fairly easy to identify. During the field capacity phase, the ballast settled steadily and at a high rate of approximately 0.02 in/MGT. Once the saturated phase is reached, a large settlement and tie rotation indicate the failure. This can be readily identified as a basal failure, not dissimilar to a bearing capacity failure of a shallow foundation footing. It should be noted here that such a failure is unlikely to occur in real track. The rotation that occurred in this case would be prevented by the rail being secured to adjacent ties.

The failure mechanism occurring in the 15 and 30 percent fouled tests with the Prestige fouling mixture is more difficult to identify. Observationally, it was noted that the tie was undergoing slow rotations and potentially some lateral sliding, particularly after field capacity and saturation were reached. These movements were evident largely by use of spirit levels applied to the surface of the tie. It is also observed that the center line of the rail and the actuator began to deviate. In both cases, failure occurred once the center lines deviated enough that the actuator rotates around the top of the rail, causing a lateral sliding of the tie. However, the rotation and sliding did not appear to be progressive, and there was no major settlement occurring, so predicting when such a behavior could occur may be difficult based on these results.

These box test failures are not necessarily indicative of failures that would occur in the track. These tests only use a single quarter-length of tie with no fixity. Therefore it is not restrained in any way other than by the surrounding ballast. The restraint provided by the rails in actual track would prevent these failures from happening.

4. Conclusion

This report outlines the testing procedures used to perform the triaxial tests and box tests for Phase II of this project at the University of Massachusetts, Amherst. The results of both Phase I and Phase II are presented and compared. Phase I tested freshly quarried Connecticut granite ballast with granitic stone dust fouling. Phase IIa tested abraded ballast sourced from in-service railway track and the natural fouling material found in that track. Phase IIb used the same ballast, but the fouling was mixed with Prestige clay in order to achieve a fouling material with plastic behavior. These three ballast and fouling combinations were tested under the same conditions so that direct comparisons could be drawn between the results.

The triaxial tests showed that the Connecticut granite and abraded ballast achieved similar strengths and friction angles to one another in all fouling and water content conditions. It was initially expected that the abraded ballast strength would be lower due to lack of angularity, but these results may be an effect of the two ballasts having differing parent rock. The abraded ballast with the Prestige mixture fouling had lower strengths and friction angles than the abraded ballast with natural fouling alone. While the two ballasts had similar strength properties, the volumetric strain curves showed that the abraded ballast was more susceptible to deformations, with higher initial contractions occurring in most testing cases. This supports the earlier work by Indraratna et al., which showed increased initial contractions and loss of strength with a purely clay fouling material [9]. The tests performed in this study show that a fouling material does not need to be purely clay to impose these negative effects on ballast performance. These results suggest that a mixed fouling with enough clay to cause plastic behavior will further increase deformations in ballast.

The box test results help support some of the findings in the triaxial tests. The tests with abraded ballast often saw higher initial settlements during each phase, similar to the higher initial contractions in the triaxial tests. The elastic settlement in the abraded ballast tests were about 0.07 inches (1.8 mm), while the granite elastic settlement was 0.02 inches (0.5 mm). The larger elastic settlement of the abraded ballast, indicating a lower modulus. For each ballast and fouling combination, increased fouling led to increased settlement, as might be expected. The abraded ballast with 30 percent natural fouling resulted in the first known basal failure of ballast in a box test setting in the laboratory. A large settlement and tie rotation indicated loss of support below the tie. This box failure, and the overall higher settlements of the abraded ballast with natural fouling suggest that the highly angular ballast is more capable of accommodating fouling and maintaining track support. The two box tests with abraded ballast and Prestige mixture fouling both experienced lateral box failures. During these tests, gradual sliding and rotations of the tie were observed, indicating a different response to loading that will likely require additional testing to better understand. While box failures may indicate problematic soils, they do not equate to failures in actual track, since restraint from rails is not present in the test environment.

The box tests also showed that at 15 percent fouling, the settlement behaviors of the three tests were similar, while at 30 percent fouling, the settlement behaviors of the ballast begin to vary. This seems to indicate that at 30 percent fouling, the fouling itself begins to have a larger influence on the behavior of the ballast.

The testing completed in Phase I and Phase II of this project show that while ballast that has become abraded from use may still be serviceable in track, its higher susceptibility to deformations can be problematic, particularly at higher fouling contents. This testing also

showed that fouling containing plastic fines has the potential to further increase deformations as well as change behavior and failure modes of ballast. These results highlight the importance of considering not only fouling quantity, but also the fouling type and ballast condition, when assessing the suitability of the railway substructure.

5. References

1. American Society for Testing and Materials. Annual Book of Standards. Philadelphia, PA.
2. Aursudkij, B., McDowell, G. R., and Collop A. C. Cyclic loading of railway ballast under triaxial conditions and in a railway test facility. *Granular Matter*, 2009, 11(6):391–401.
3. Chang, C. S., Adegoke, C. W., and Selig, E. T. Geotrack Model for Railroad Track Performance. *Journal of Geotechnical and Environmental Engineering*, 1980, 106(11), 1201–1218.
4. Duong, T., Tang, A. M., Cui, Y. -J., Trinh, V. N., Dupla, J. -C., Callon, N., Canou, J., and Robinet, A. Effects of fines and water contents on the mechanical behavior of interlayer soil in ancient railway sub-structure. *Soils and Foundations*, 2013, 53(6):868–78.
5. Feldman, F., and Nissen D. Alternative testing method for the measurement of ballast fouling: Percentage void contamination. Conference on Railway Engineering. Wollongong, Australia, 10–13, November 2002. Railway Technical Society of Australia, Canberra, Australia, 101–109.
6. Han, X. and Selig, E. Investigation of the effects of fouling material and degree of fouling on the settlement of ballast bed by ballast box. Report AAR95-426R for Association of American Railroads. University of Massachusetts, Amherst, 1996.
7. Indraratna, B., Ionescu, D., and Christie, H. D. Shear Behavior of Railway Ballast Based on Large-Scale Triaxial Tests. *Journal of Geotechnical and Geoenvironmental Engineering*, 1998, 124(5):439–49.
8. Indraratna, B., Kabbaz, H., Salim, W., and Christie, D. Geotechnical properties of ballast and the role of geosynthetics in rail track stabilisation. Proceedings of the Institute of Civil Engineering Ground Improvement, 2006, 10(3):91–101.
9. Indraratna, B., Tennakoon, N., Nimbalkar, S., and Rujikiatkamjorn, C. [Behaviour of clay-fouled ballast under drained triaxial testing](#). *Geotechnique: international journal of soil mechanics*, 2013, 63(5):410–9.
10. Kashani, H. F. “[Evaluating the Influence of Breakdown Fouling and Moisture Content on the Mechanical and Electromagnetic Properties of Ballasted Railroad Track](#).” PhD Dissertation. University of Massachusetts, Amherst, 2016.
11. Knutson, R. M., and Thompson, M. R. Resilient response of railway ballast. *Transportation Research Record*, 1977, 651.
12. Norman, G. M. Ballast box experiments for evaluating ballast field performance. concrete tie correlation study report. Report FRA82-291P. University of Massachusetts, Amherst, 1982.
13. Selig, E., and Boucher, D. [Abrasion Tests for Railroad Ballast](#). *Geotechnical Testing Journal*, 13(4), 1990, 301–311.
14. Selig, E. T., and Waters, J. M. Track Geotechnology and Substructure Management. New York: Thomas Telford Publications, 1994.

15. Suiker, A. S., Selig, E. T., Frenkel, R. Static and Cyclic Triaxial Testing of Ballast and Subballast. *Journal of Geotechnical and Geoenvironmental Engineering*, 2005, 131(6):771–82
16. Trinh, V. N., Tang, A. M., Cui, Y., Dupla, J., Canou, J., Calon, N., Lambert, L., Robinet, A., Schoen, O. Mechanical characterisation of the fouled ballast in ancient railway track substructure by large-scale triaxial tests. *Soils and Foundations – Toyko*, 2012, 52(3):511–23.

Appendix A.

Additional Figures for Triaxial Tests

50% Secant Modulus

The following plots provide the 50 percent strength secant modulus data for all triaxial tests. This data is also presented in [Table 4](#).

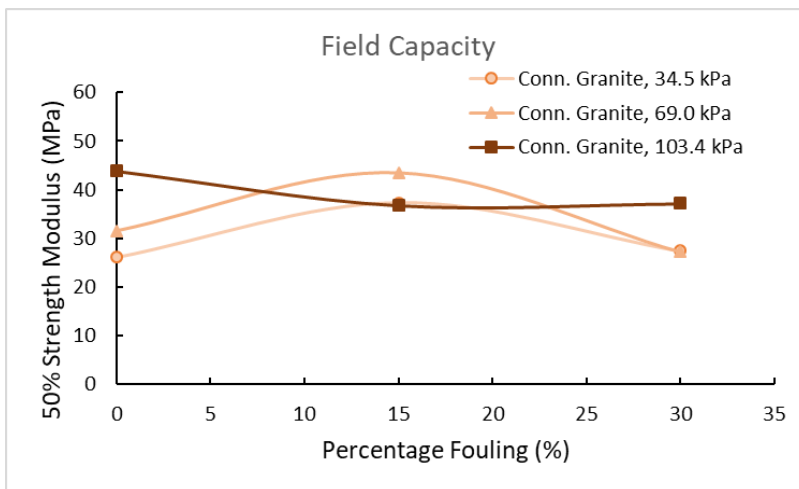
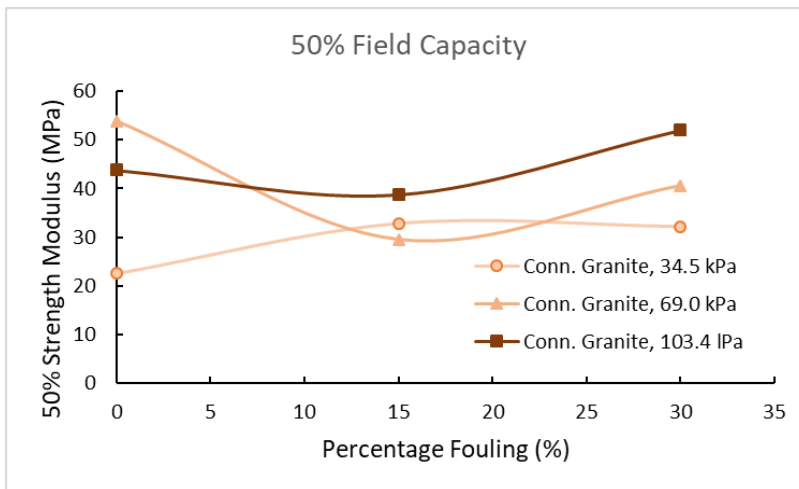
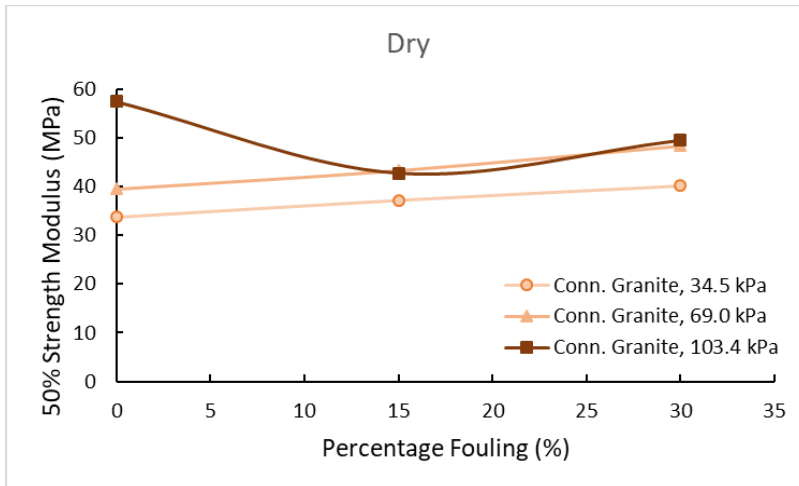


Figure 14 – 50 percent strength secant modulus for Connecticut granite ballast with breakdown fouling

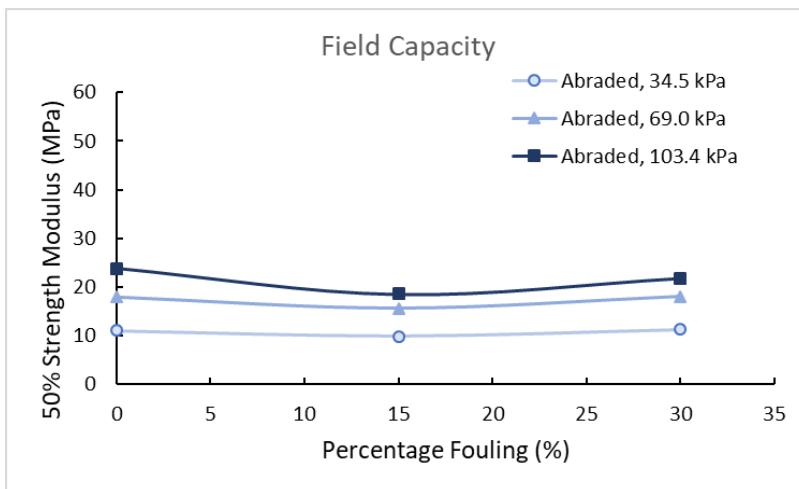
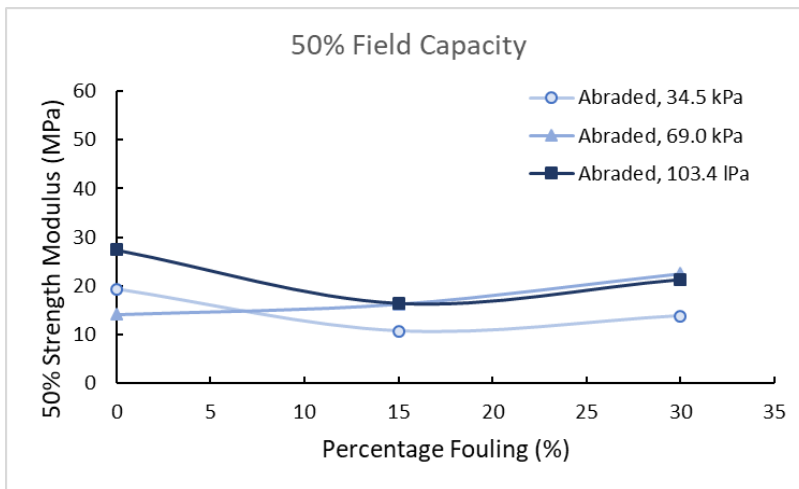
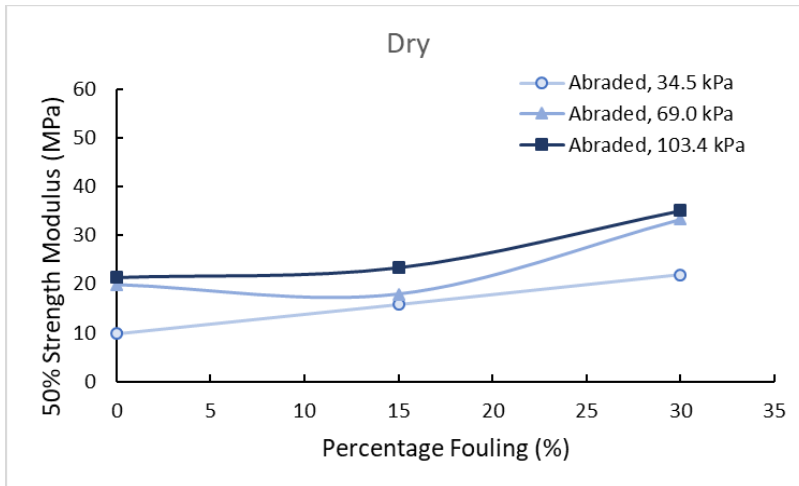


Figure 15 – 50 percent strength secant modulus for abraded ballast with natural fouling

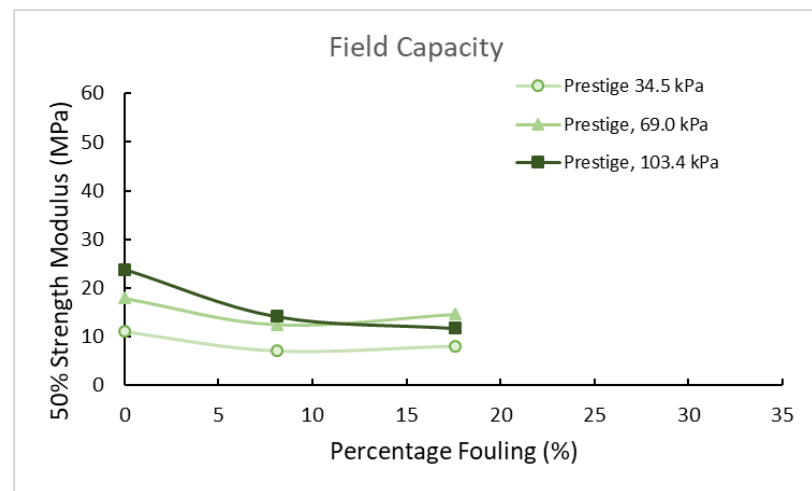
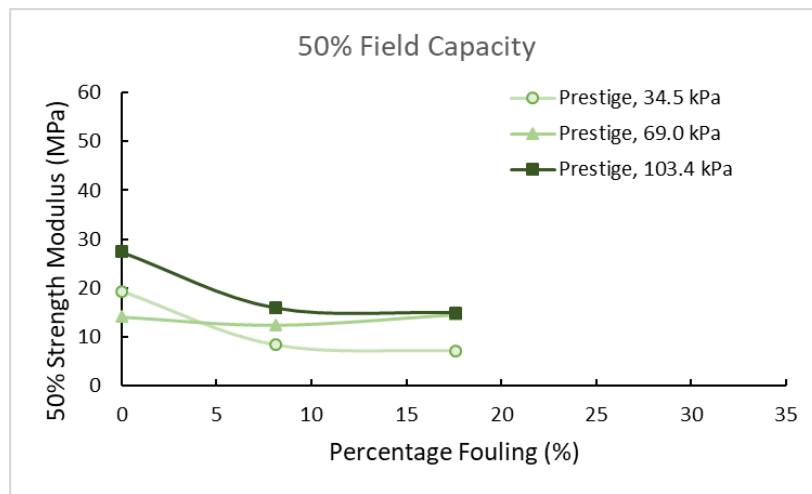
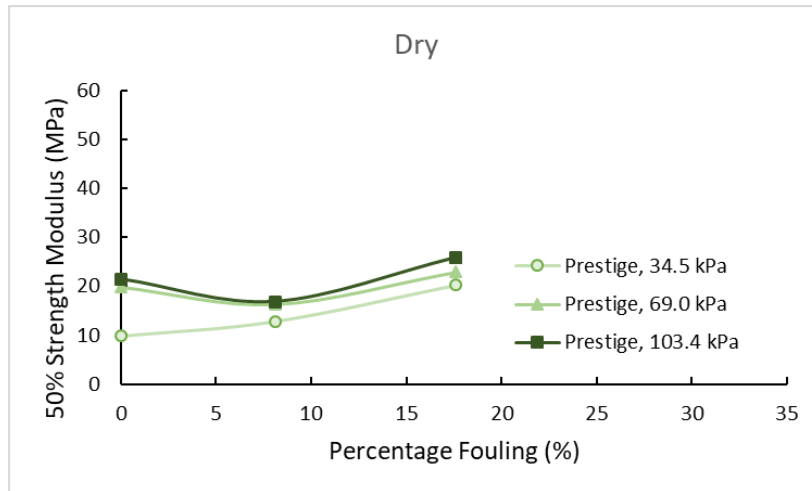


Figure 16 – 50 percent strength secant modulus for abraded ballast with Prestige mix fouling

Stress-strain and Volumetric Strain

Each of the following figures presents a set of triaxial tests performed at a specific water condition, fouling condition, and confining pressure. Each figure is composed of two plots. The first shows stress-strain curves and the second shows volumetric strain curves.

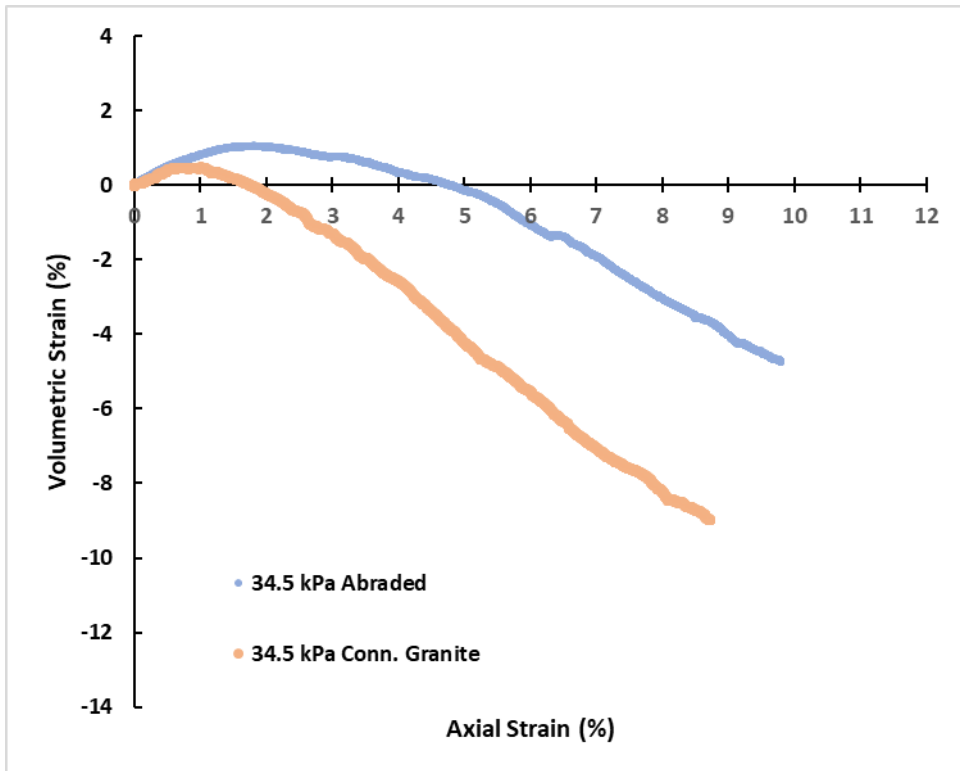
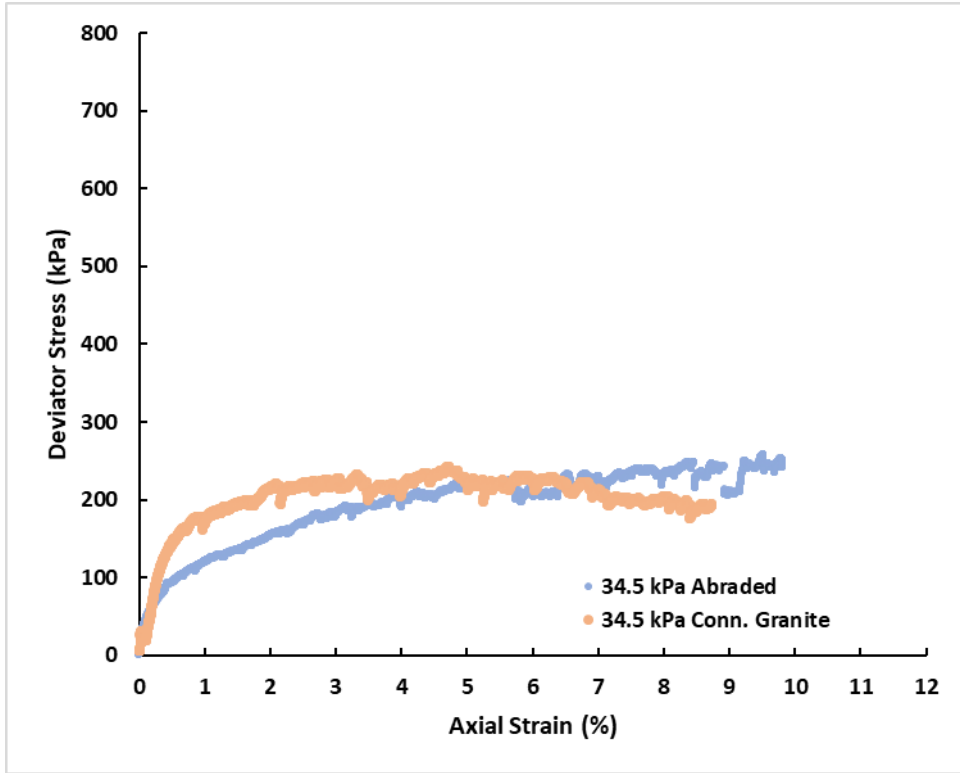


Figure 17 – Clean, dry, 5 psi confining

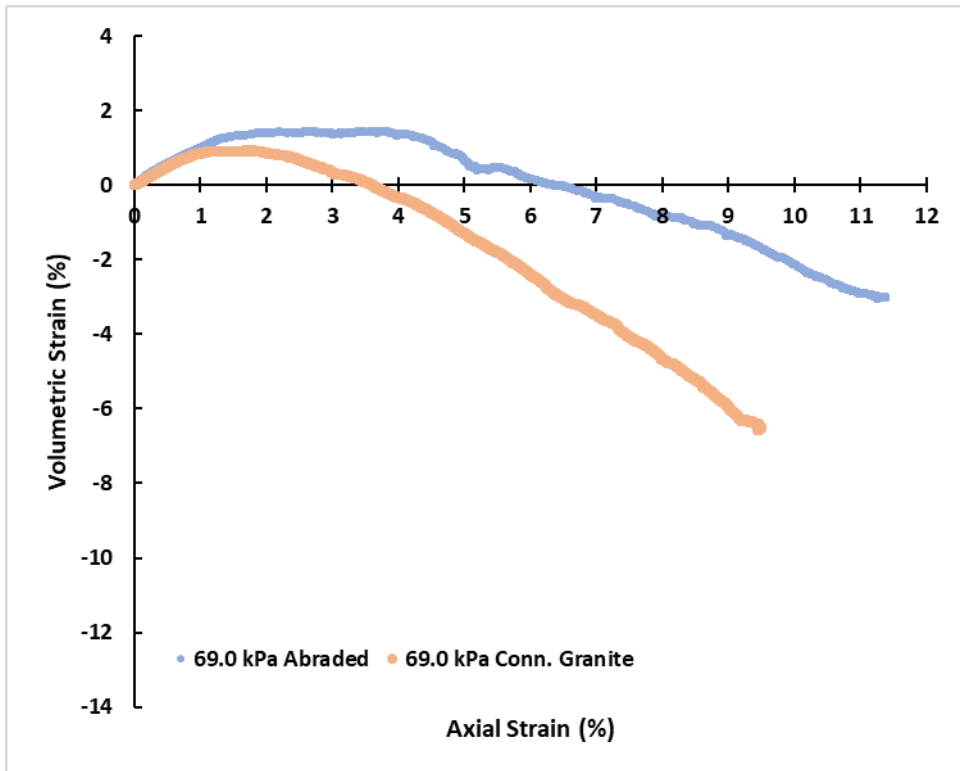
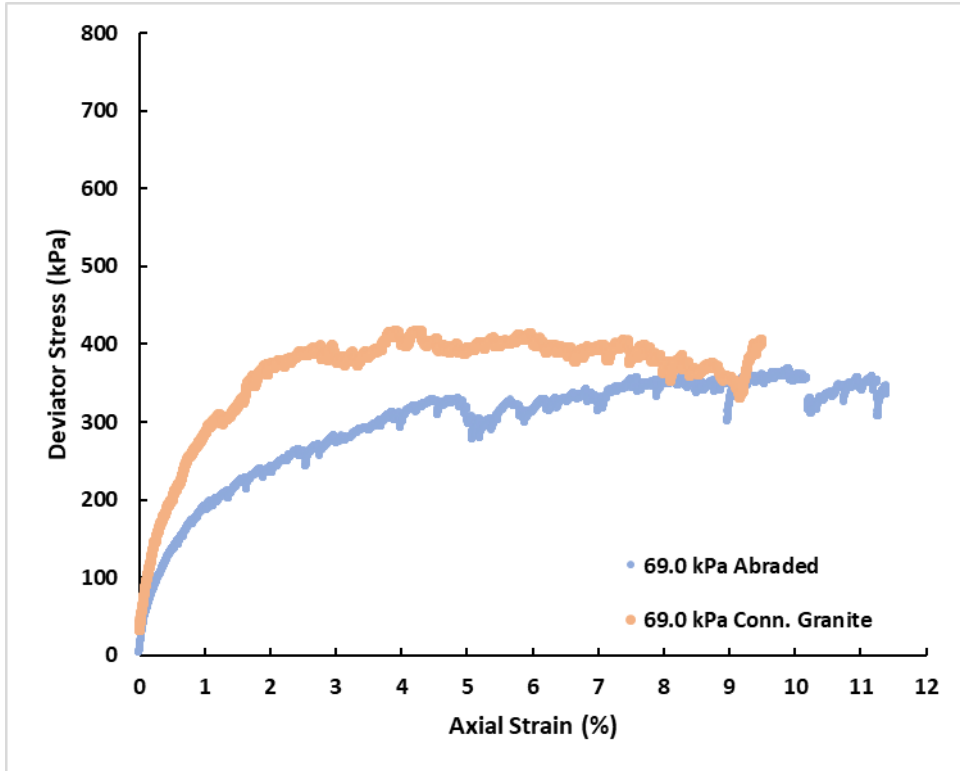


Figure 18 – Clean, dry, 10 psi confining

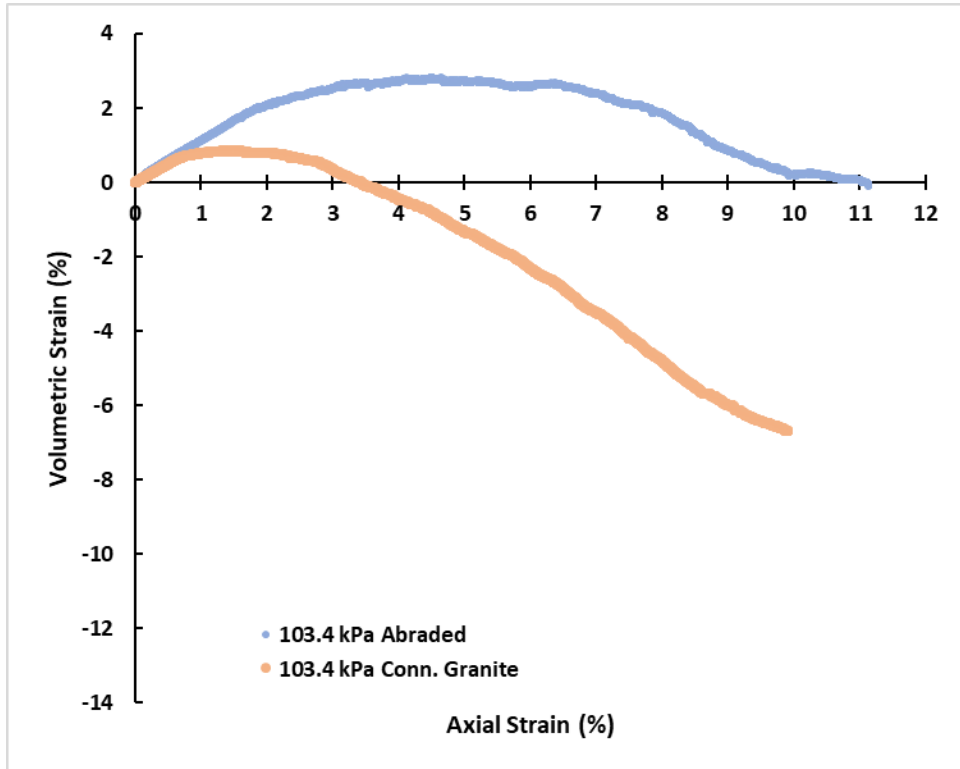
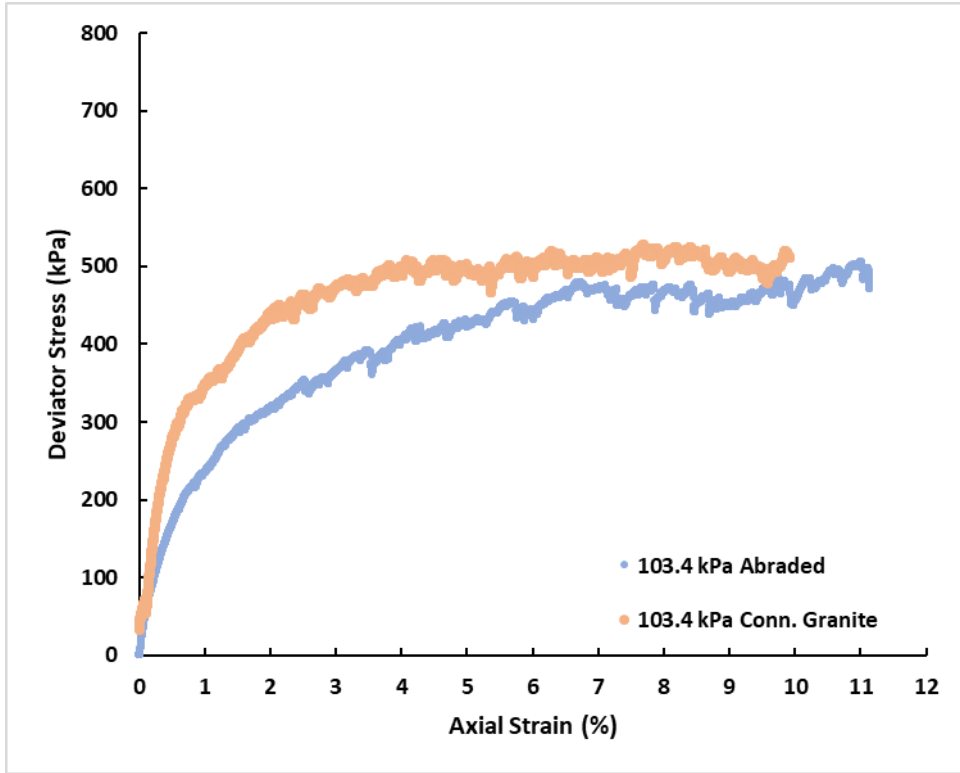


Figure 19 – Clean, dry, 15 psi confining

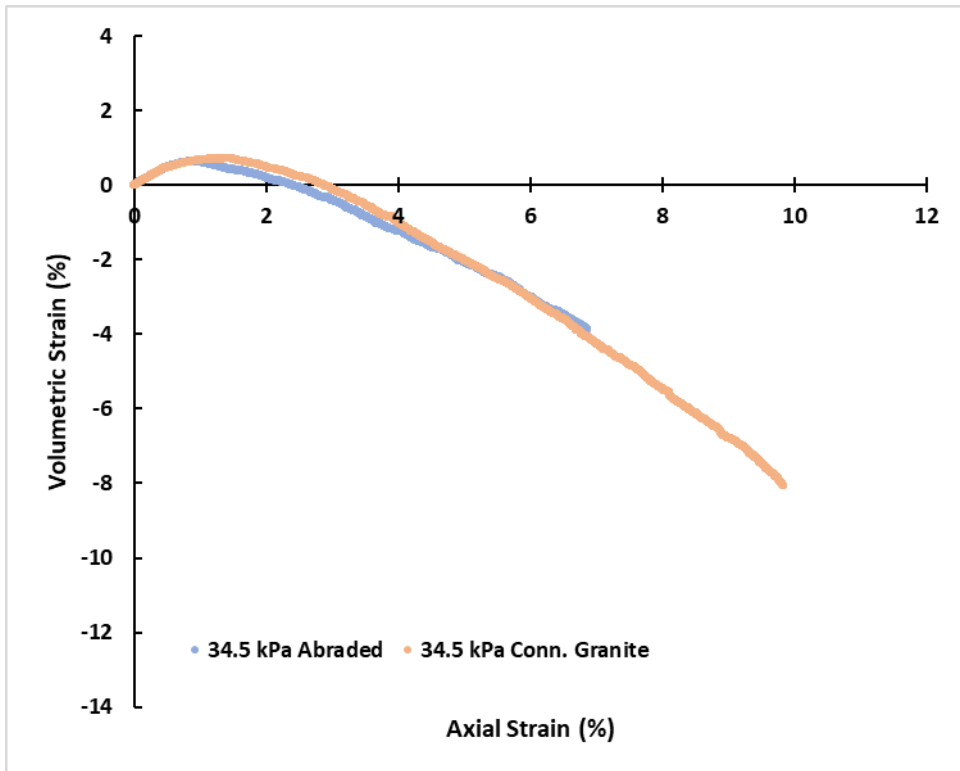
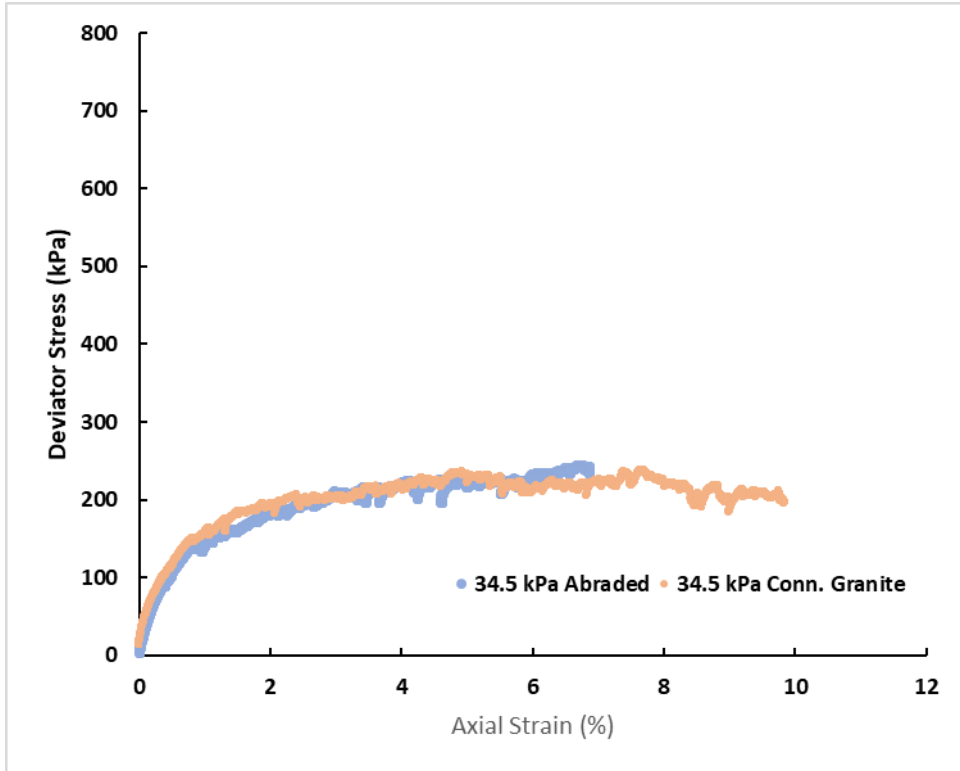


Figure 20 – Clean, 50 percent field capacity, 5 psi confining

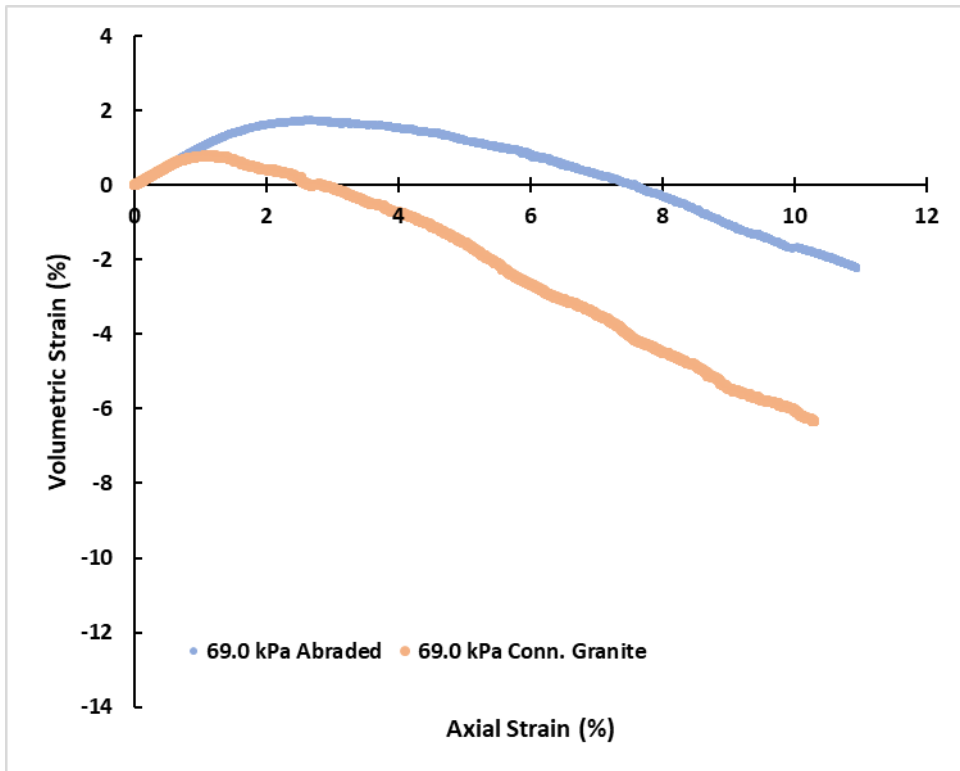
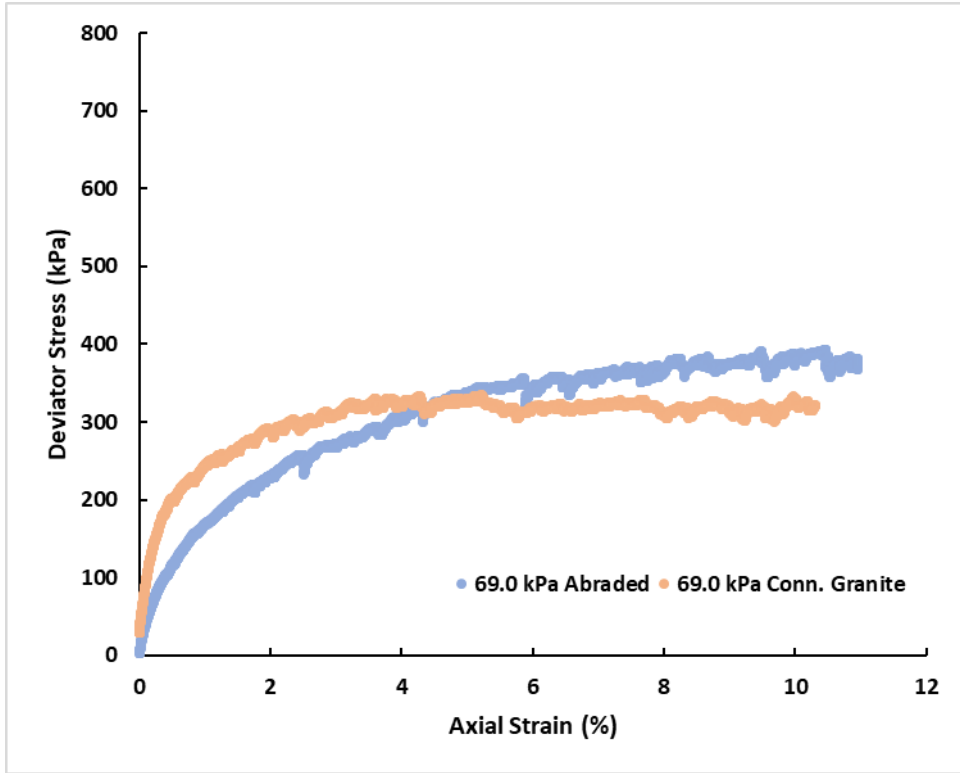


Figure 21 – Clean, 50 percent field capacity, 10 psi confining

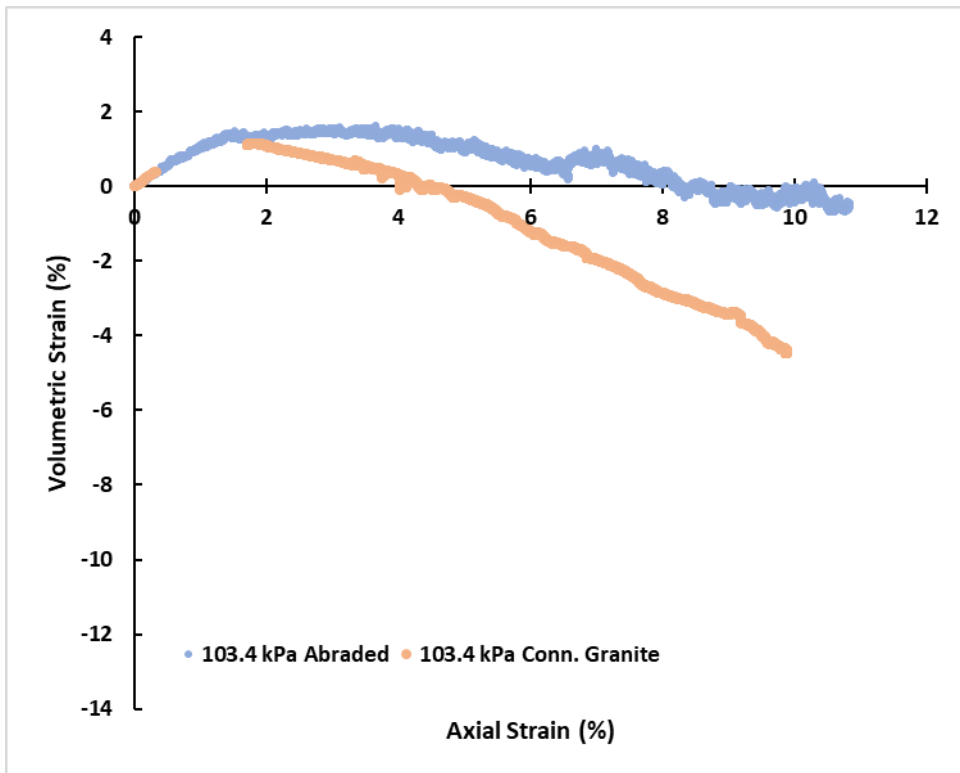
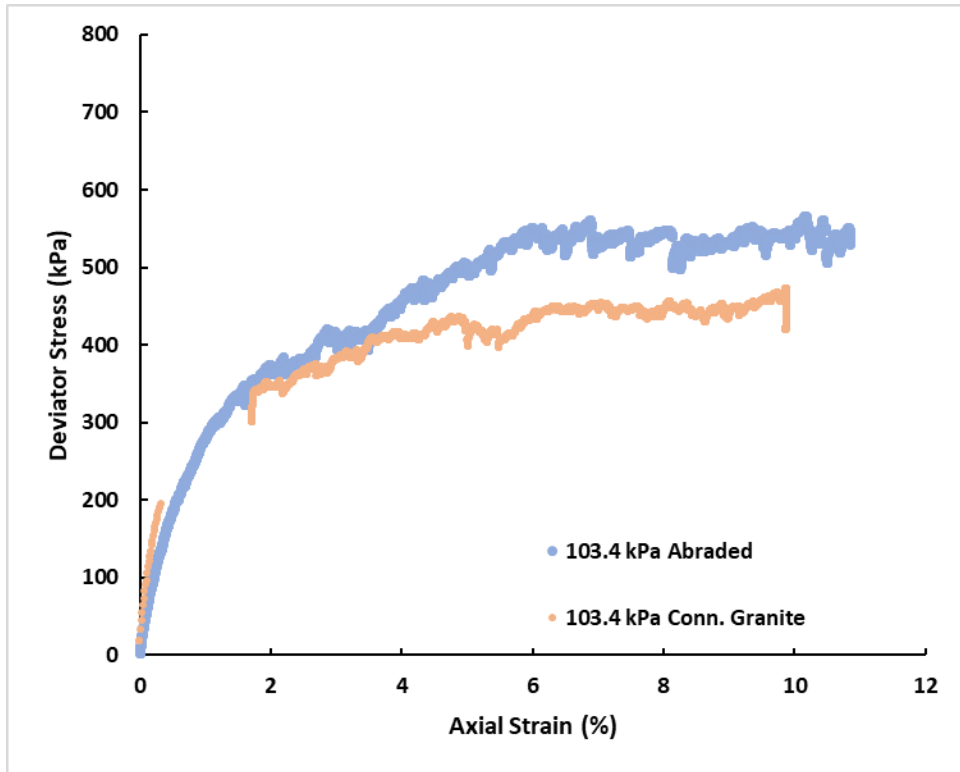


Figure 22 – Clean, 50 percent field capacity, 15 psi confining

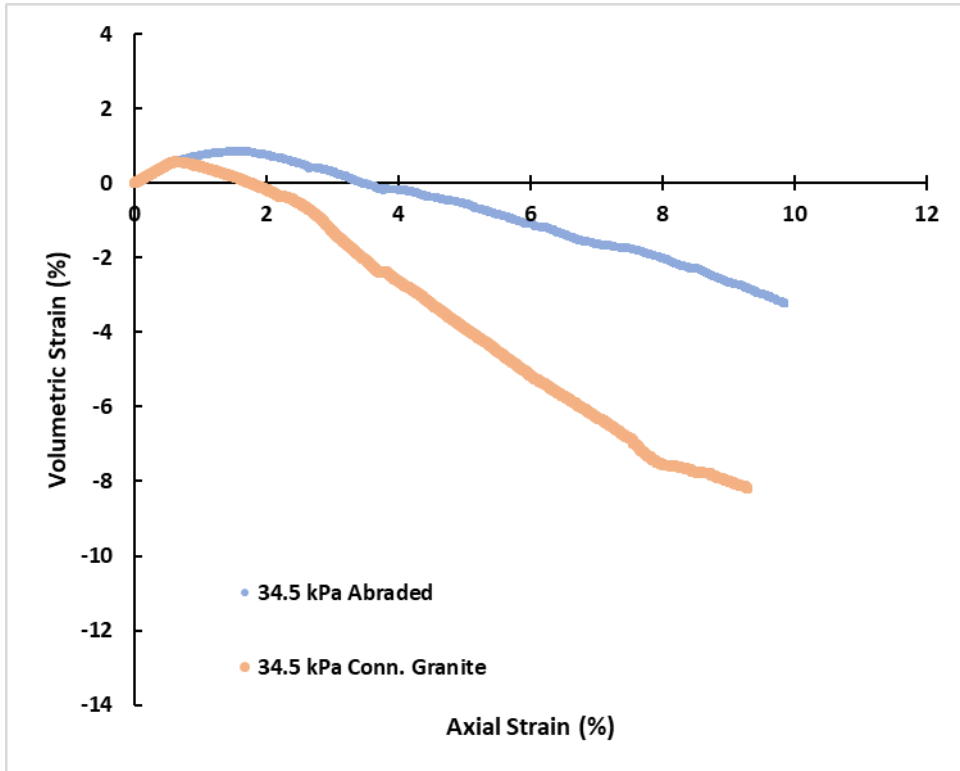
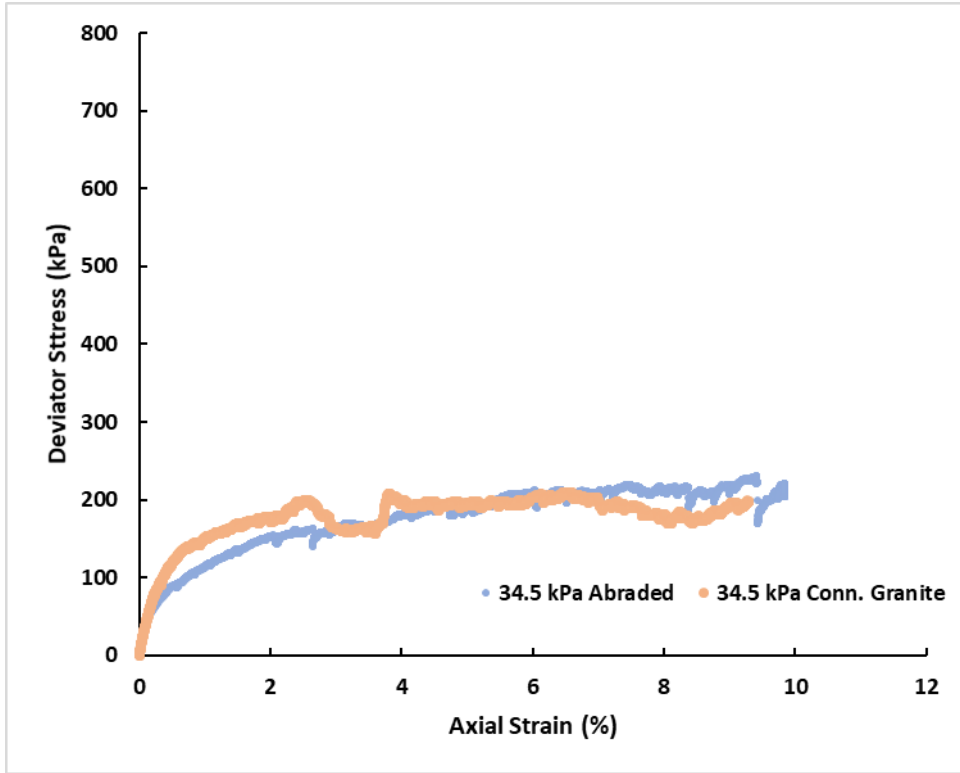


Figure 23 – Clean, field capacity, 5 psi confining

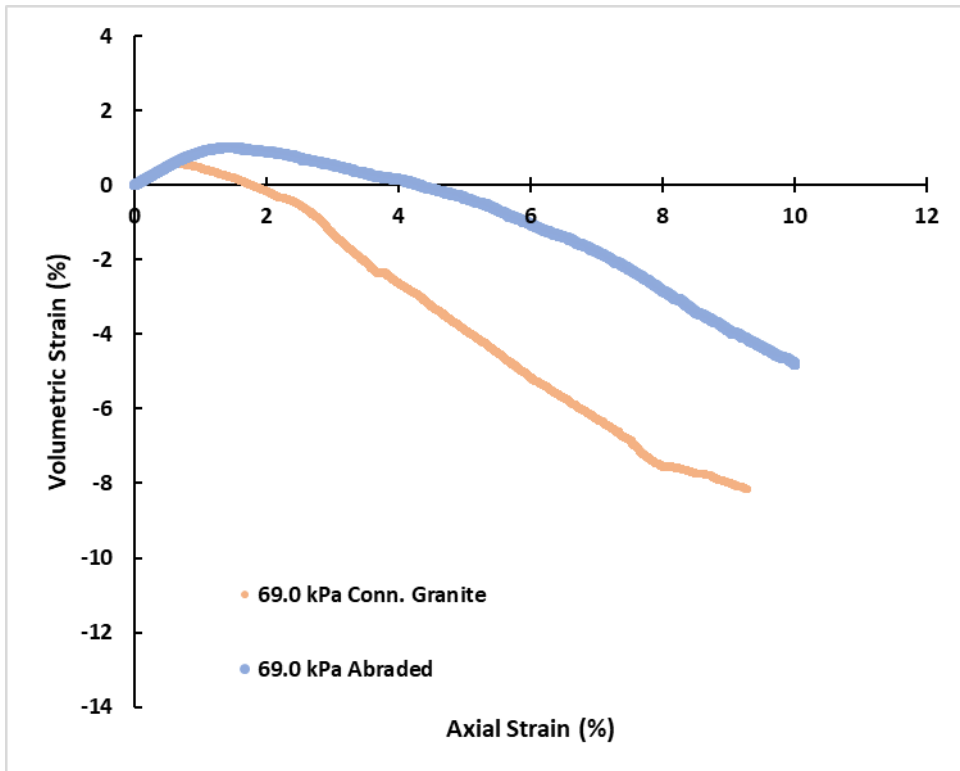
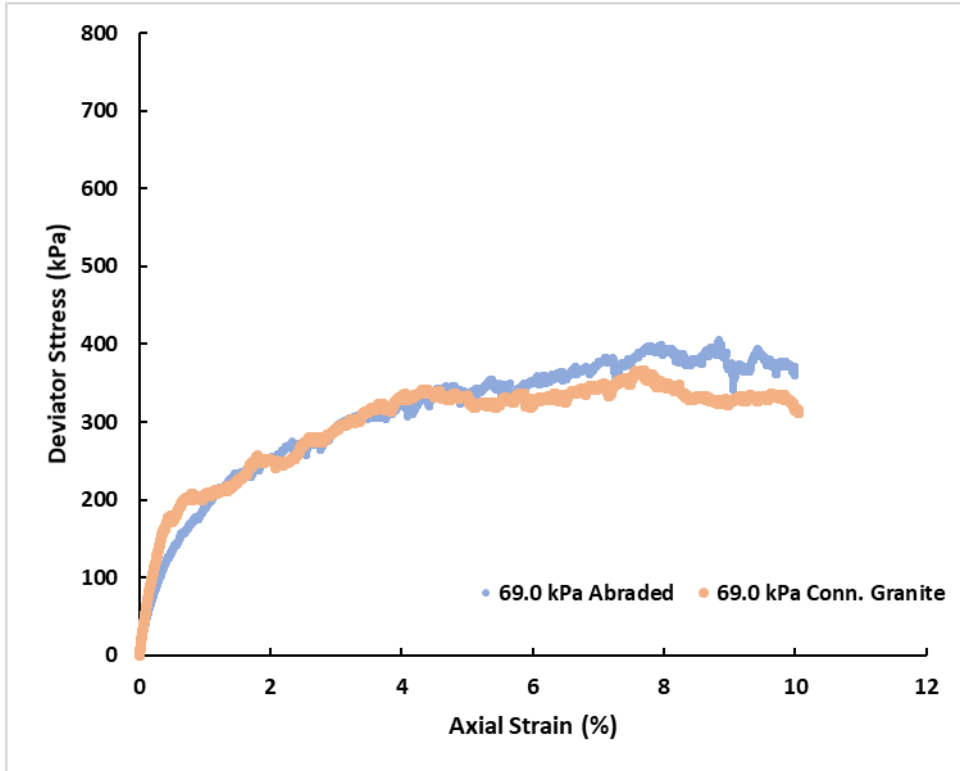


Figure 24 – Clean, field capacity, 10 psi confining

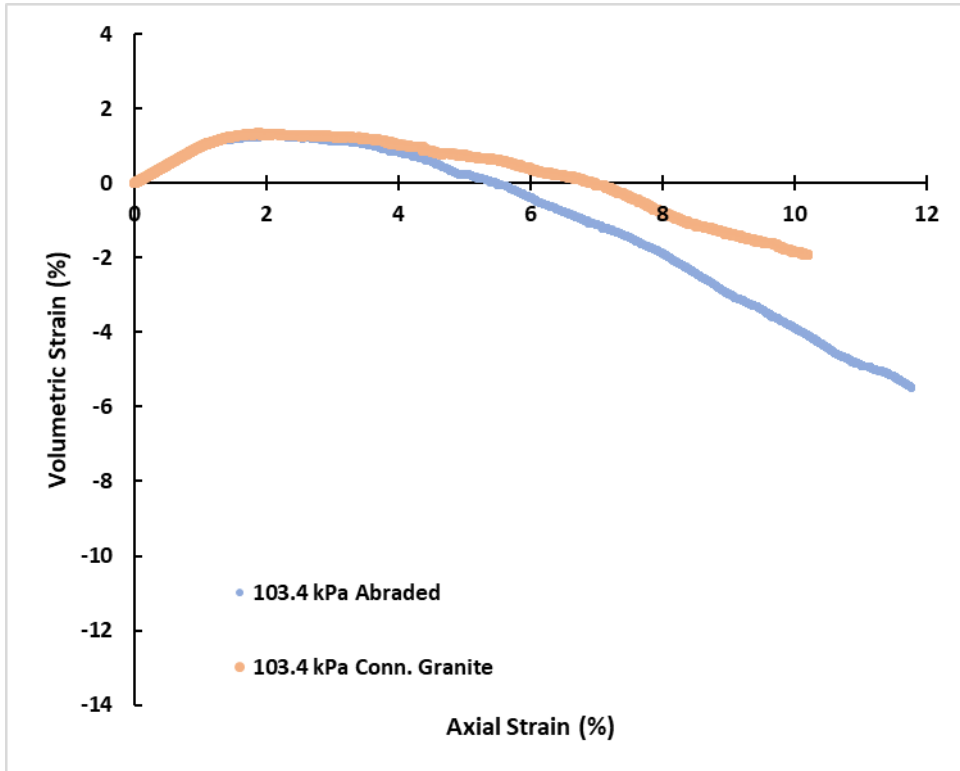
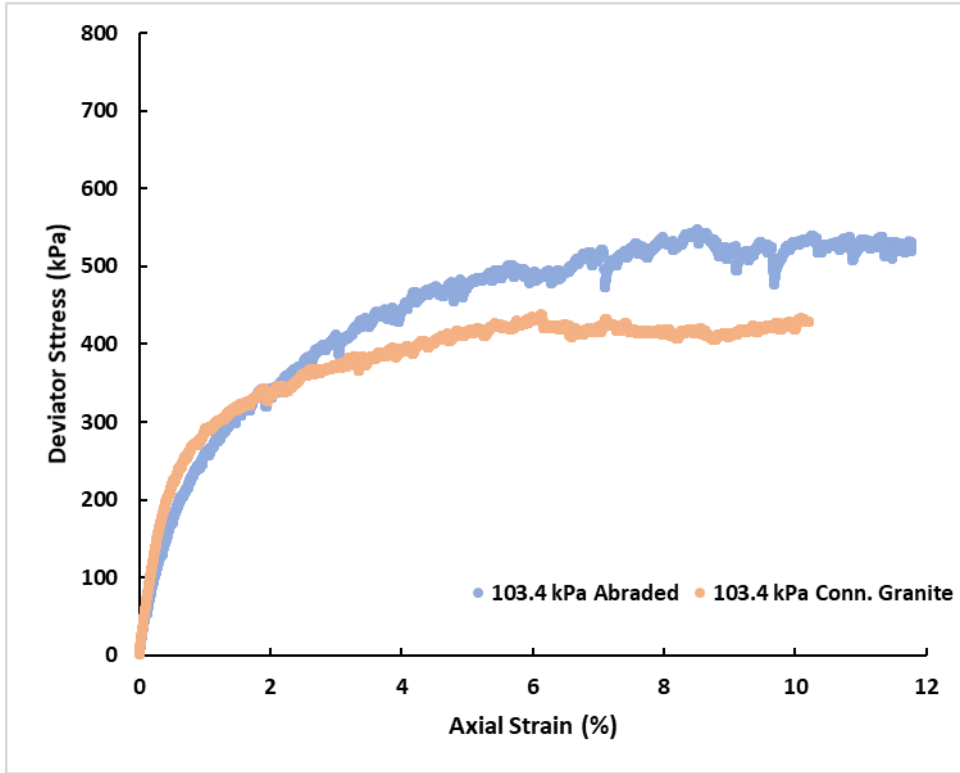


Figure 25 – Clean, field capacity, 15 psi confining

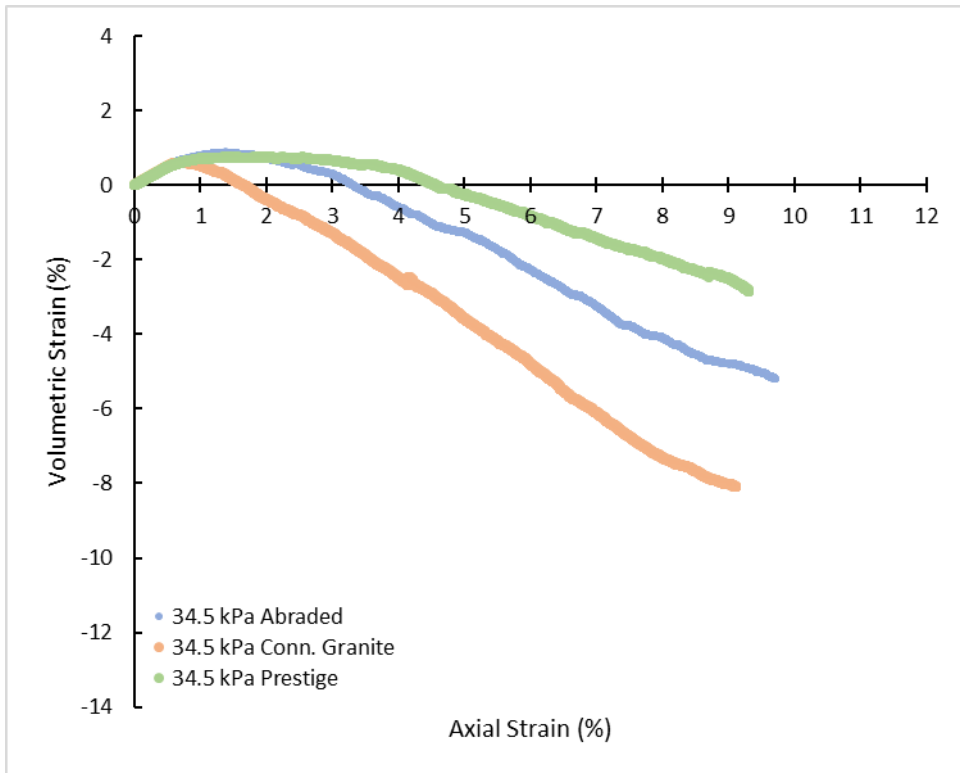
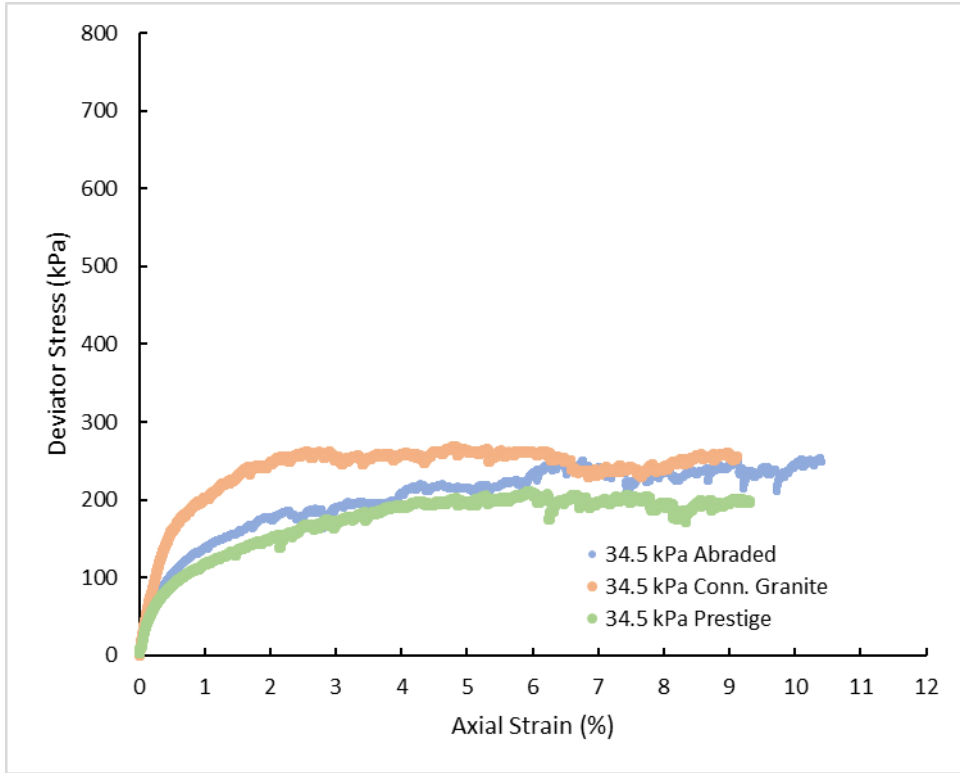


Figure 26 – 15 percent fouled, dry, 5 psi confining

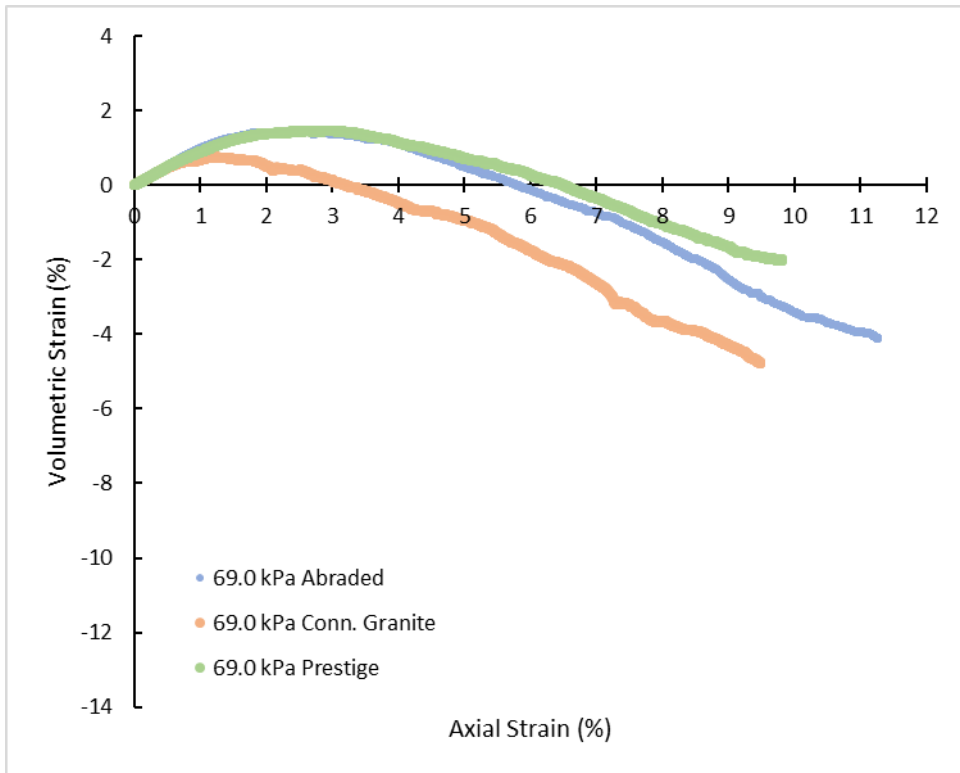
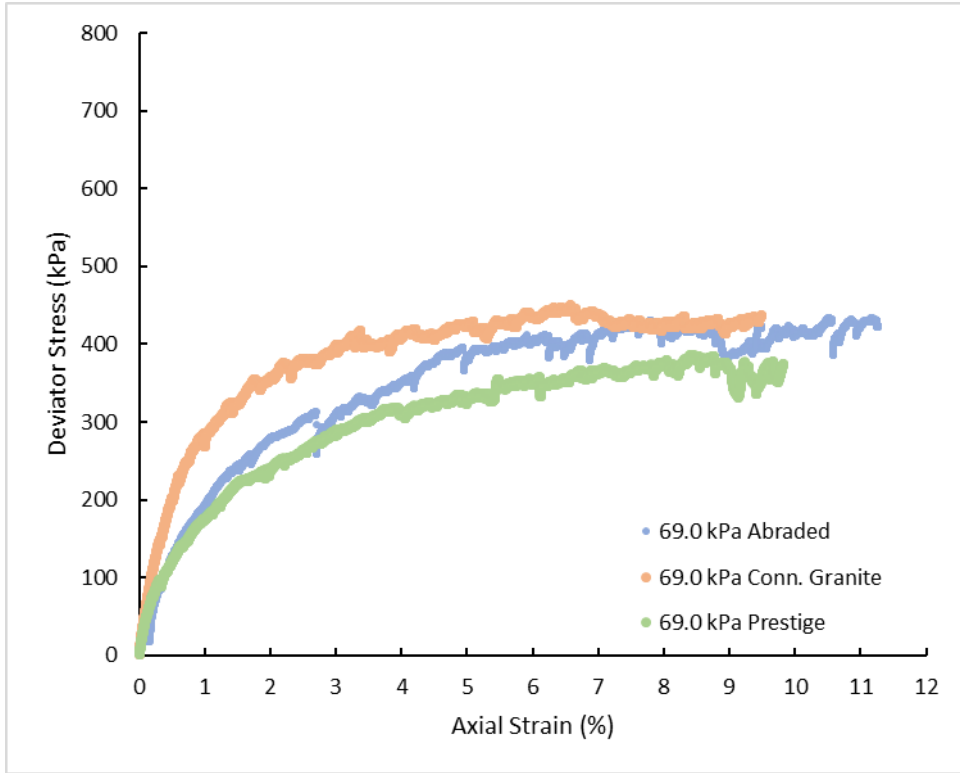


Figure 27 – 15 percent fouled, dry, 10 psi confining

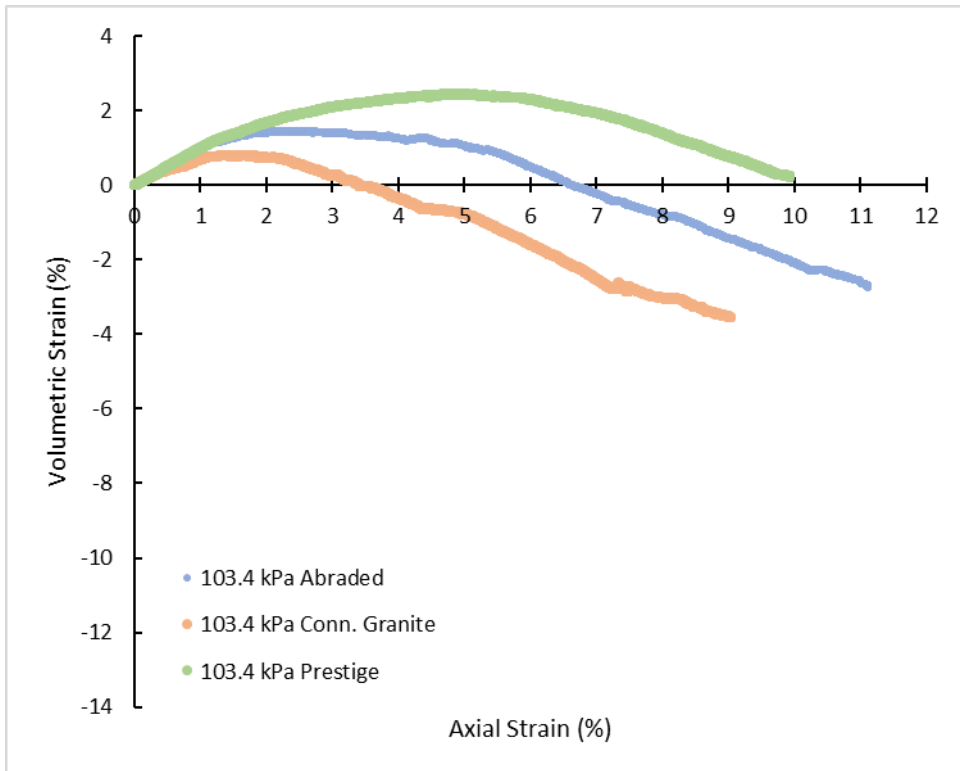
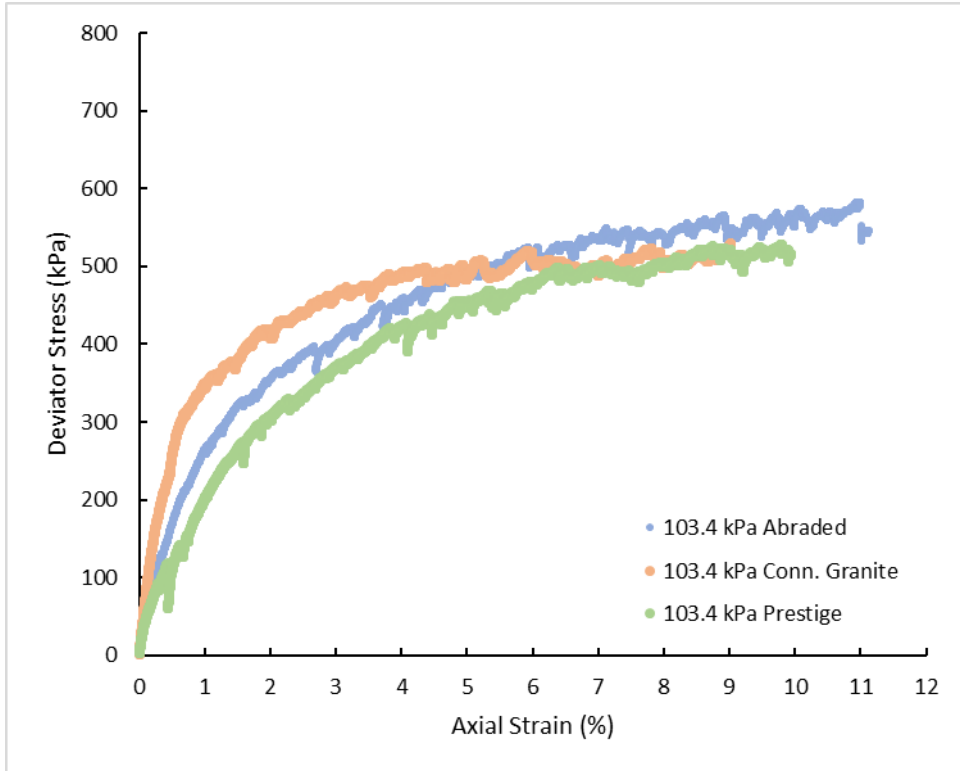


Figure 28 – 15 percent fouled, dry, 15 psi confining

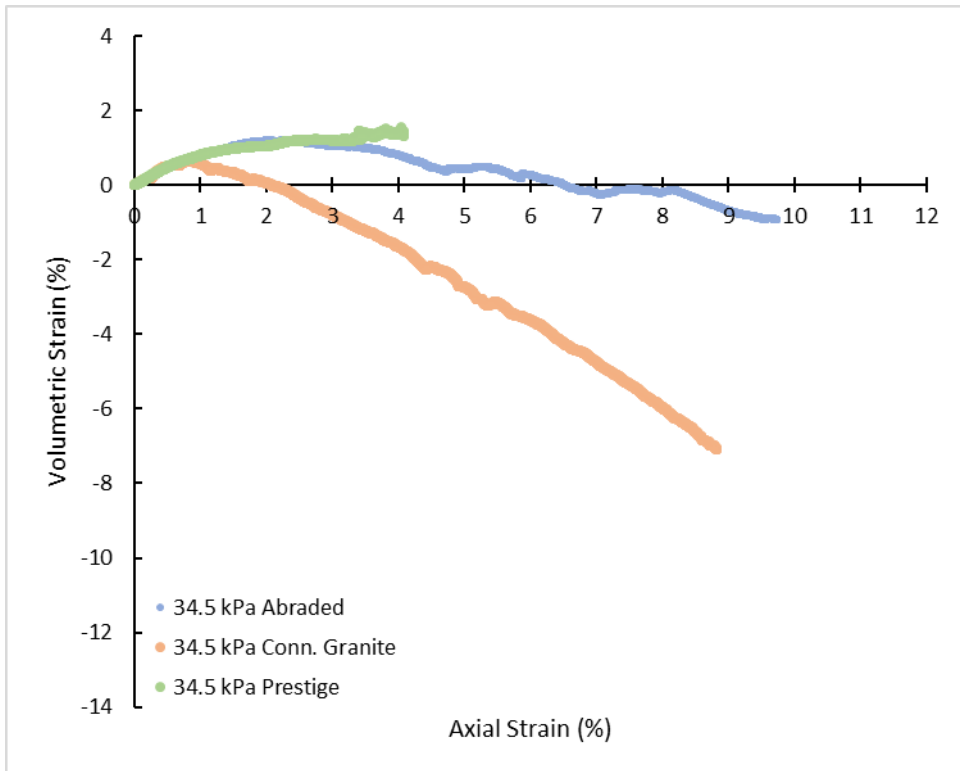
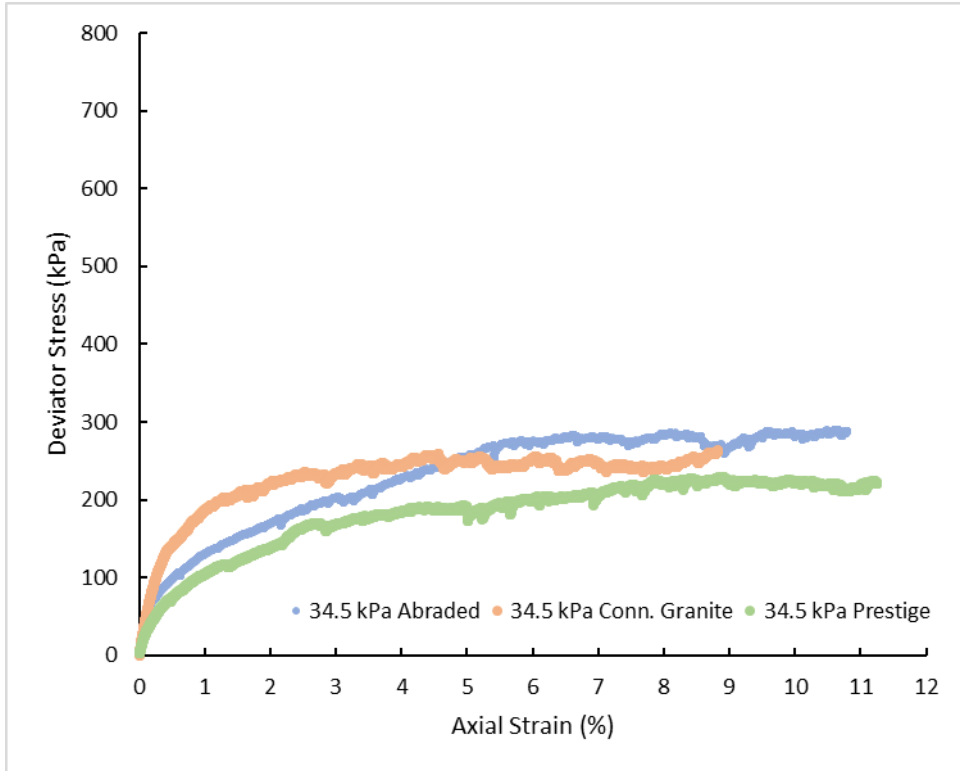


Figure 29 - 15 percent fouled, 50 percent field capacity, 5 psi confining

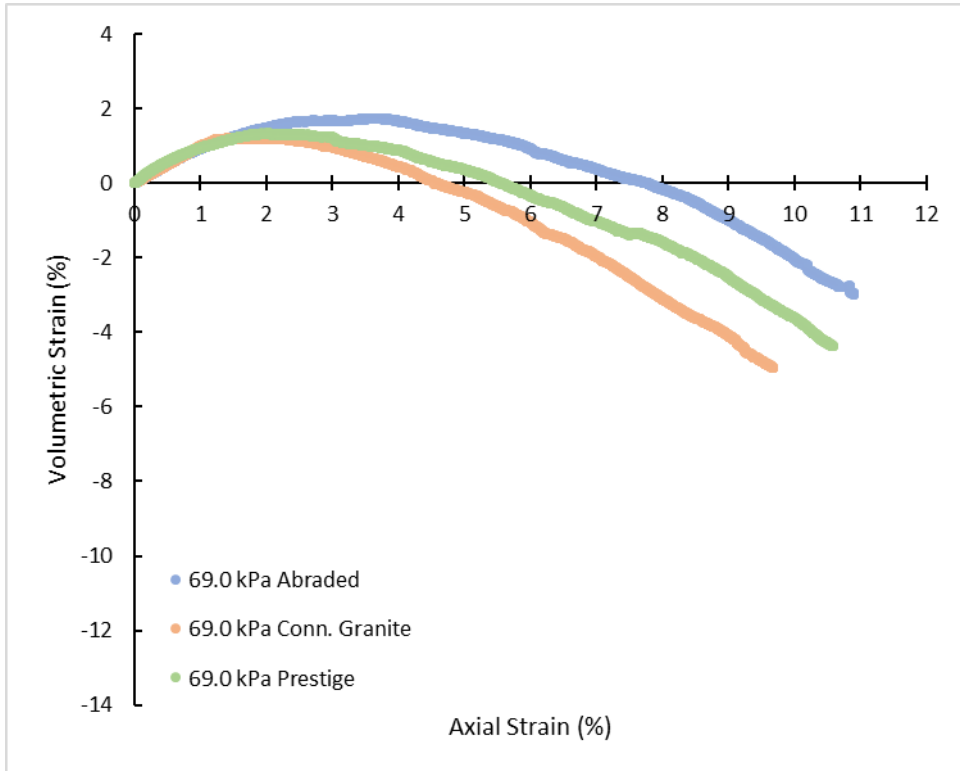
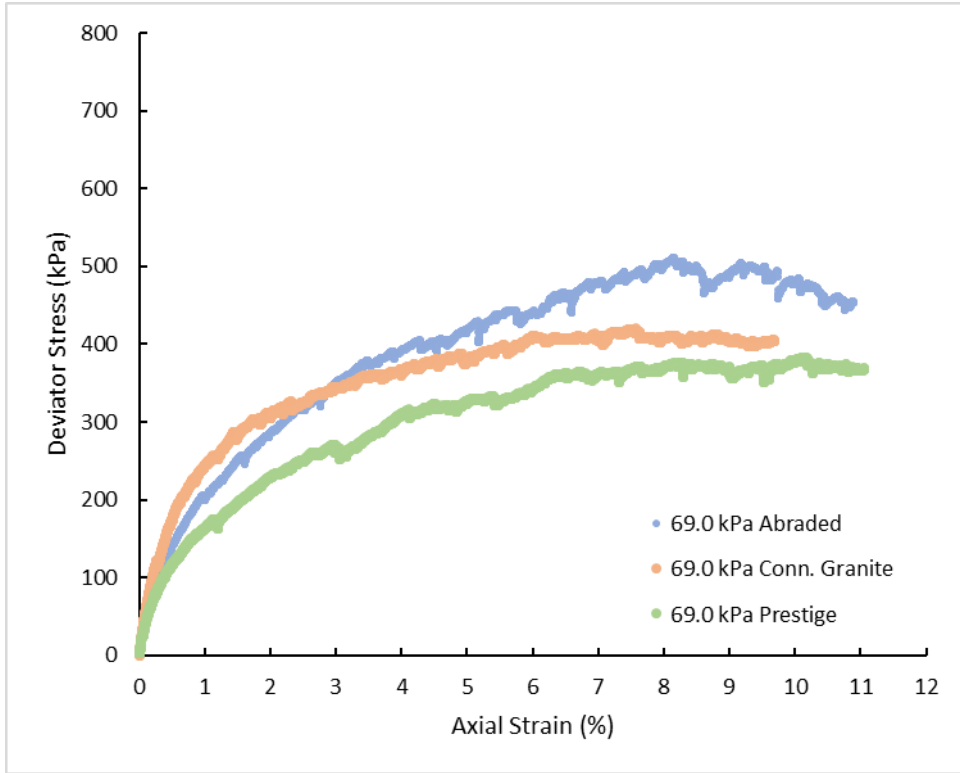


Figure 30 – 15 percent fouled, 50 percent field capacity, 10 psi confining

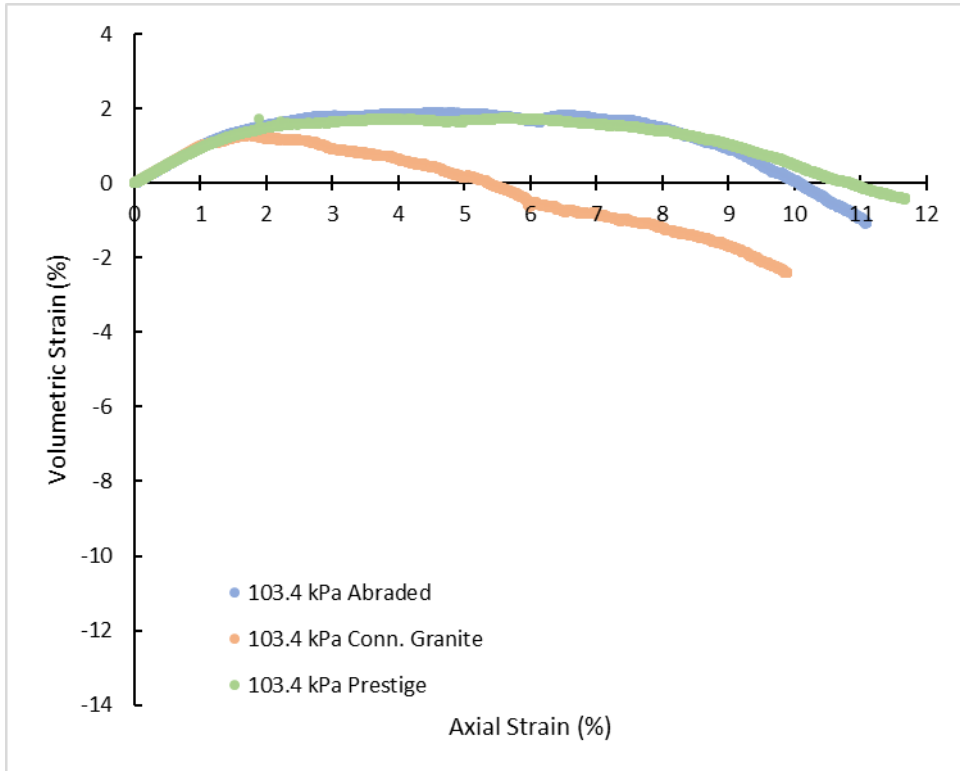
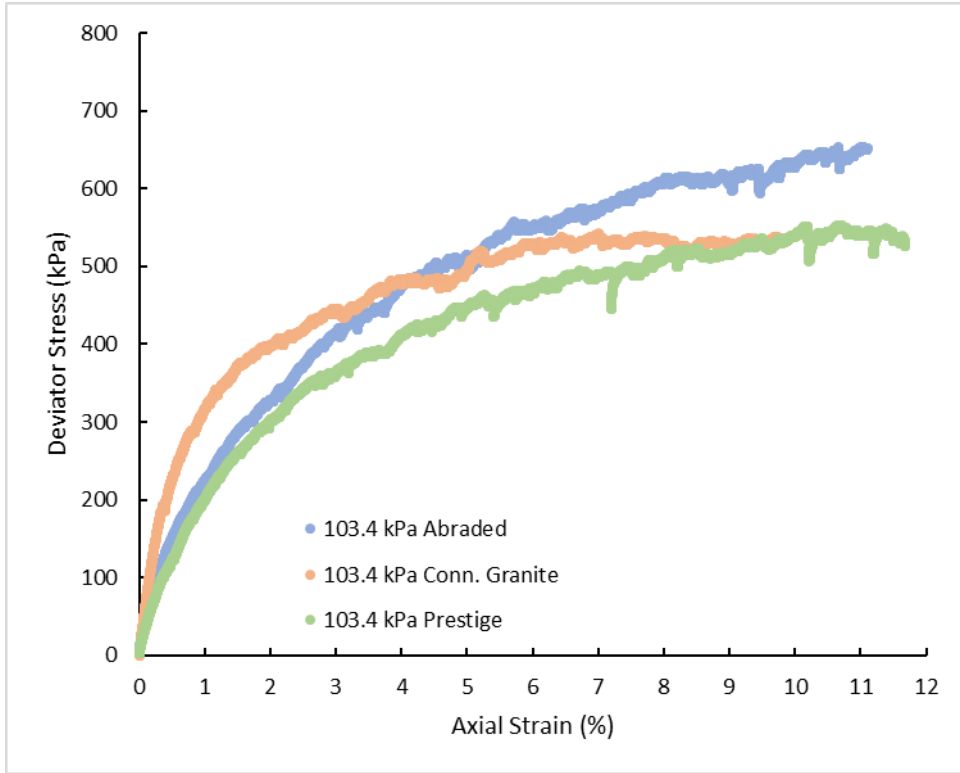


Figure 31 – 15 percent fouled, 50 percent field capacity, 15 psi confining

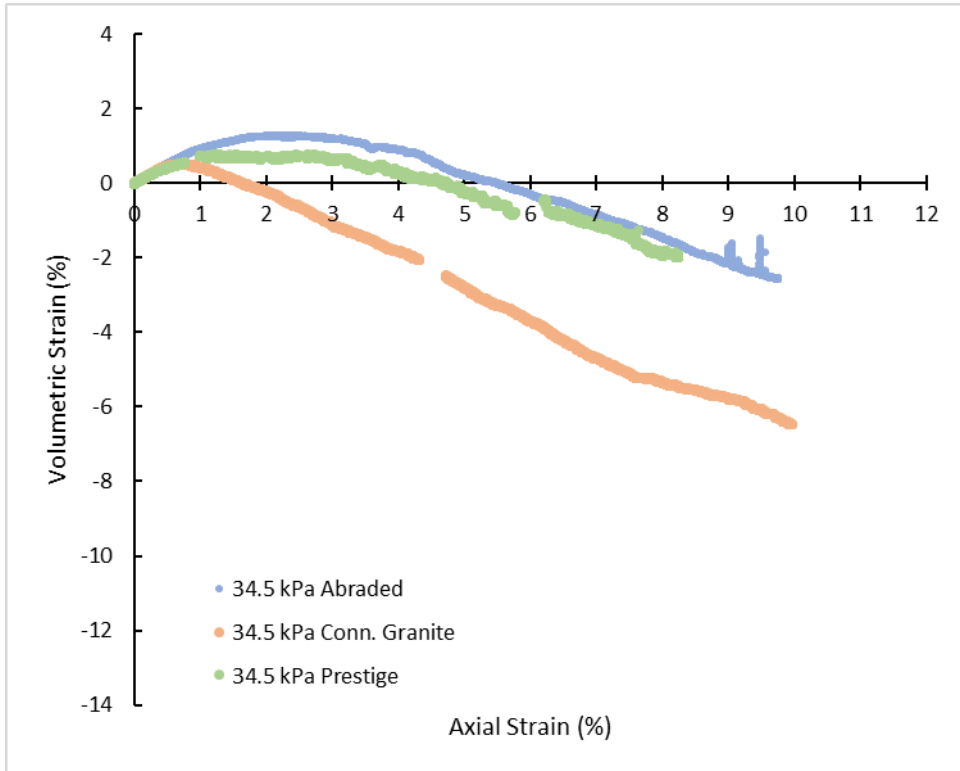
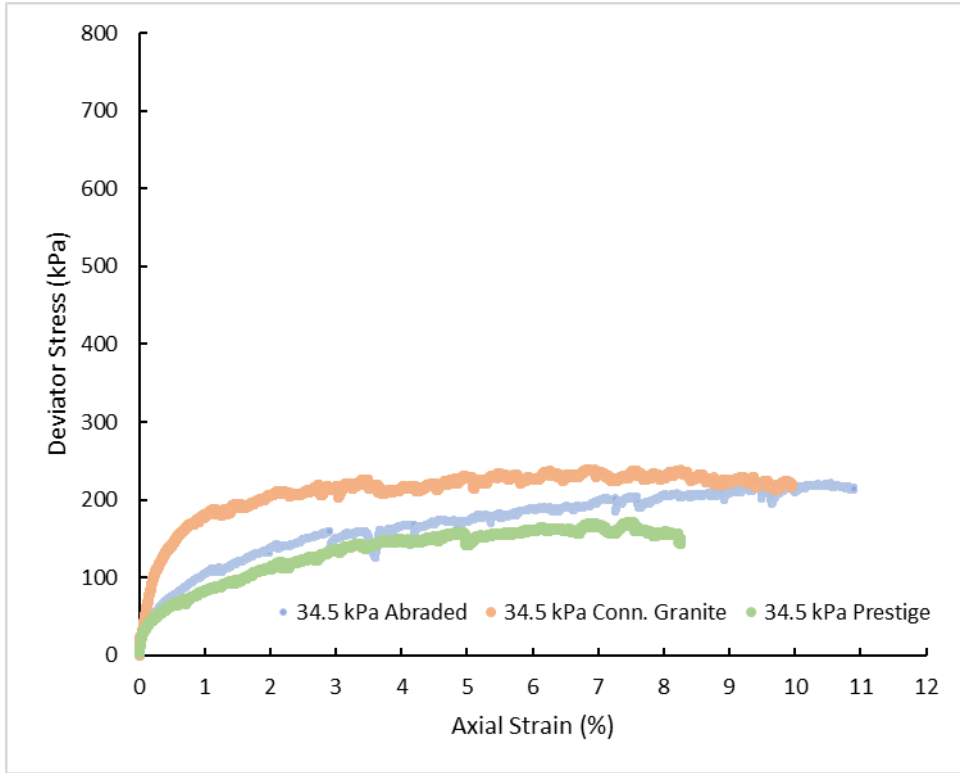


Figure 32 – 15 percent fouled, field capacity, 5 psi confining

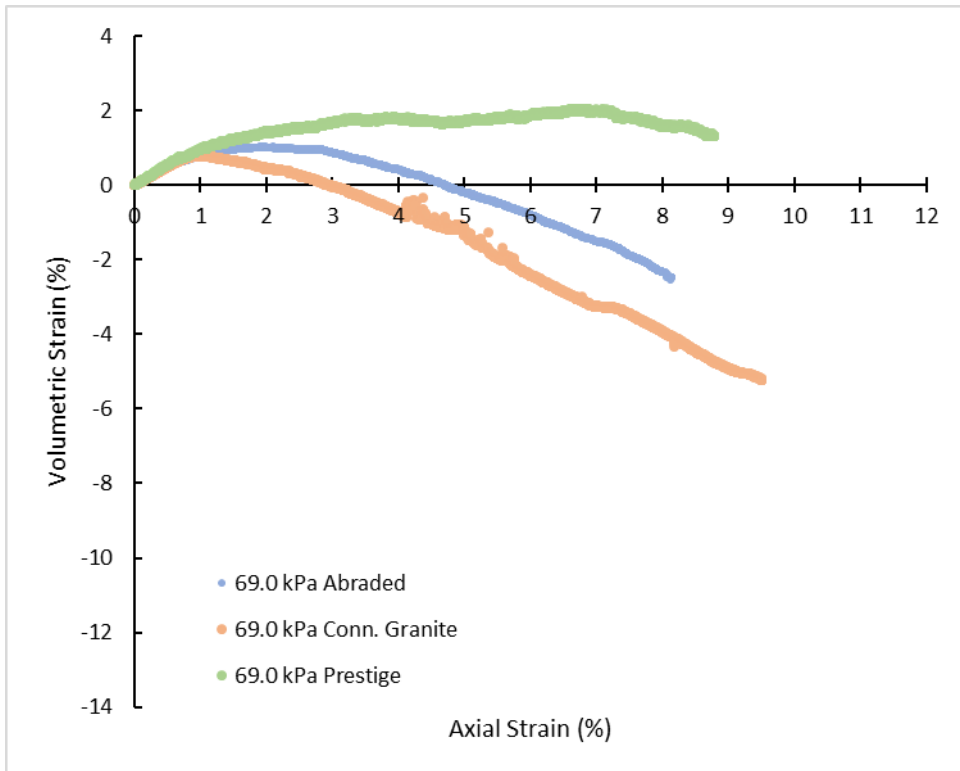
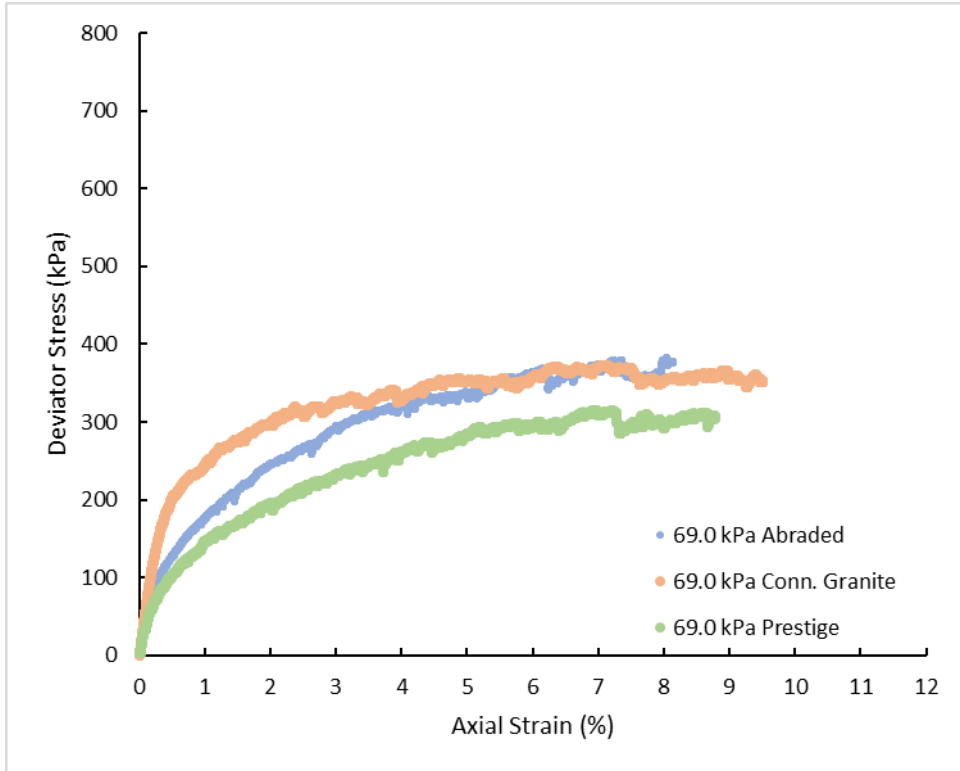


Figure 33 – 15 percent fouled, field capacity, 10 psi confining

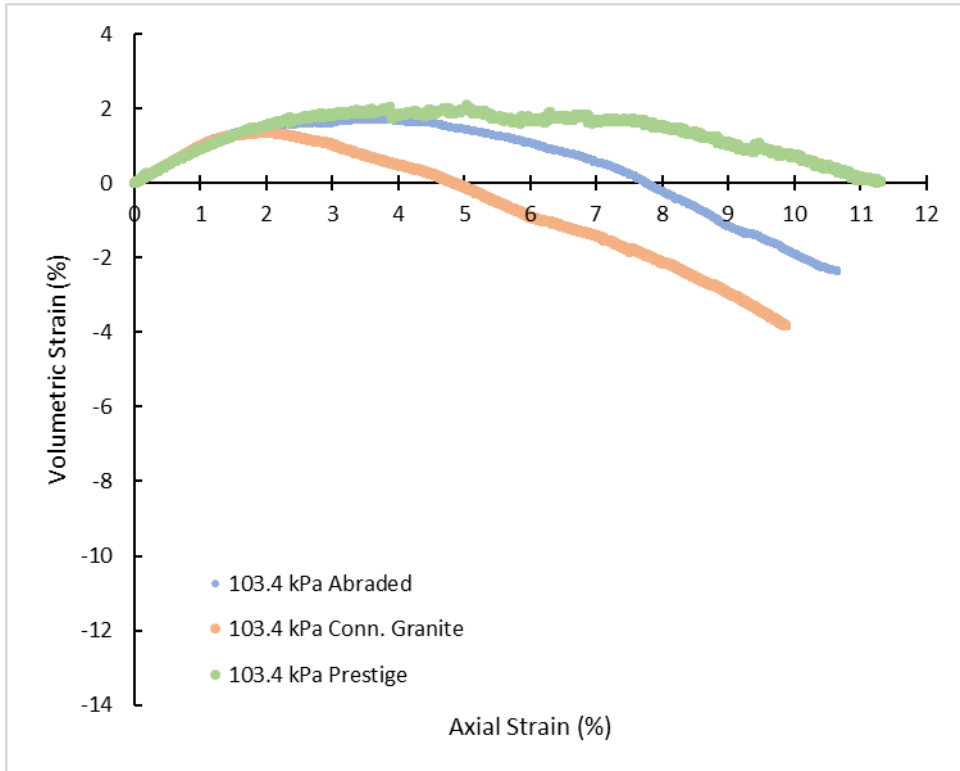
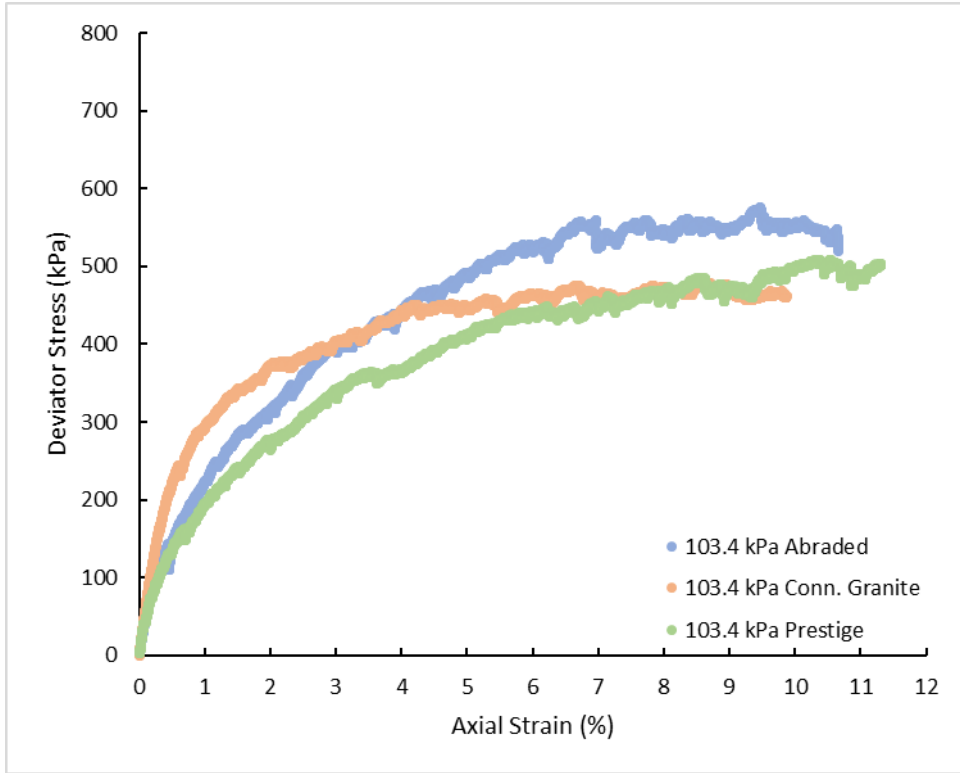


Figure 34 – 15 percent fouled, field capacity, 15 psi confining

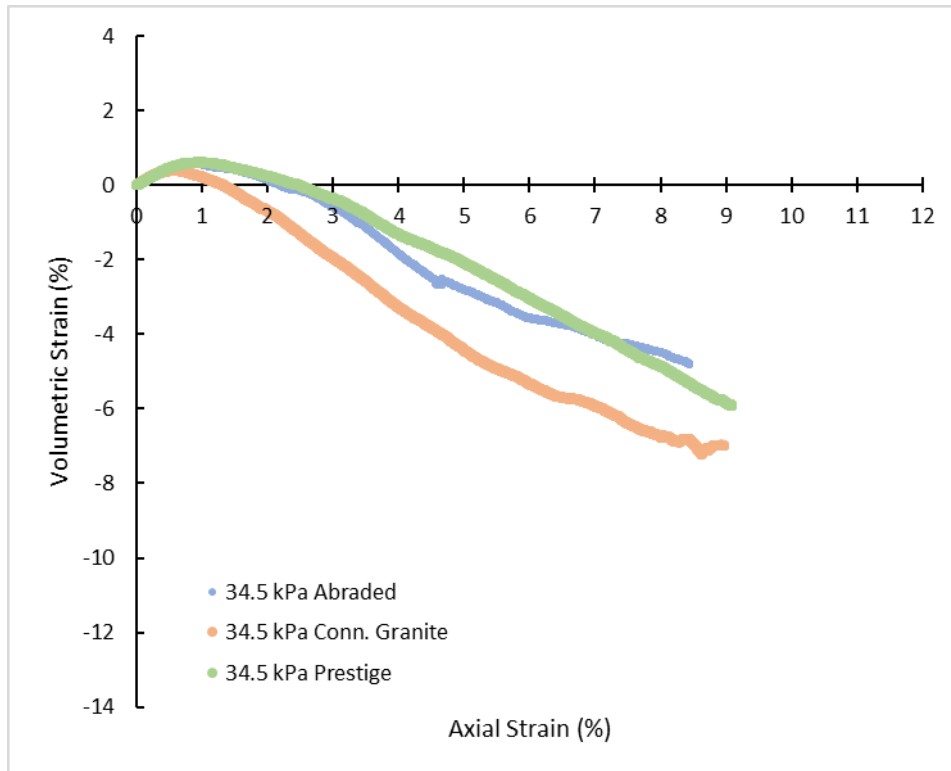
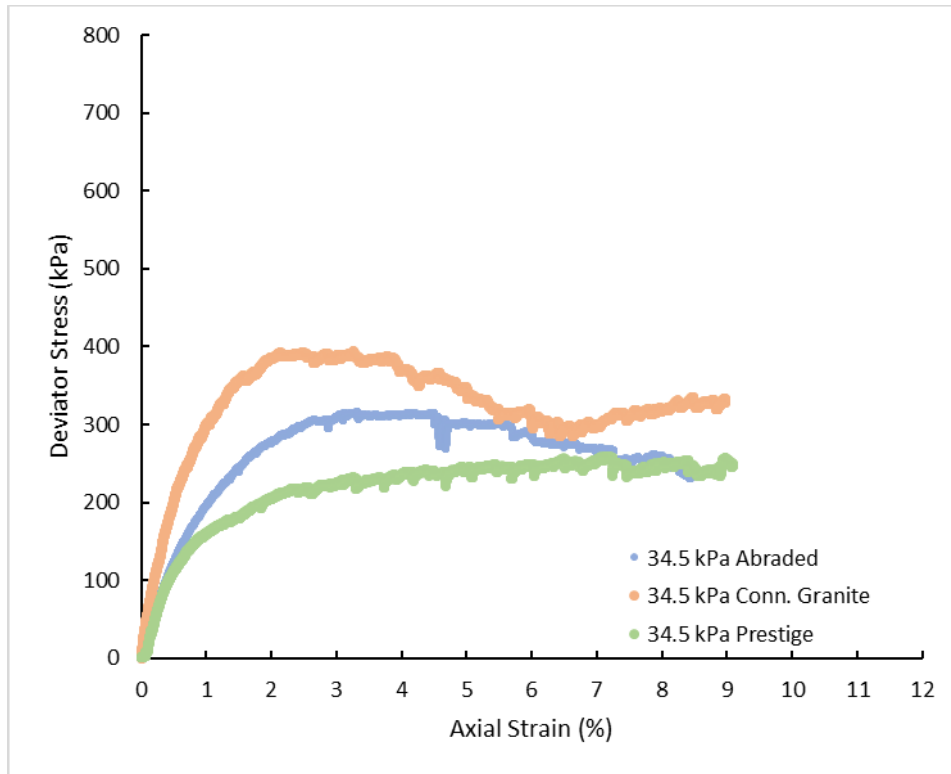


Figure 35 – 30 percent fouled, dry, 5 psi confining

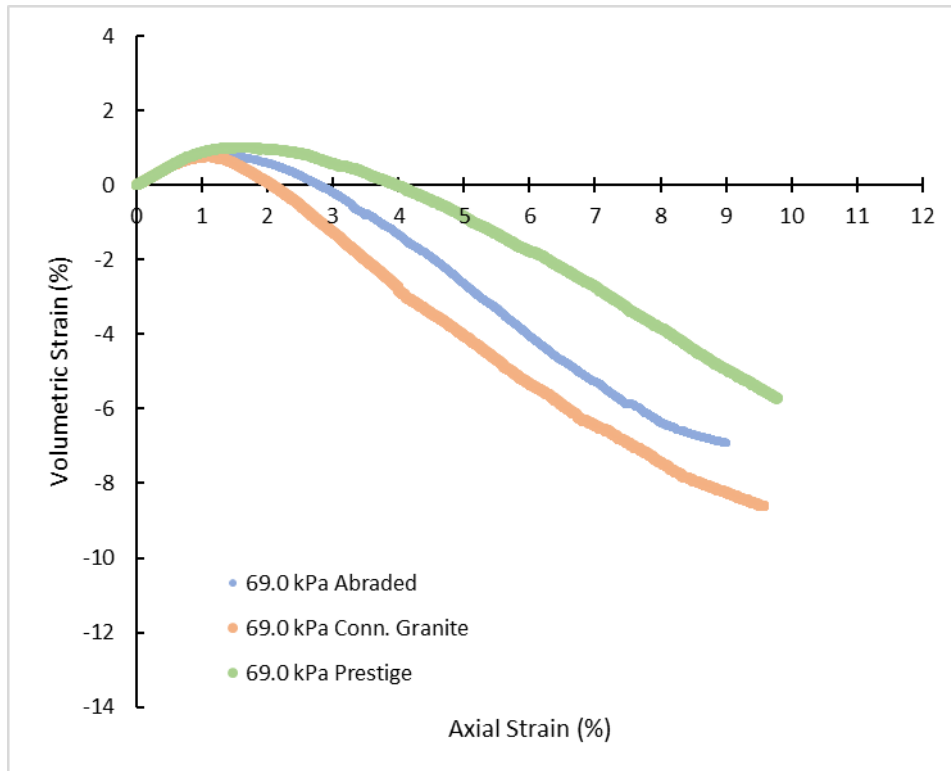
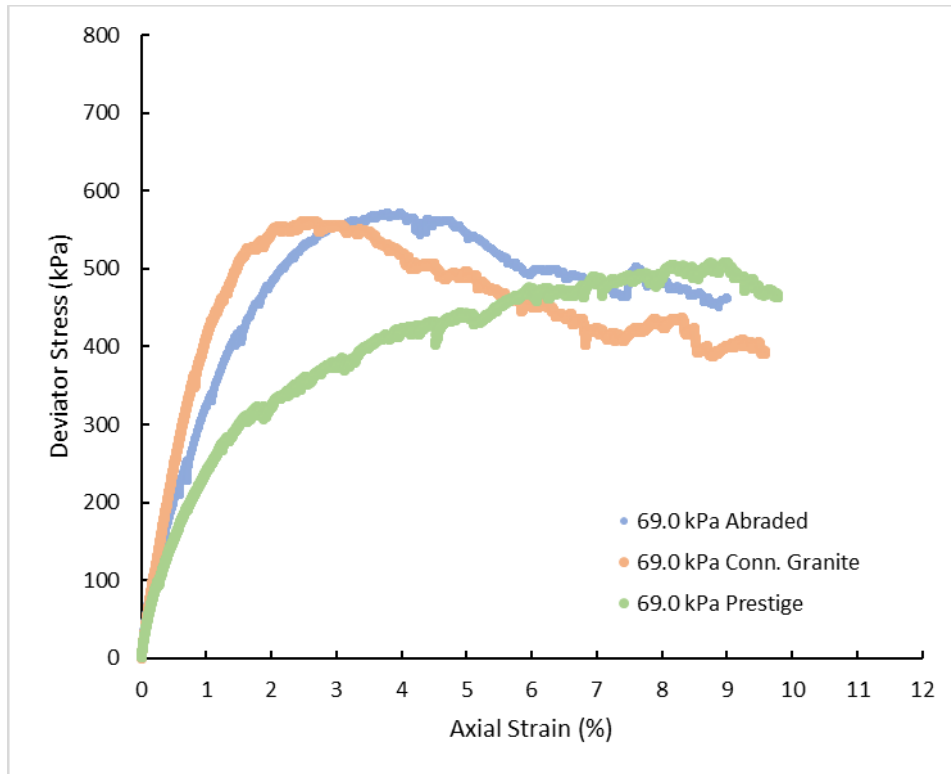


Figure 36 – 30 percent fouled, dry, 10 psi confining

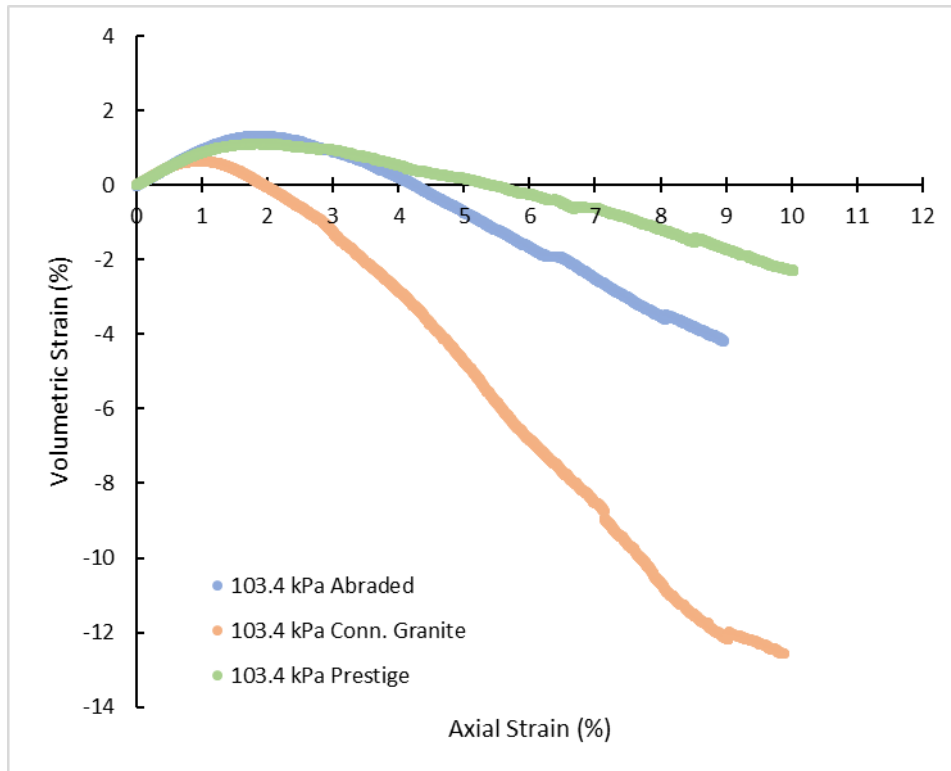
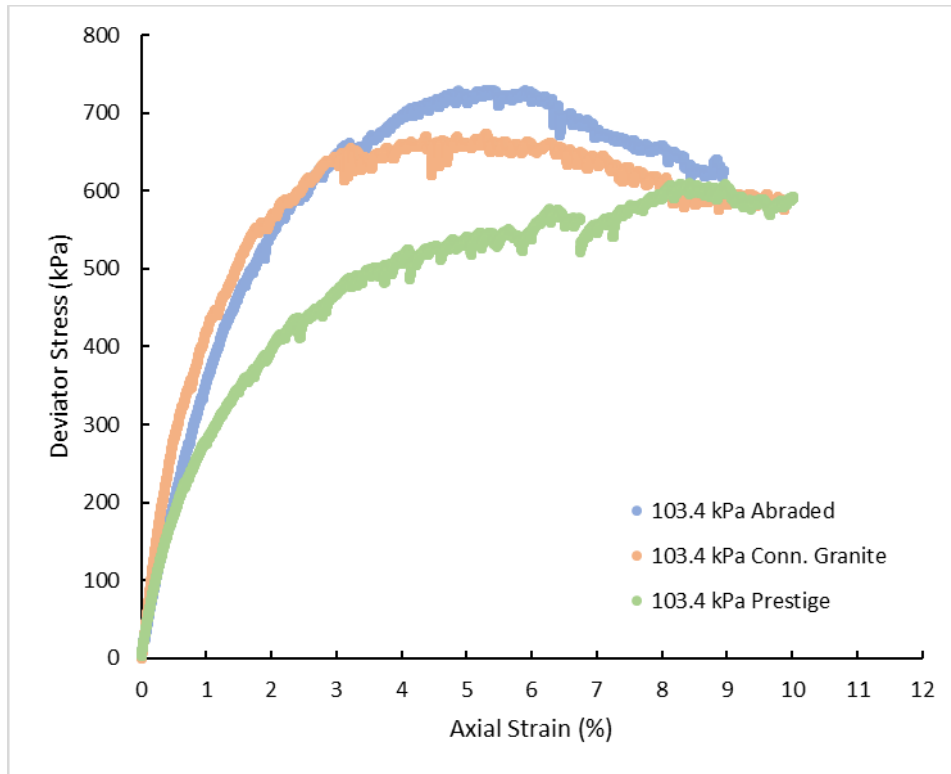


Figure 37 – 30 percent fouled, dry, 15 psi confining

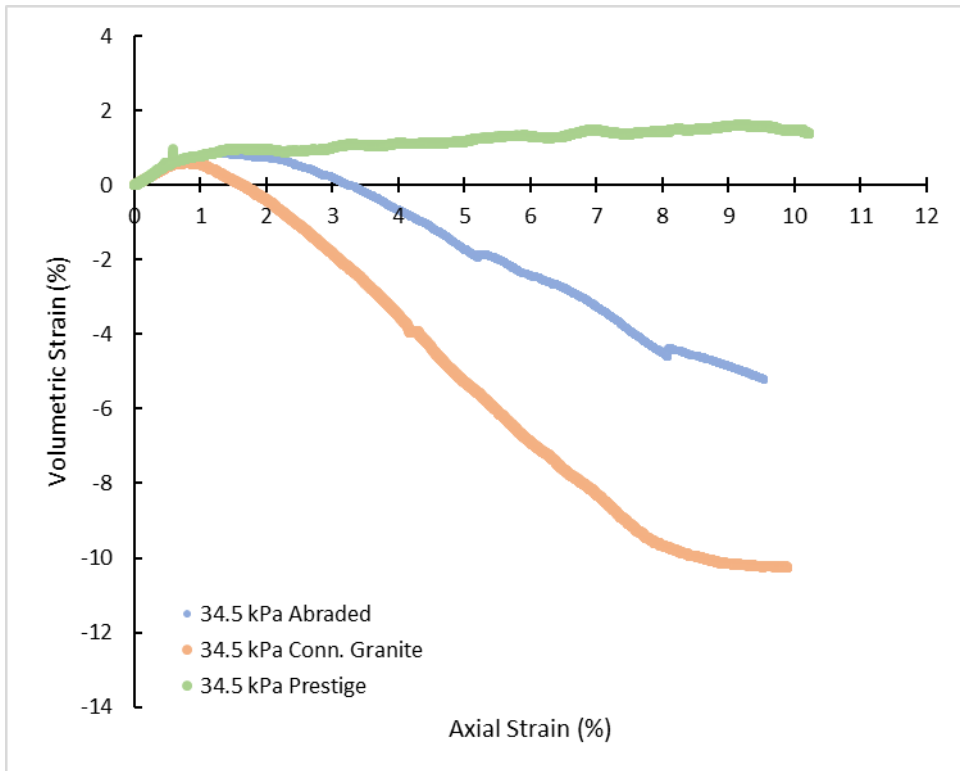
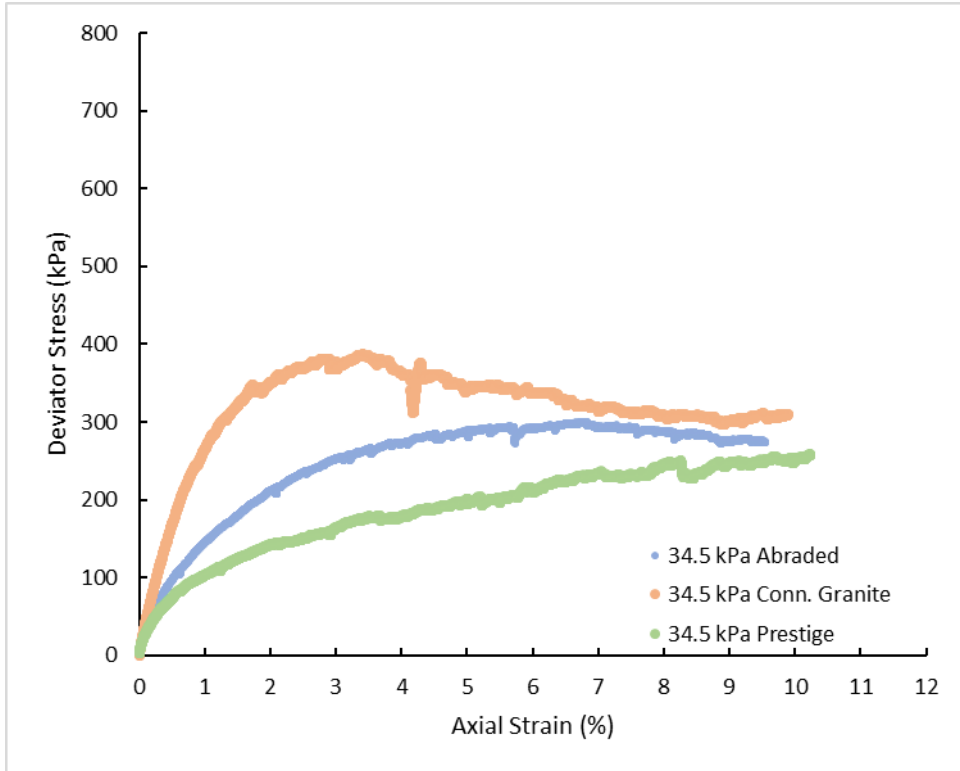


Figure 38 – 30 percent fouled, 50 percent field capacity, 5 psi confining

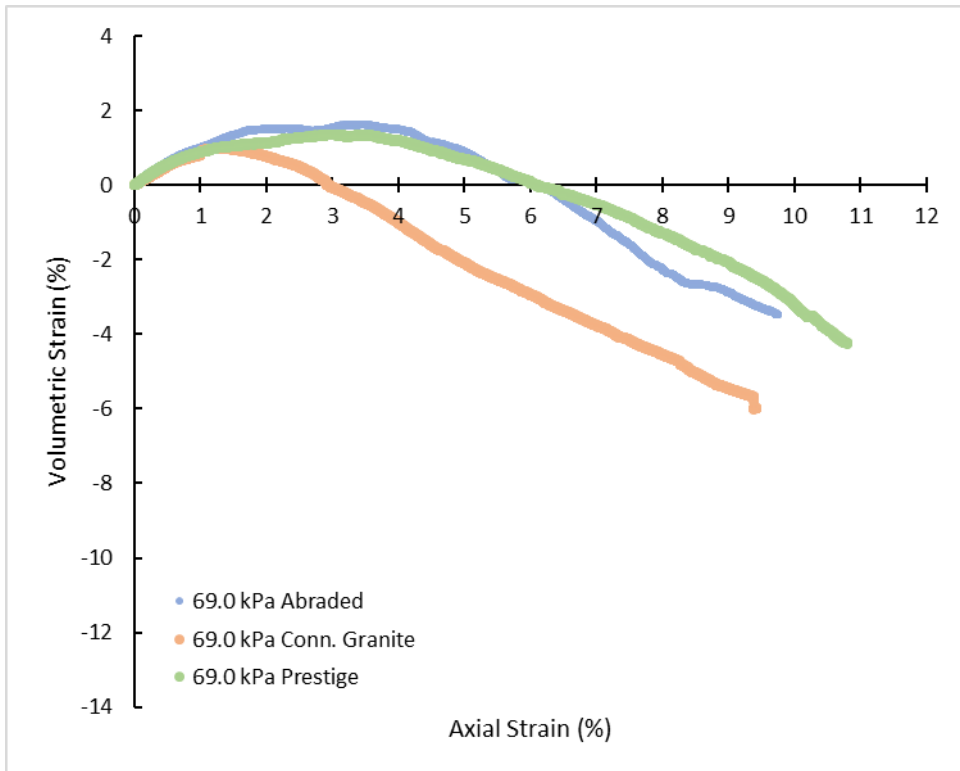
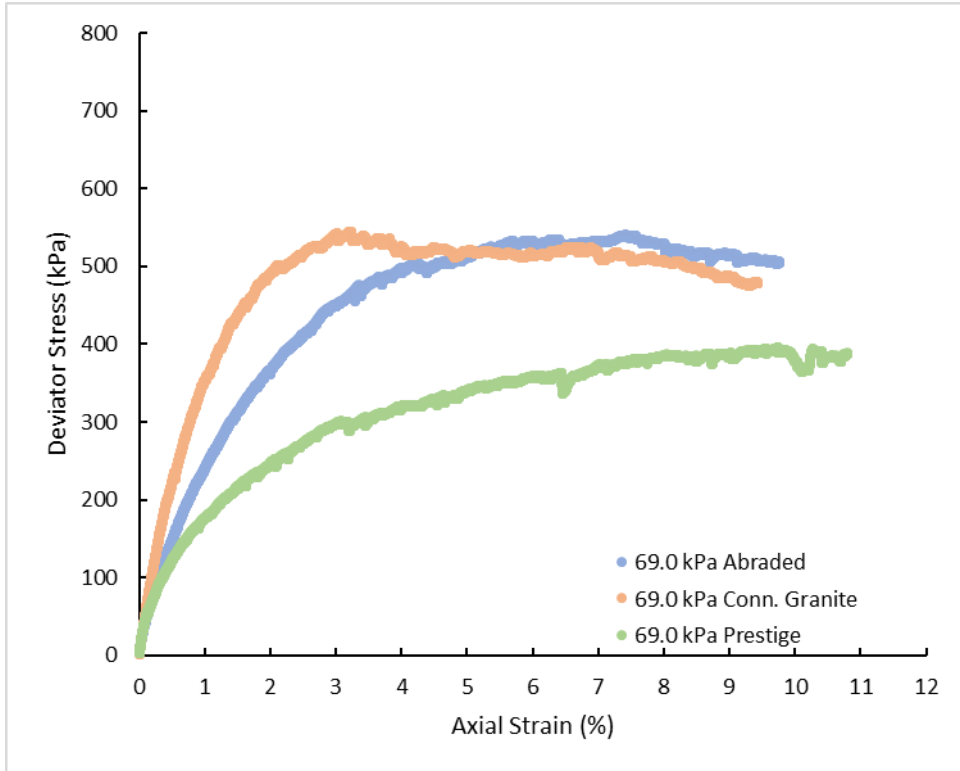


Figure 39 – 30 percent fouled, 50 percent field capacity, 10 psi confining

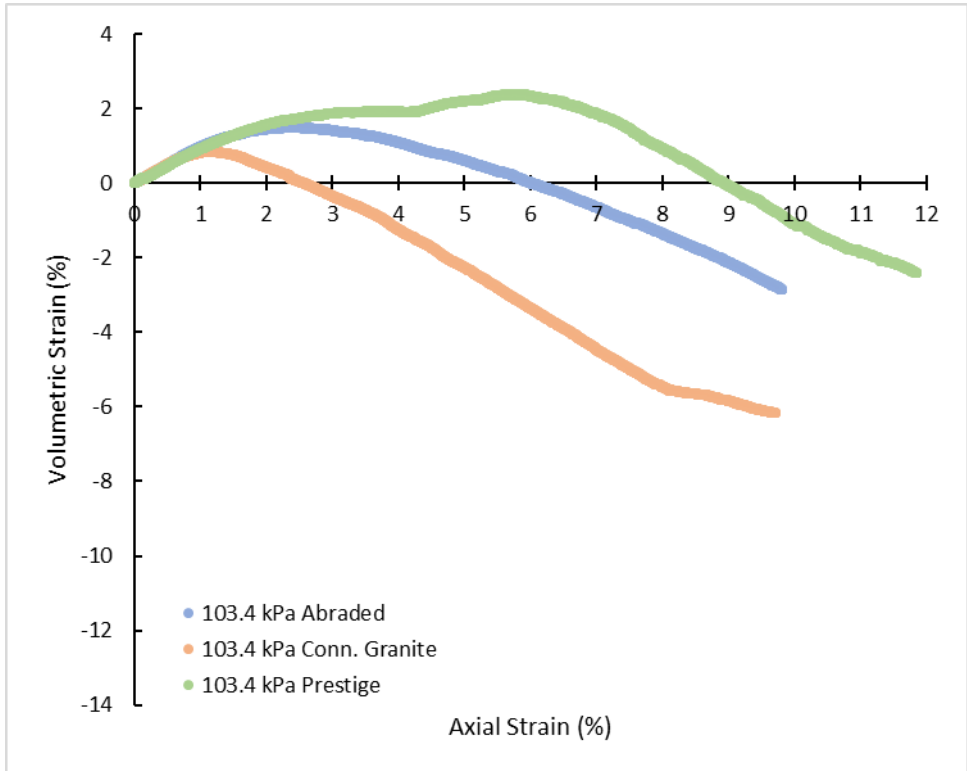
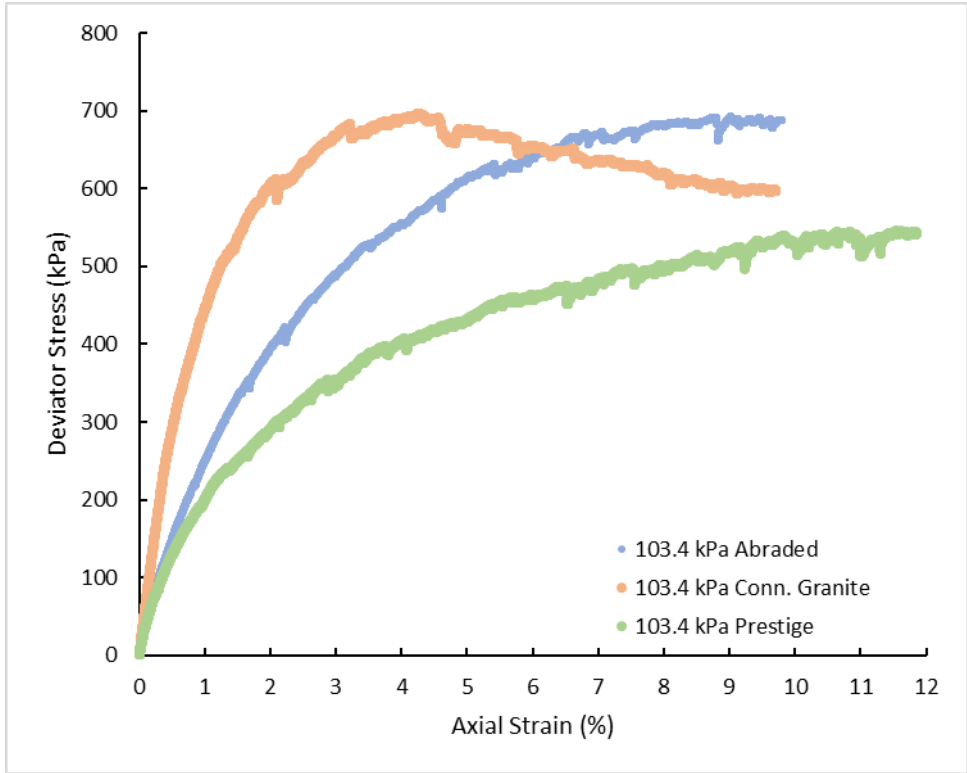


Figure 40 – 30 percent fouled, 50 percent field capacity, 15 psi confining

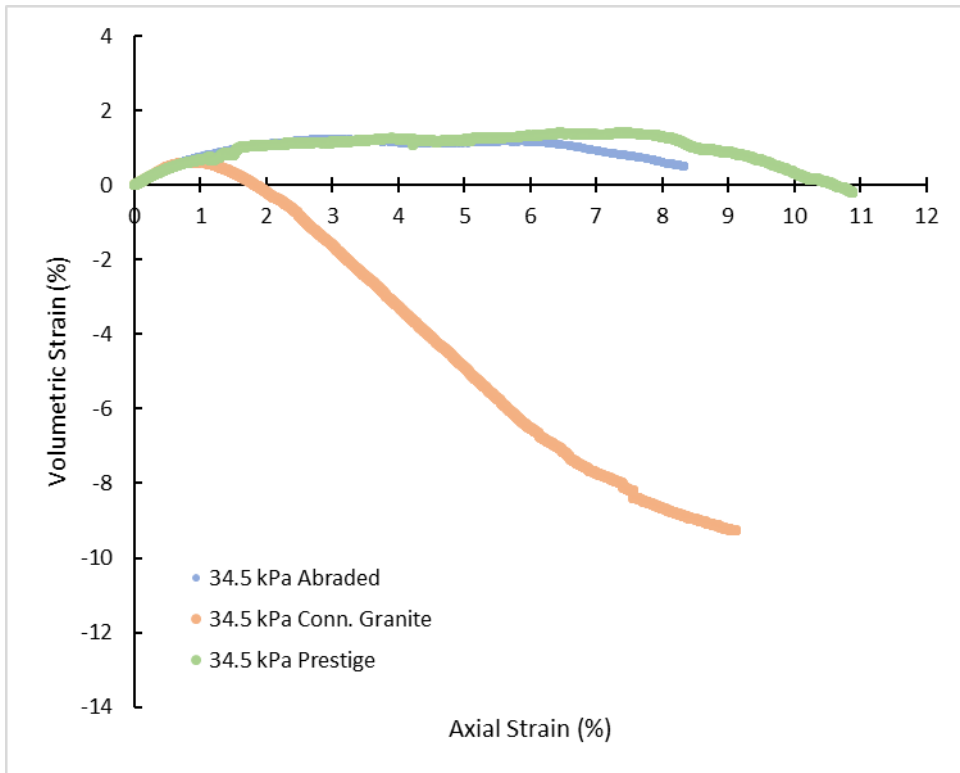
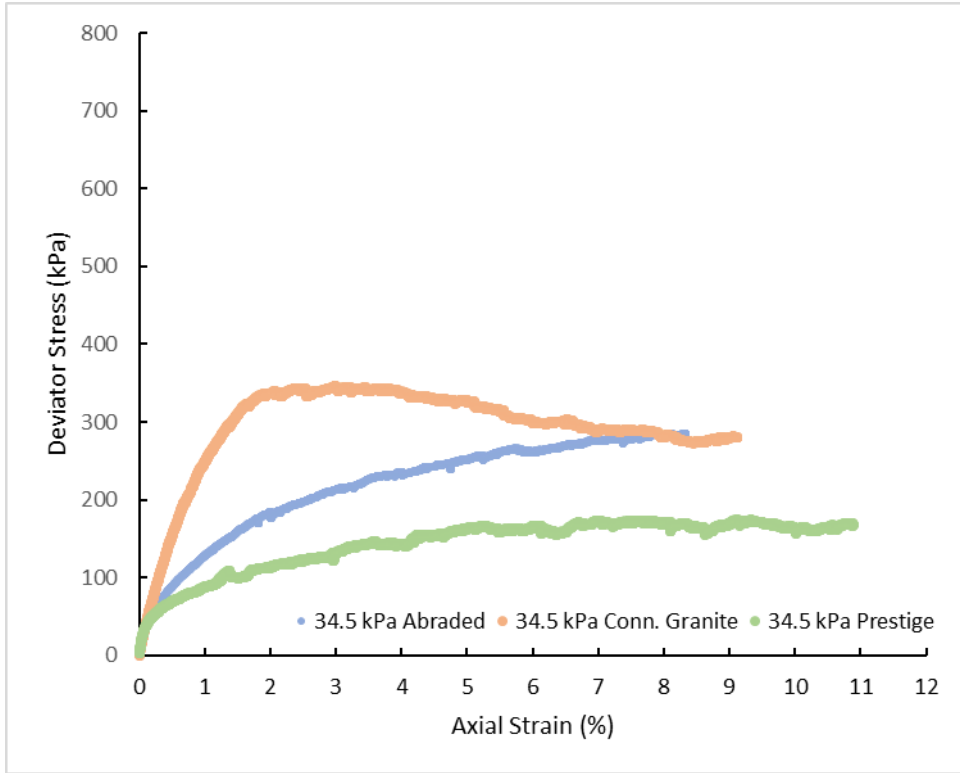


Figure 41 – 30 percent fouled, field capacity, 5 psi confining

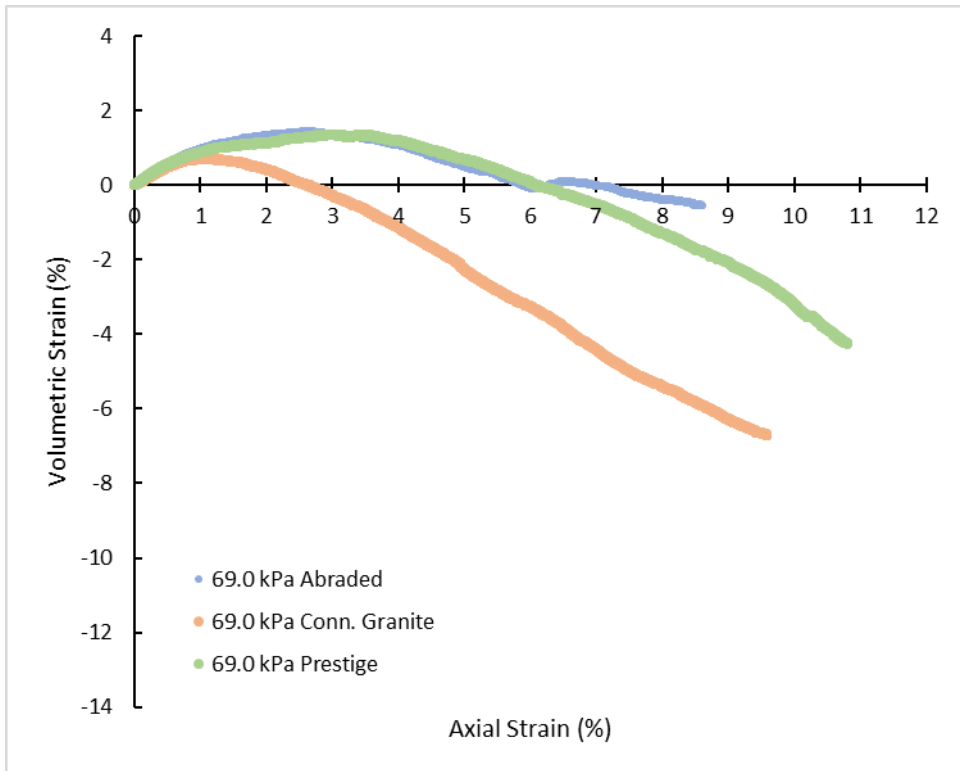
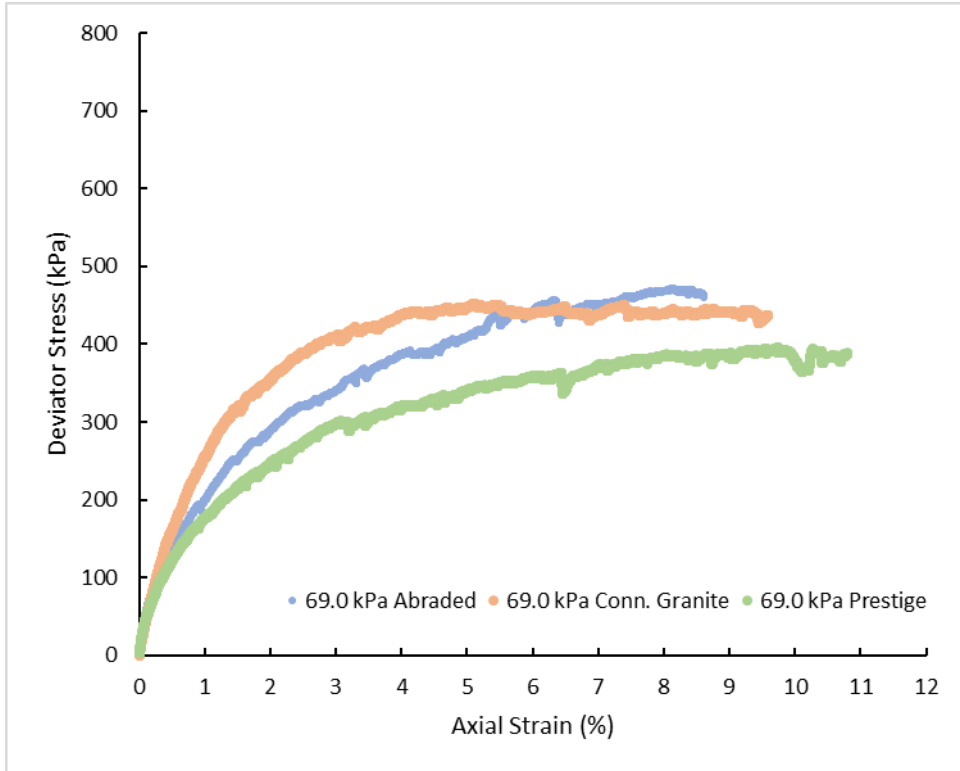


Figure 42 – 30 percent fouled, field capacity, 10 psi confining

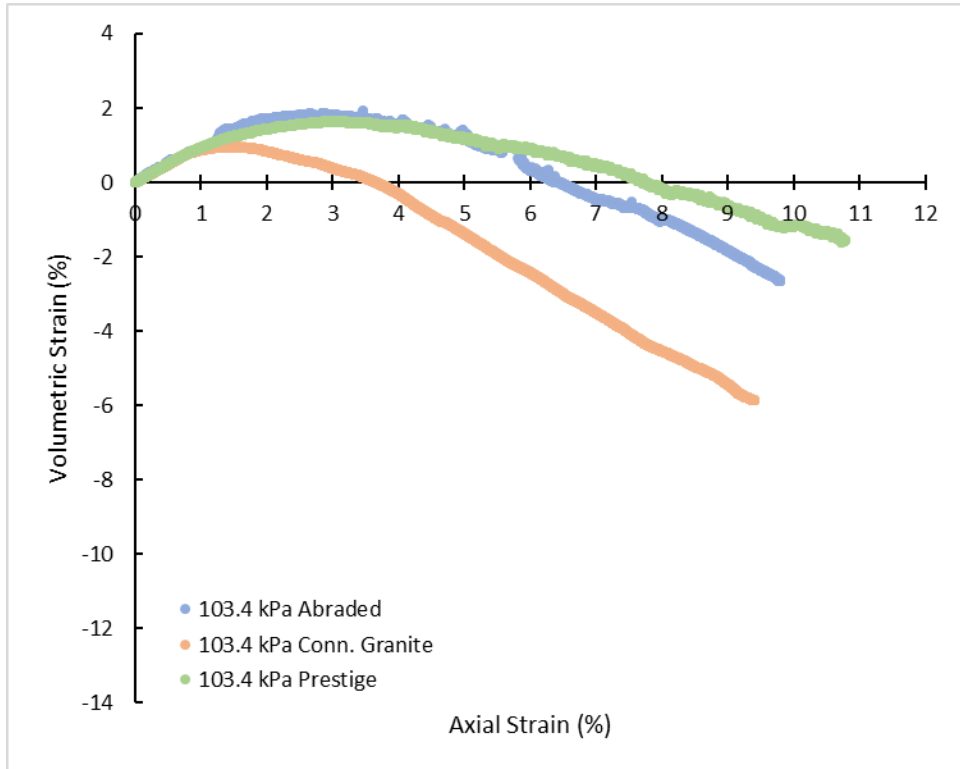
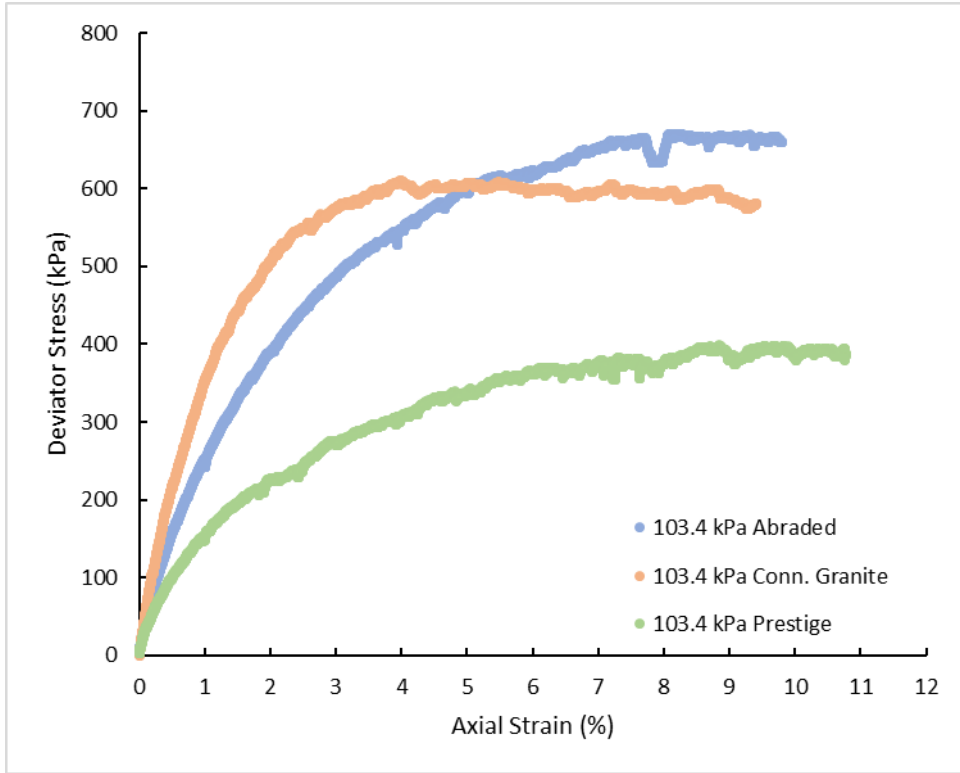


Figure 43 – 30 percent fouled, field capacity, 15 psi confining

Appendix B.

Box Test Settlement and Settlement Rate Curves

The figures in this appendix show the settlement data collected for each box test. Each plot depicts a different phase of the test. These data are presented in two different ways. The first plot for a phase shows settlement curves on a linear scale. The second plot for each phase presents the same data on a log-log plot, which presents settlement rate.

Clean Box Tests

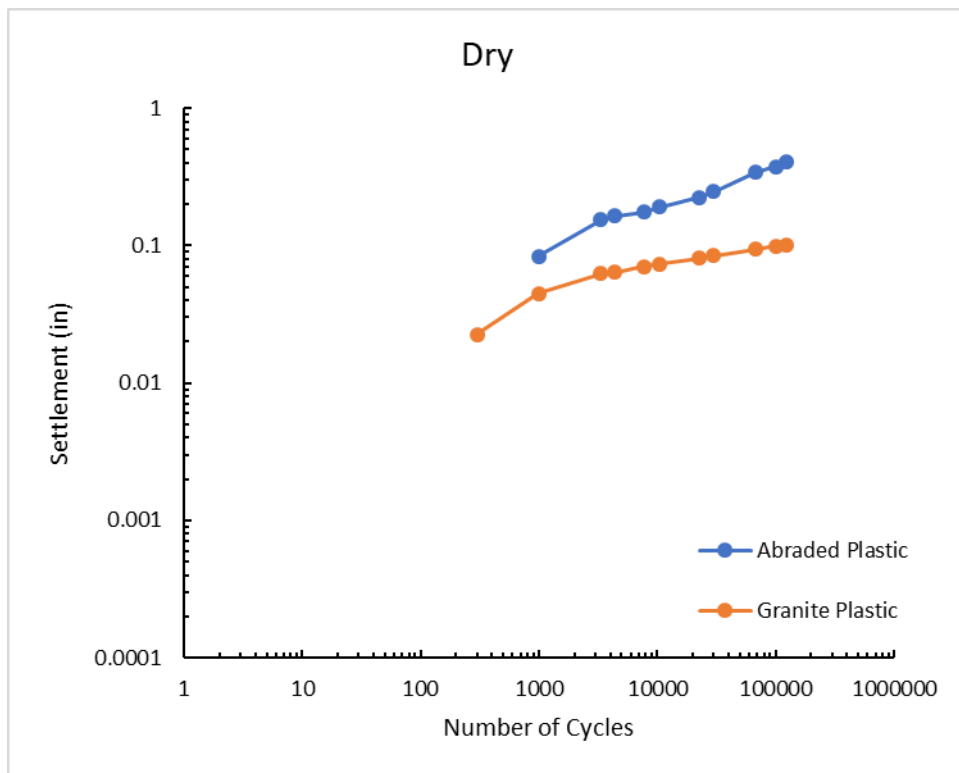
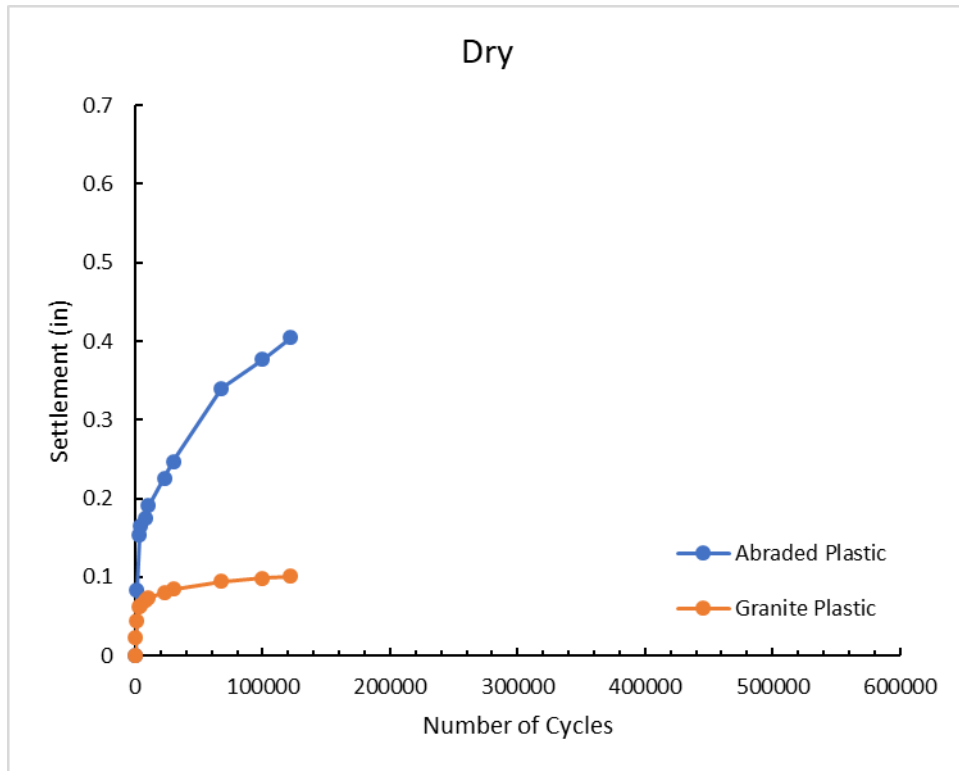


Figure 44 – Clean box tests, dry phase

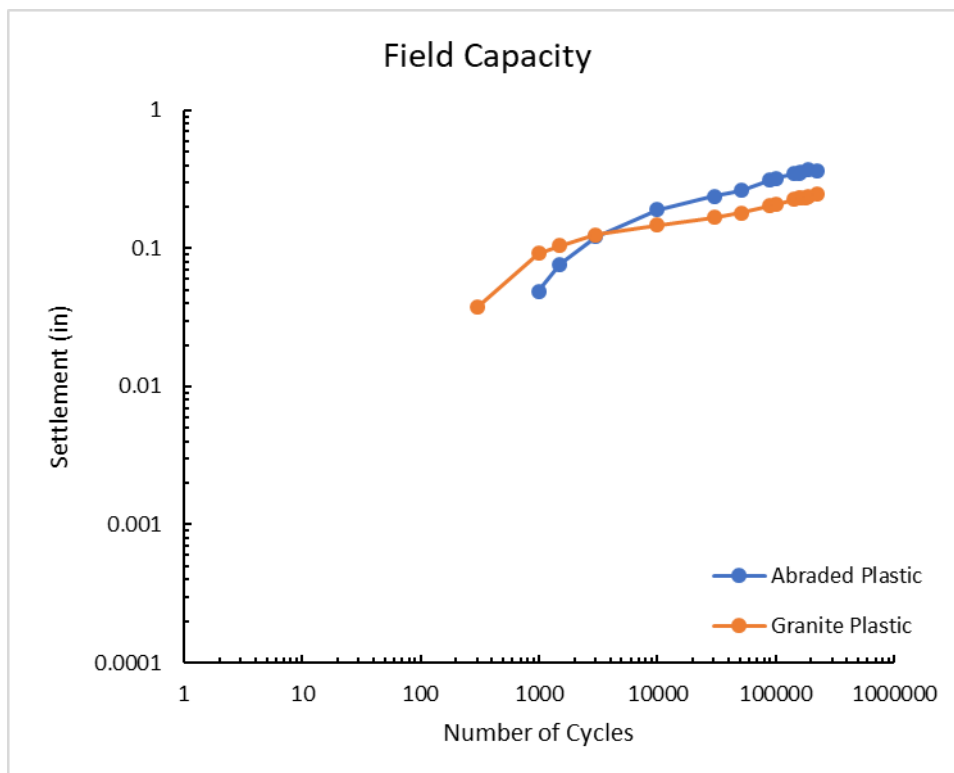
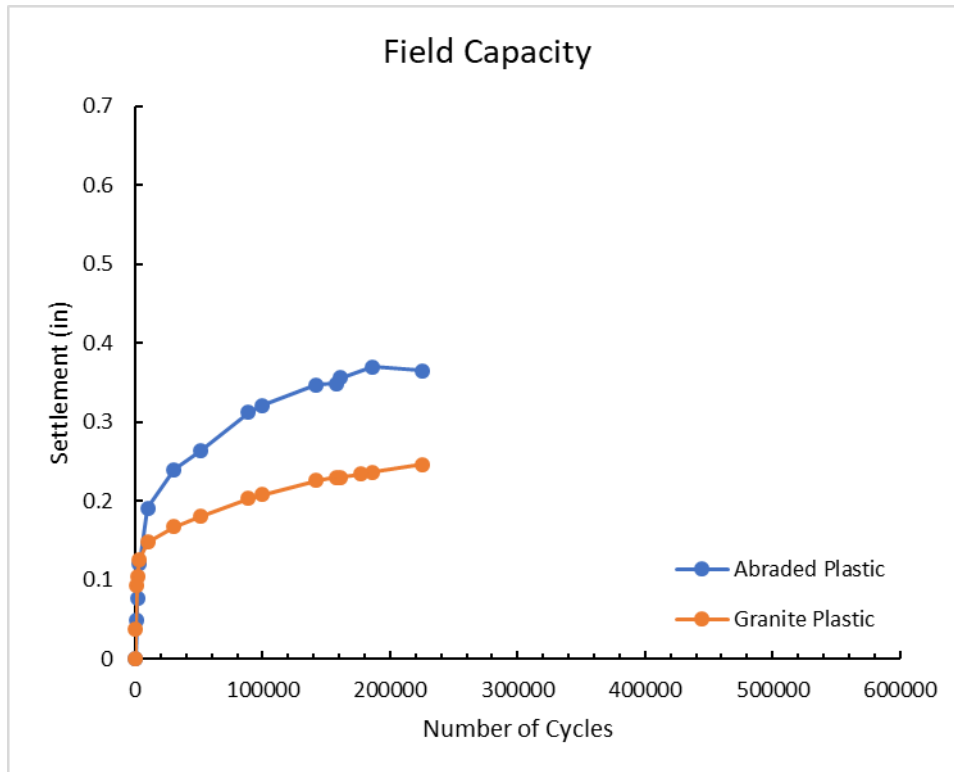


Figure 45 – Clean box tests, field capacity phase

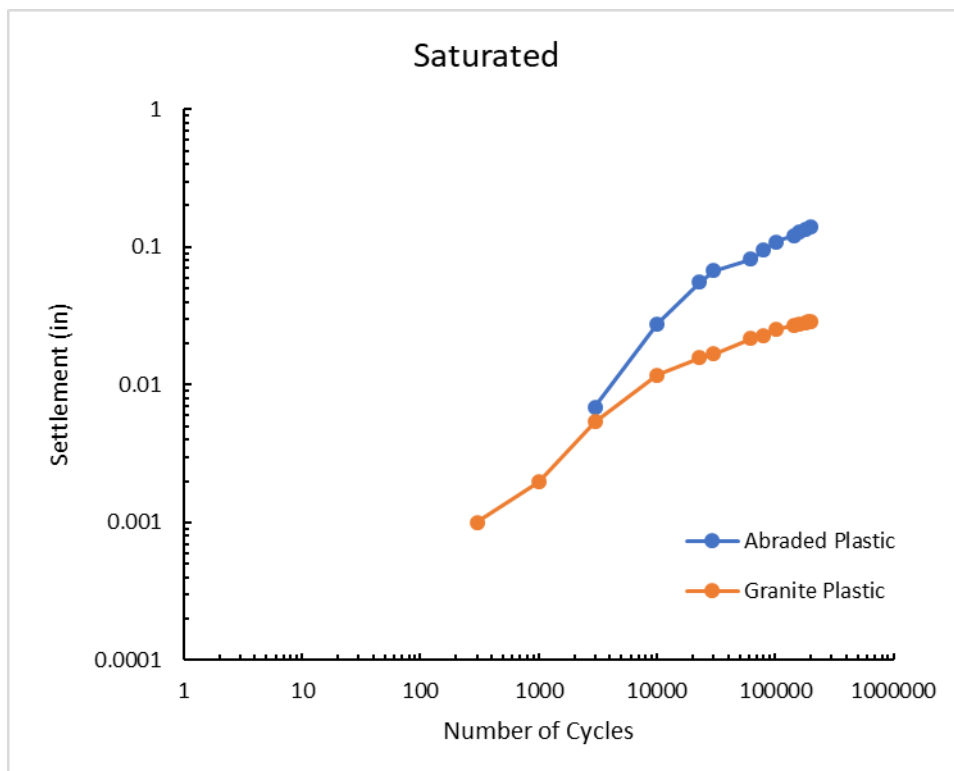
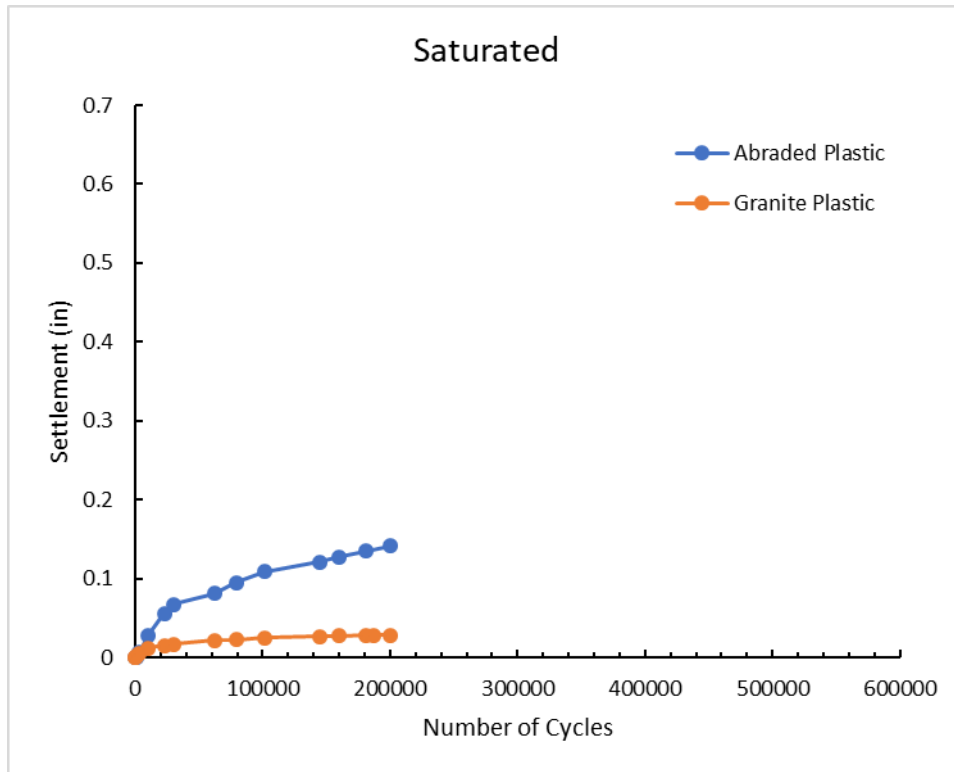


Figure 46 – Clean box tests, saturated phase

15% Fouled Tests

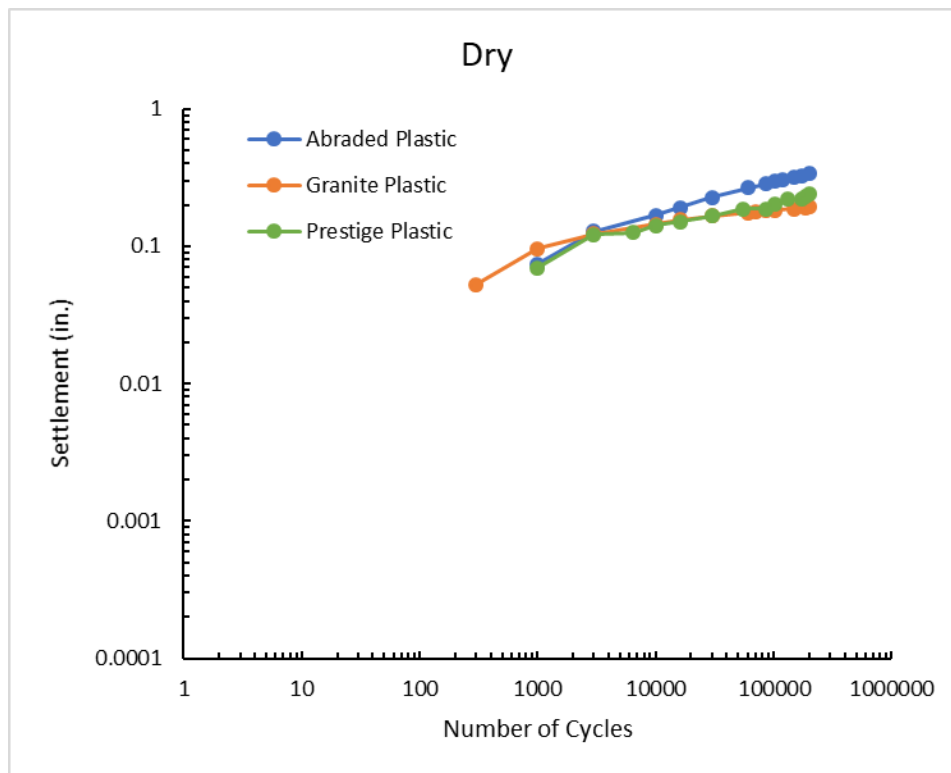
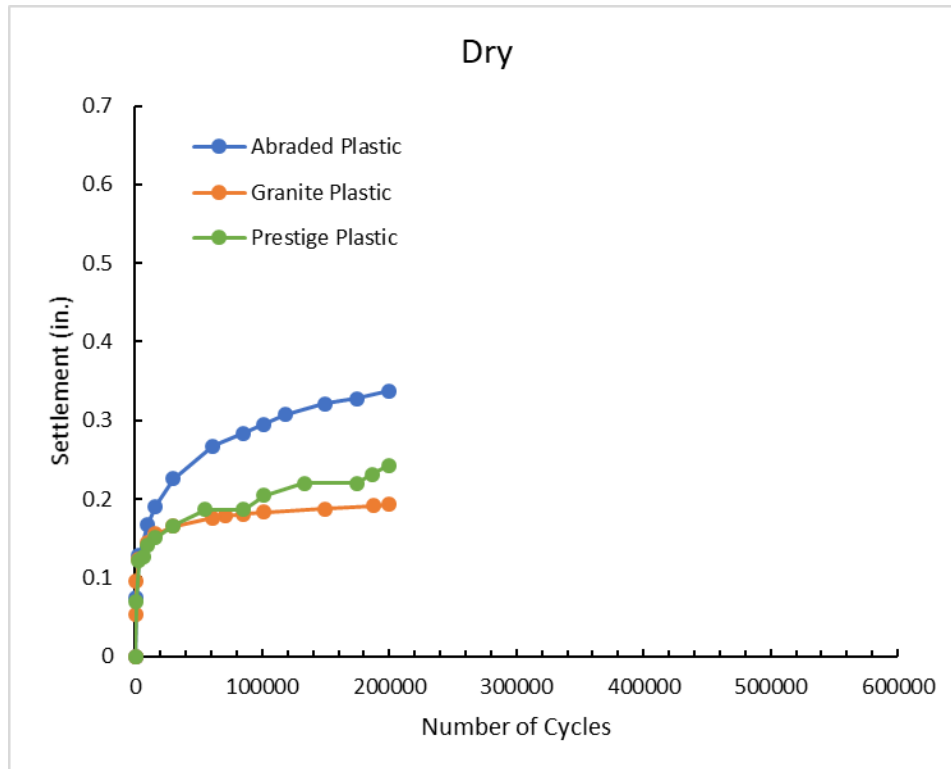


Figure 47 – 15 percent fouled box tests, dry phase

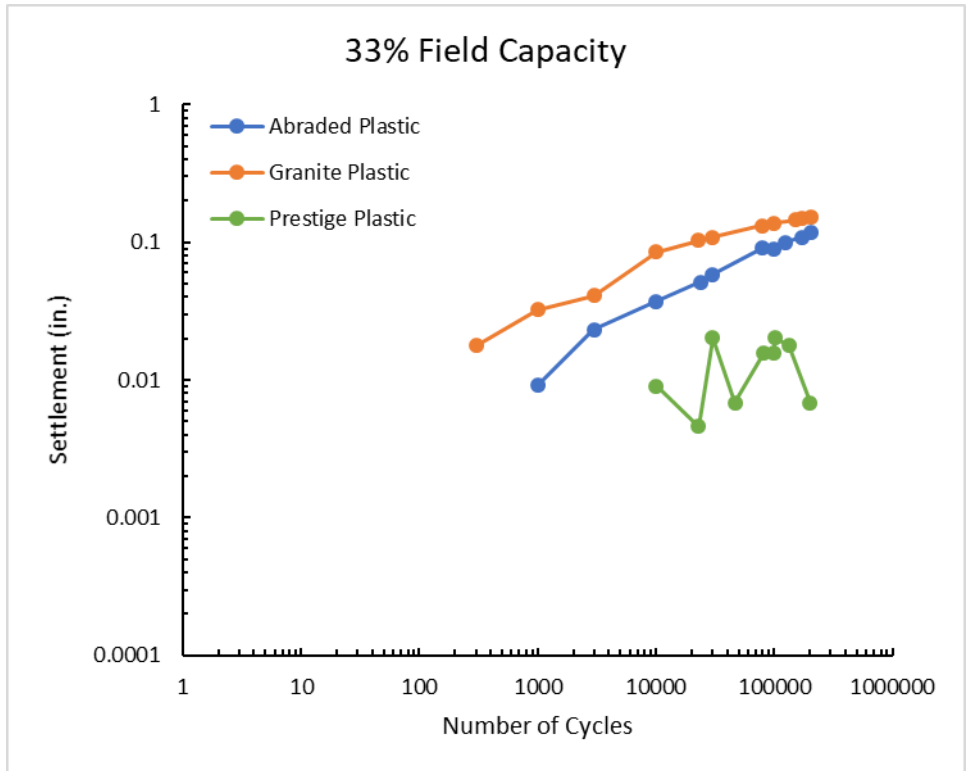
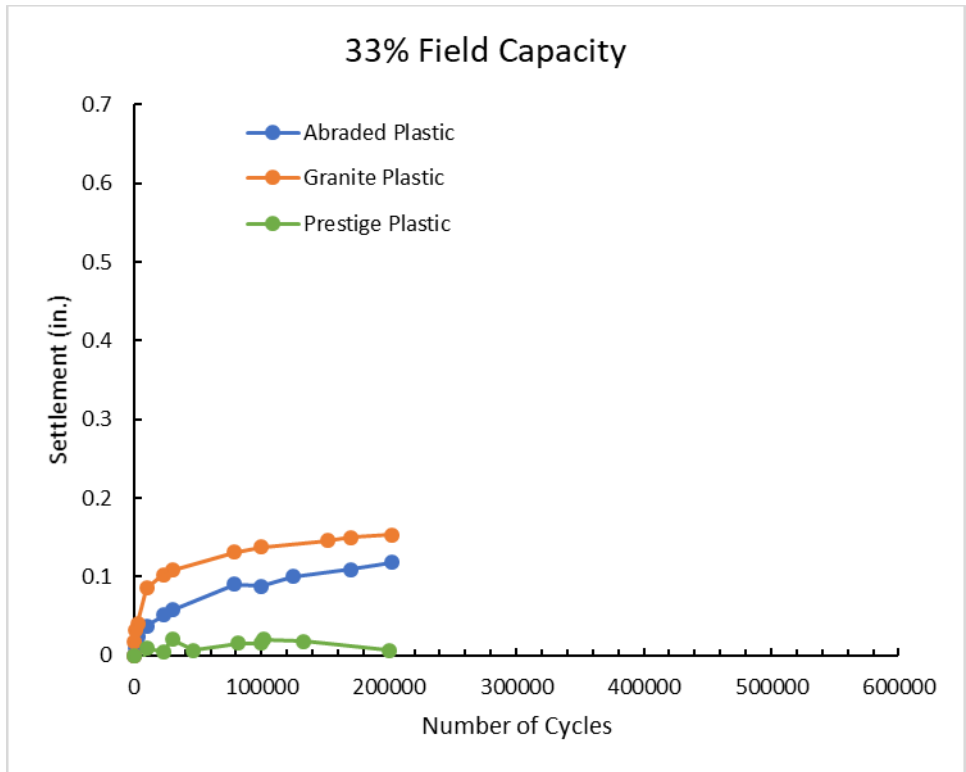


Figure 48 – 15 percent fouled box tests, 1/3 field capacity phase

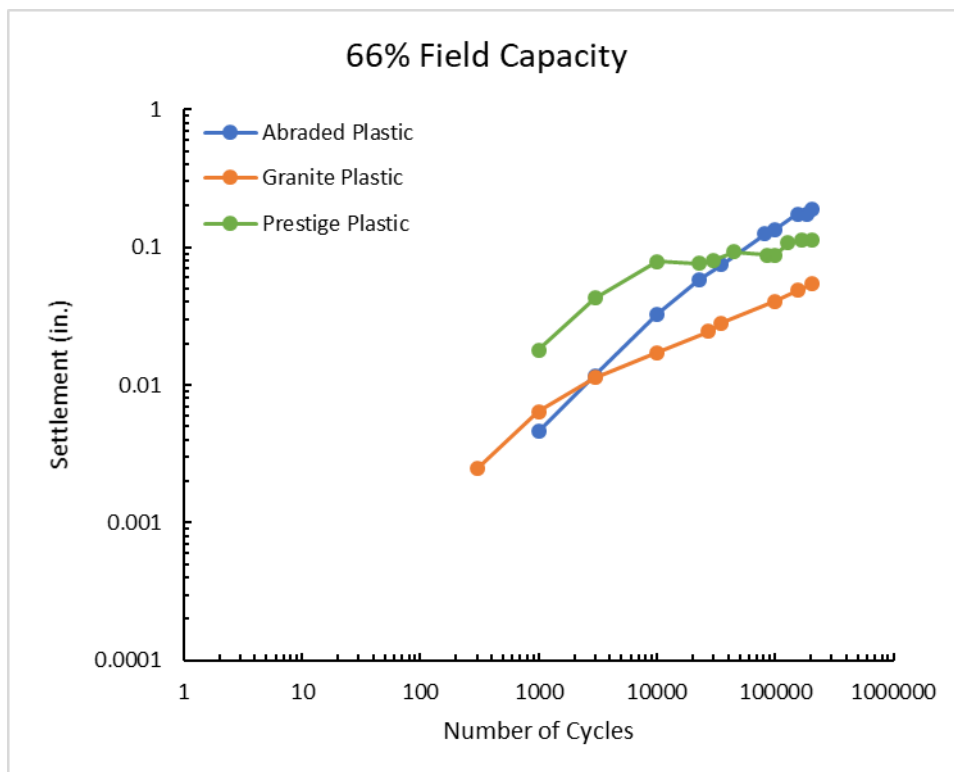
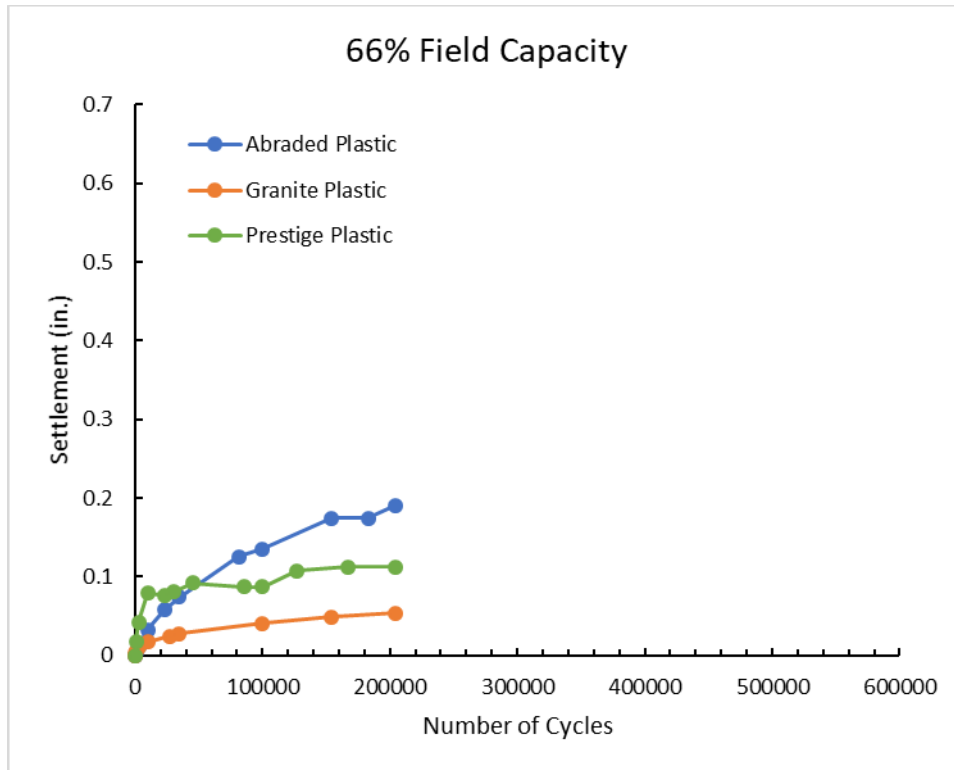


Figure 49 – 15 percent fouled box tests, 2/3 field capacity phase

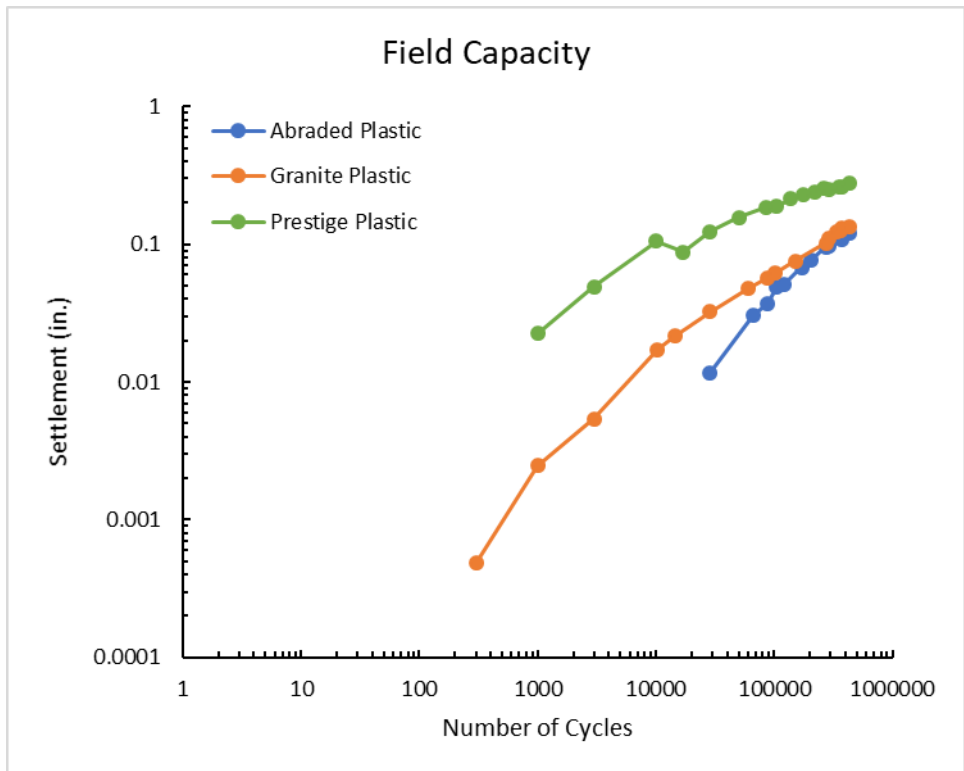
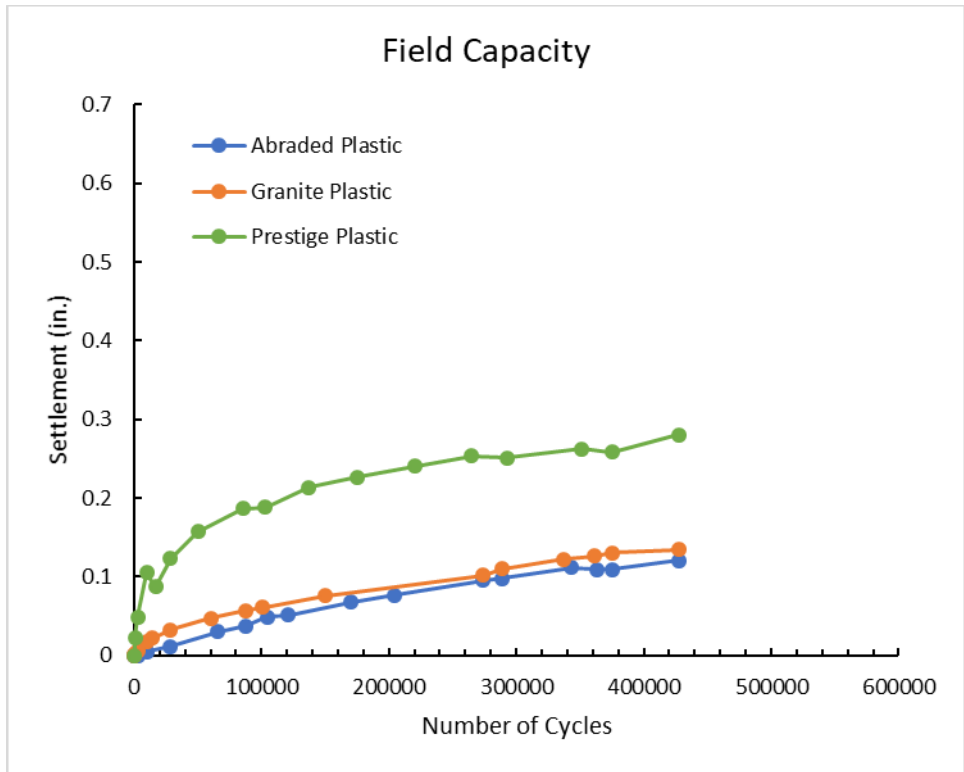


Figure 50 – 15 percent fouled box tests, field capacity phase

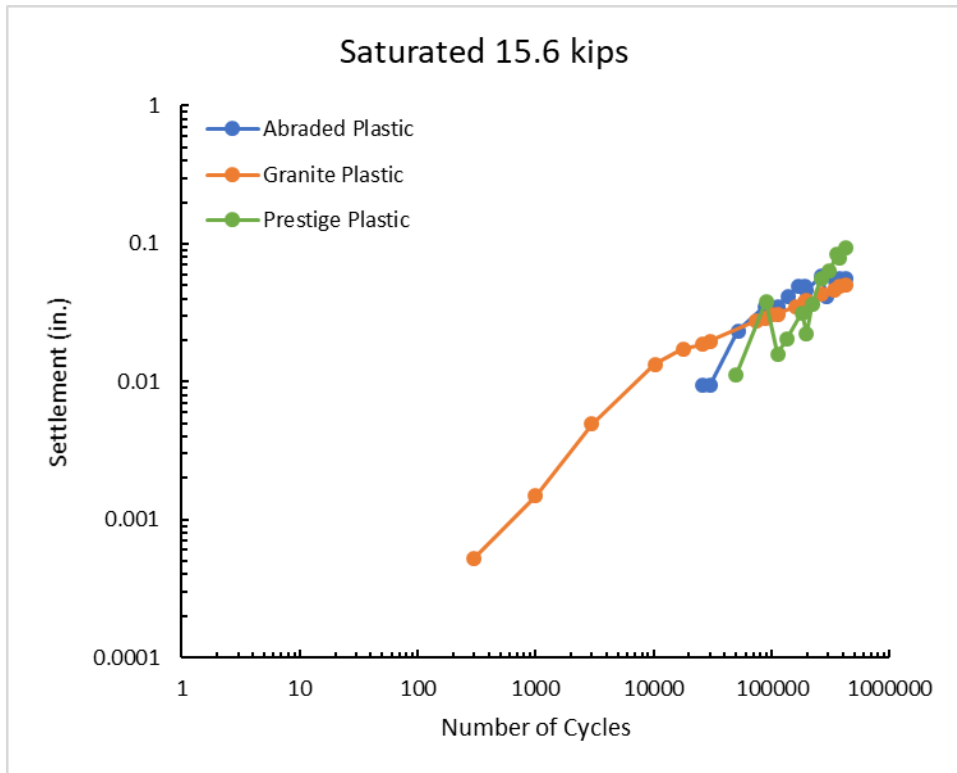
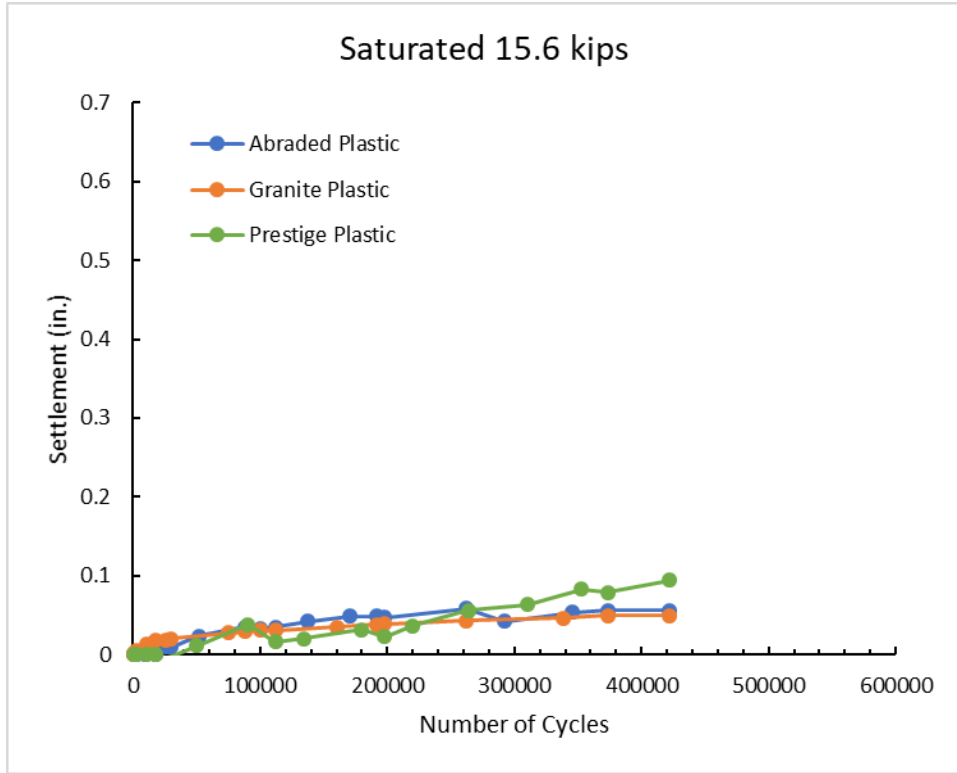


Figure 51 – 15 percent fouled box tests, saturated phase, 15.6 kip loading

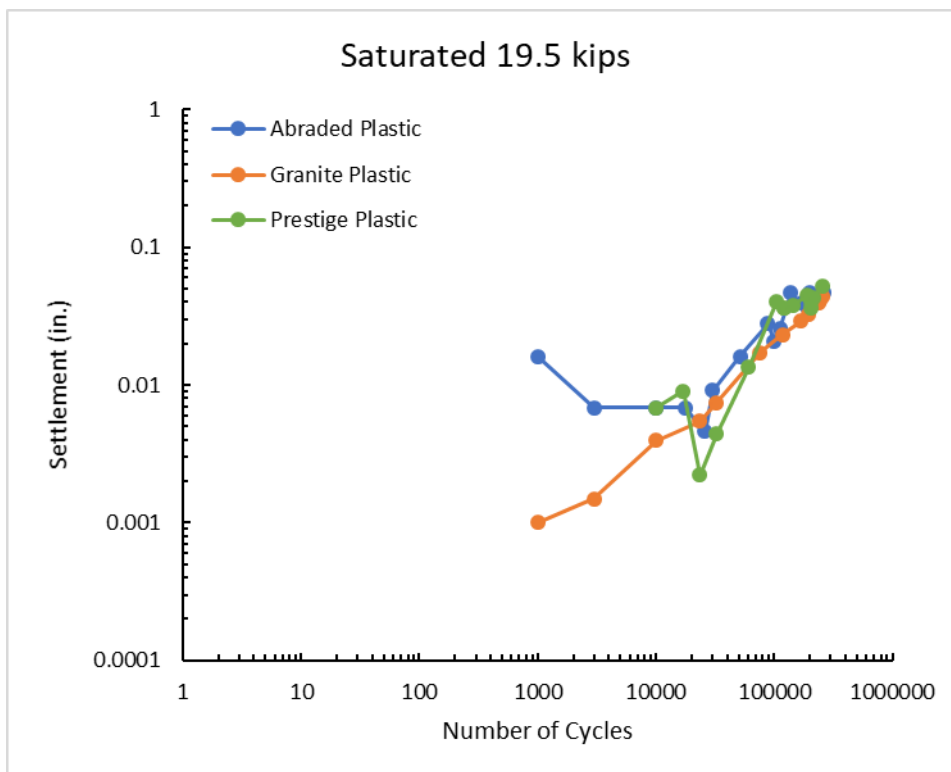
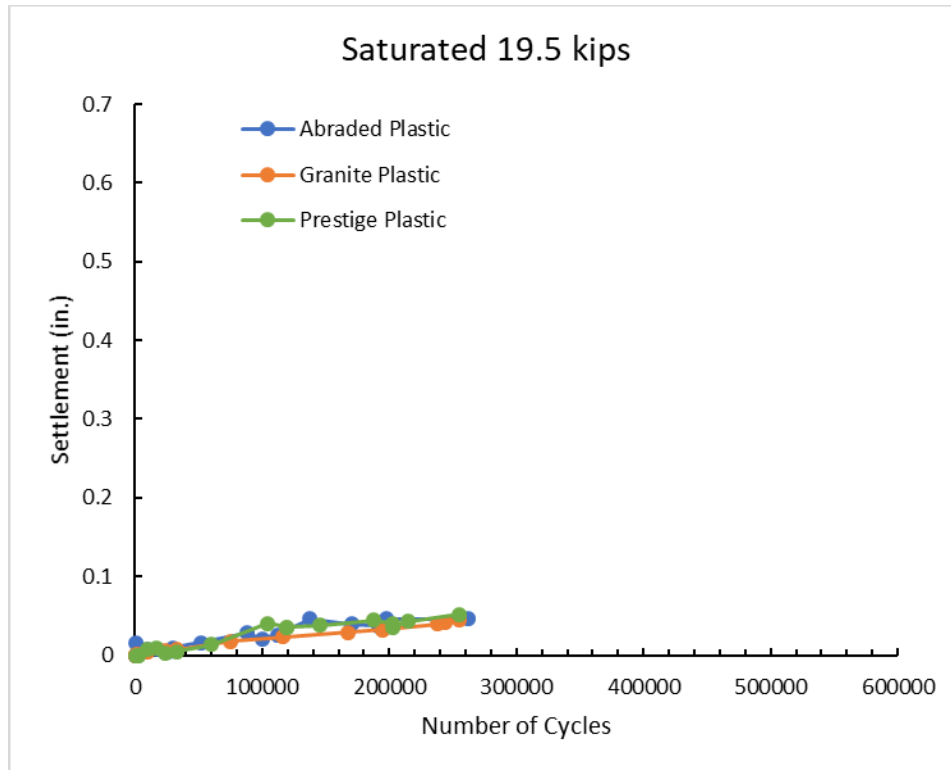


Figure 52 – 15 percent fouled box tests, saturated phase, 19.5 kip loading

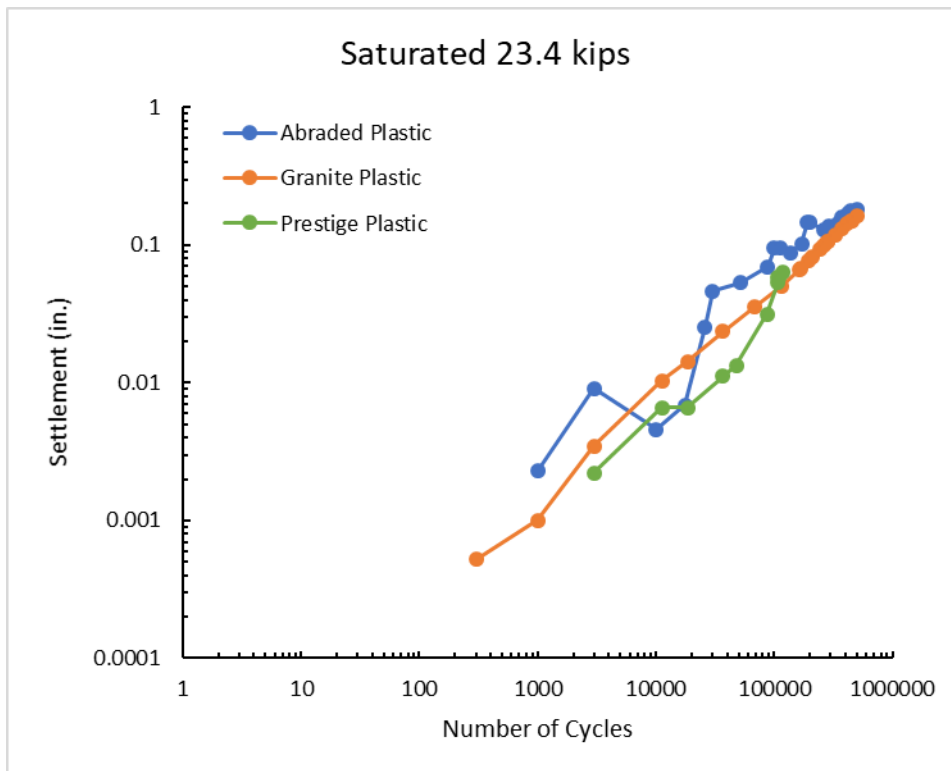
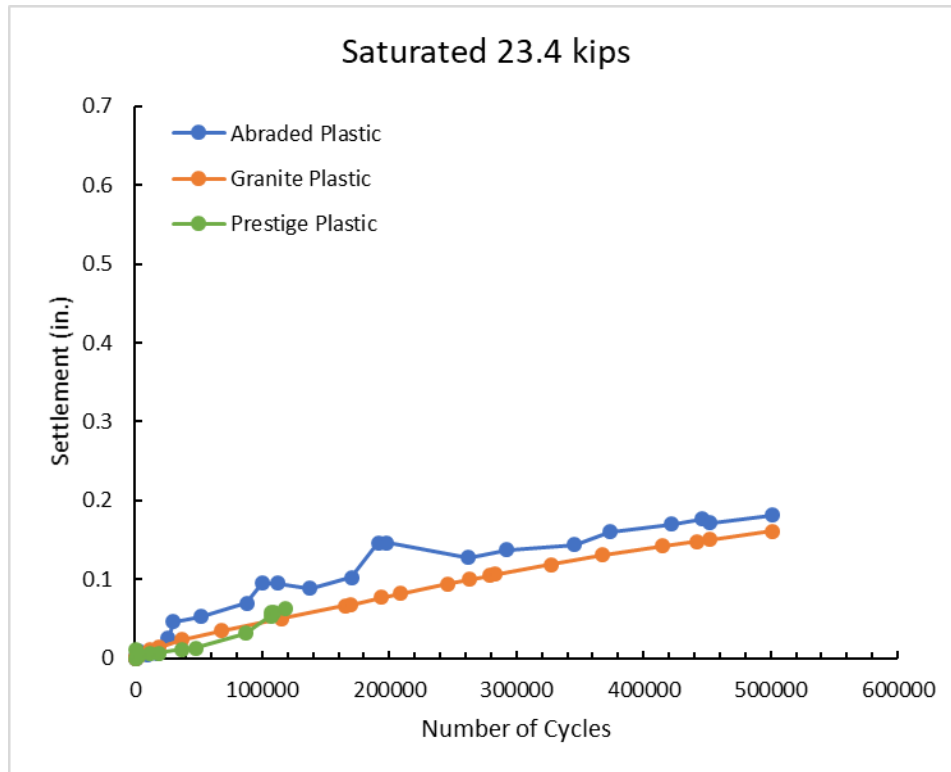


Figure 53 – 15 percent fouled box tests, saturated phase, 23.4 kip loading

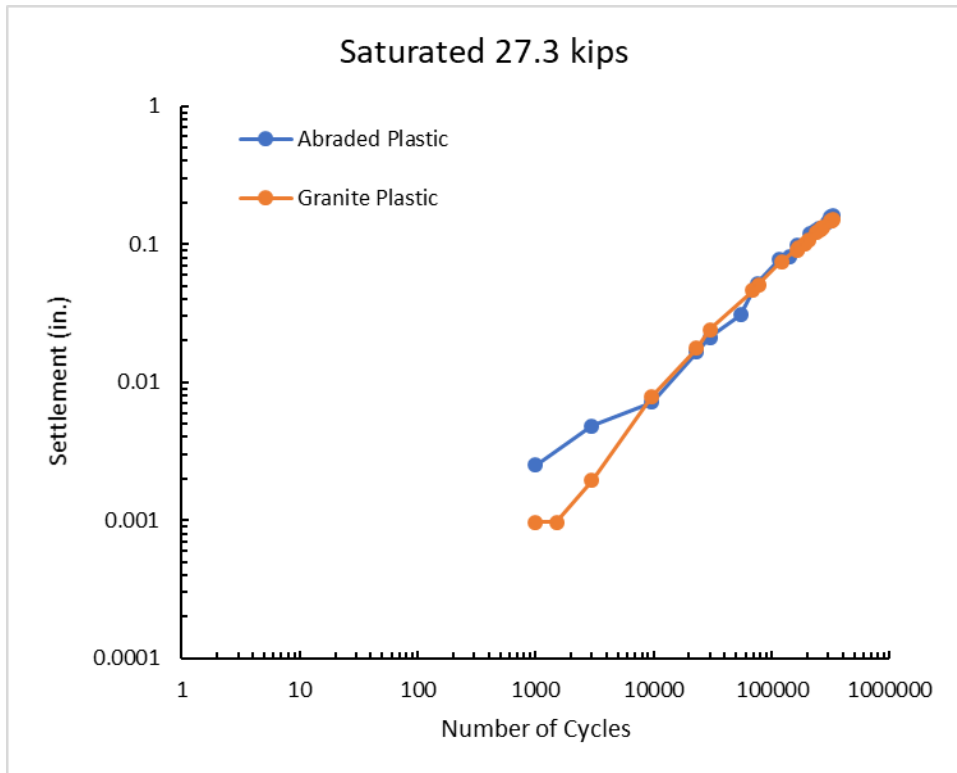
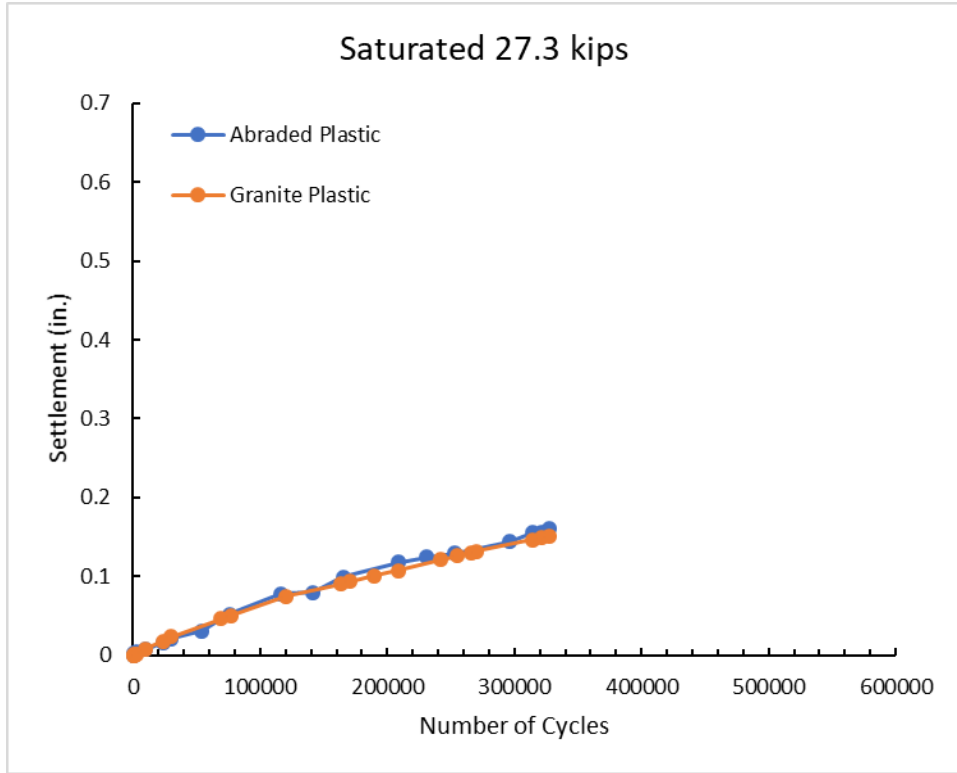


Figure 54 – 15 percent fouled box tests, saturated phase, 27.3 kip loading

30% Fouled Tests

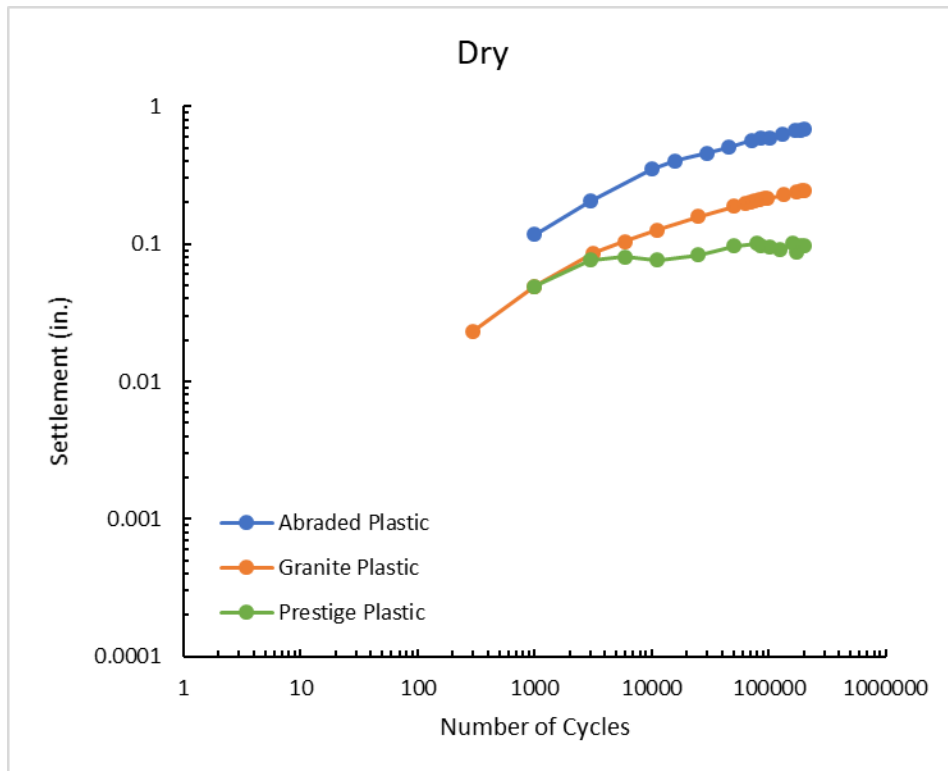
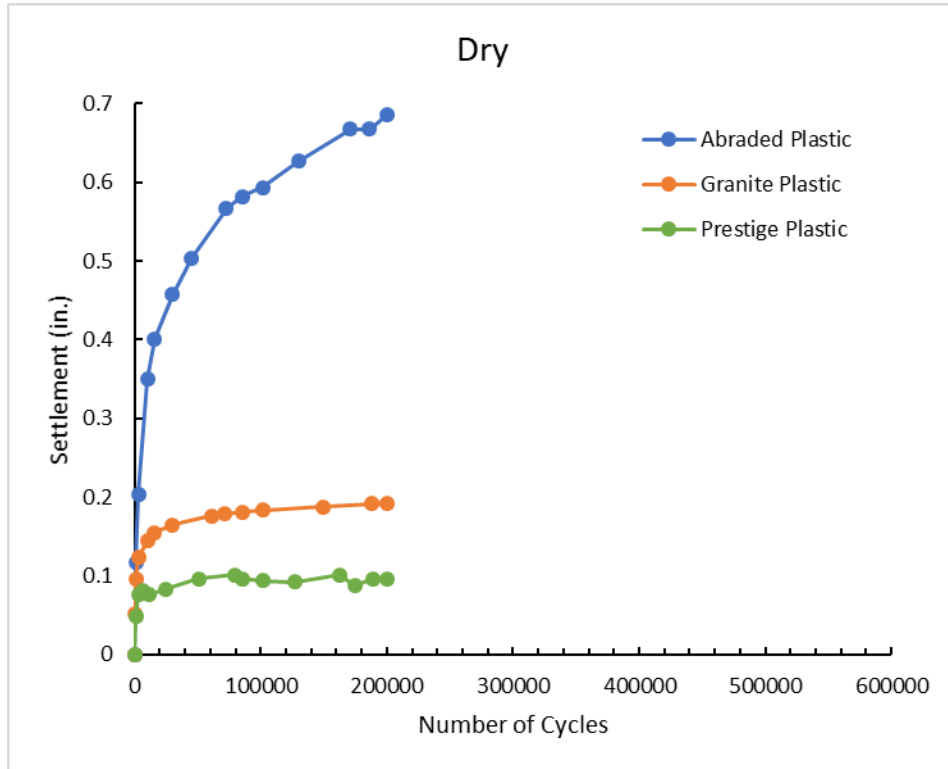


Figure 55 – 30 percent fouled tests, dry phase

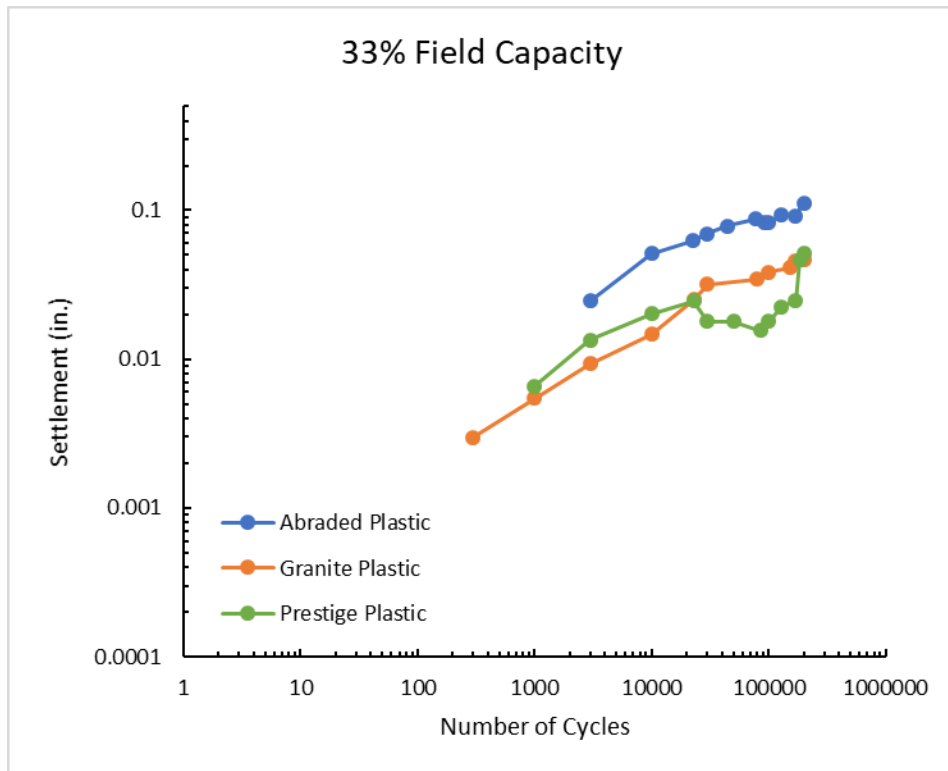
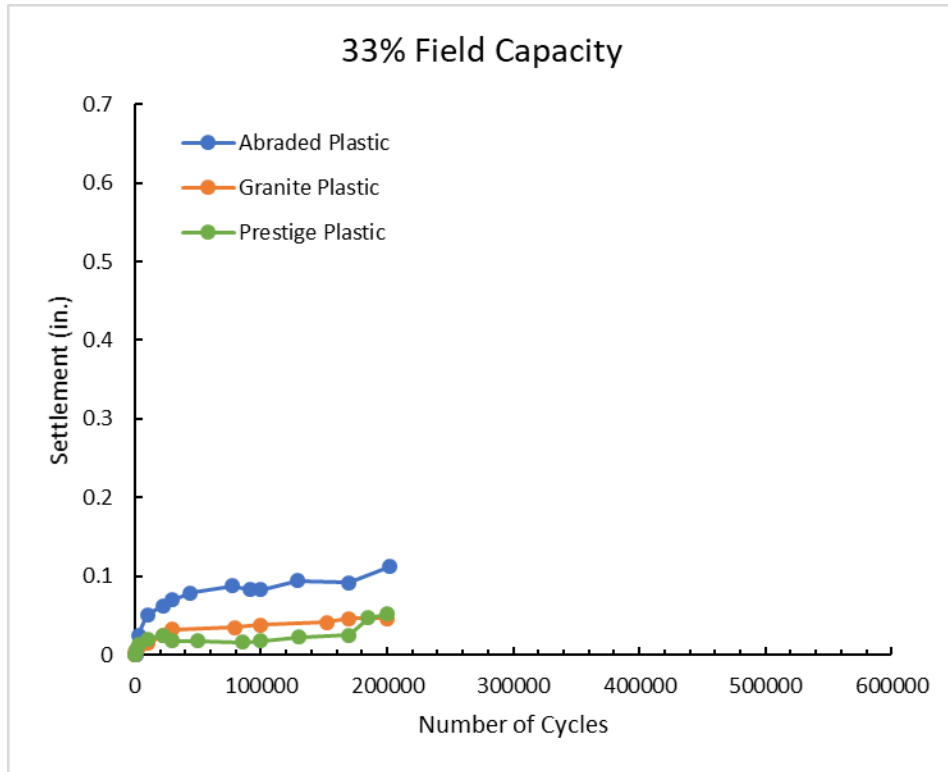


Figure 56 – 30 percent fouled tests, 1/3 field capacity phase

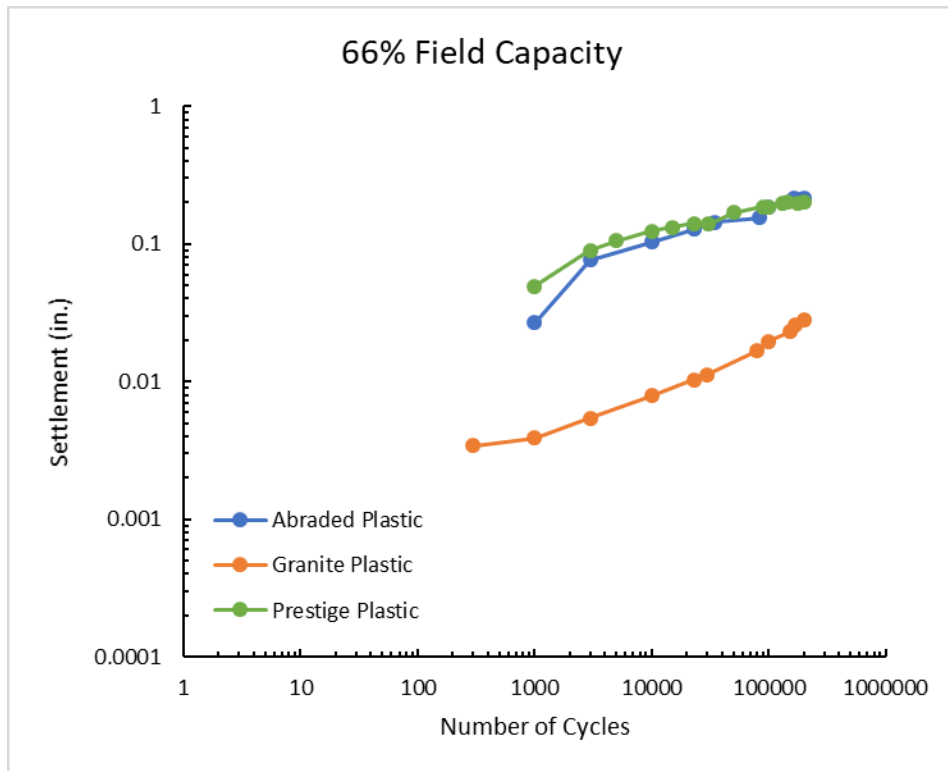
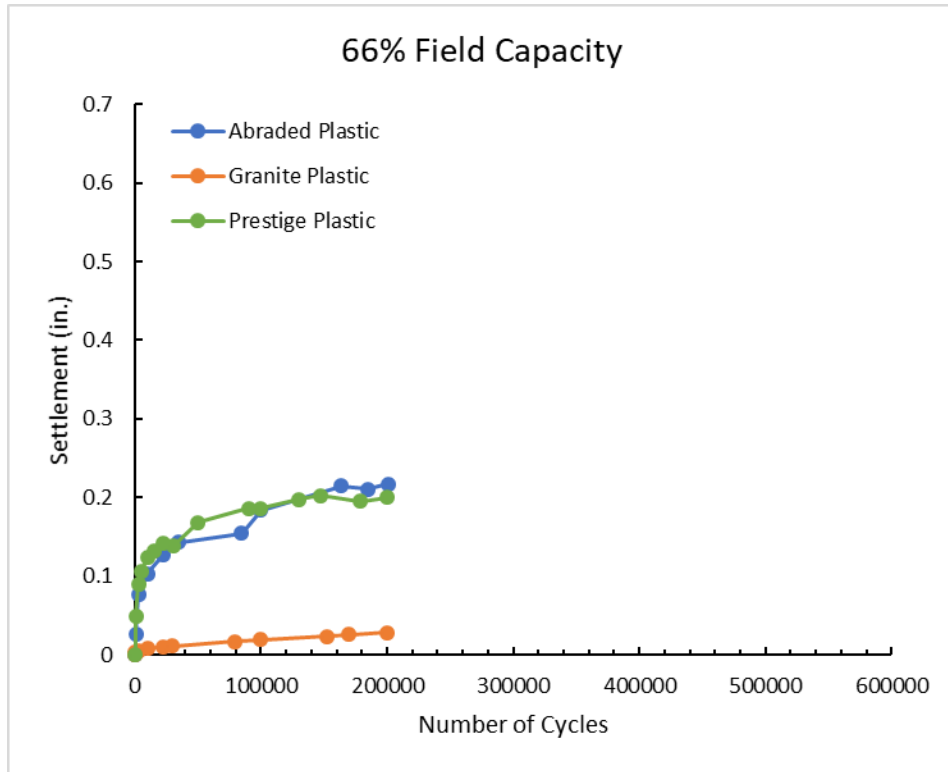


Figure 57 – 30 percent fouled tests, 2/3 field capacity phase

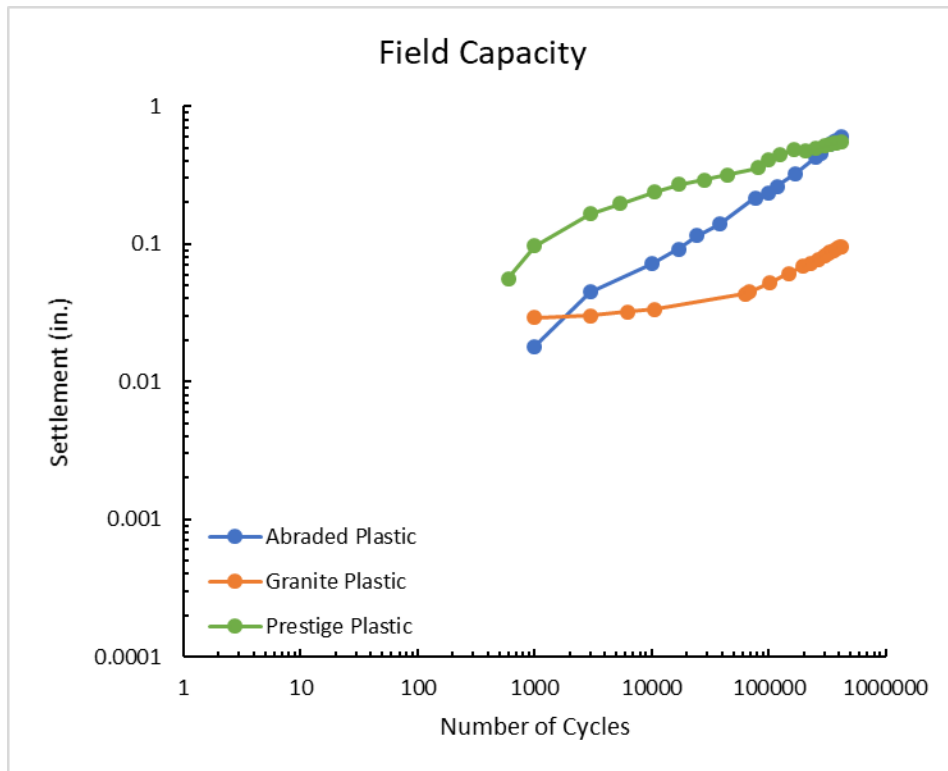
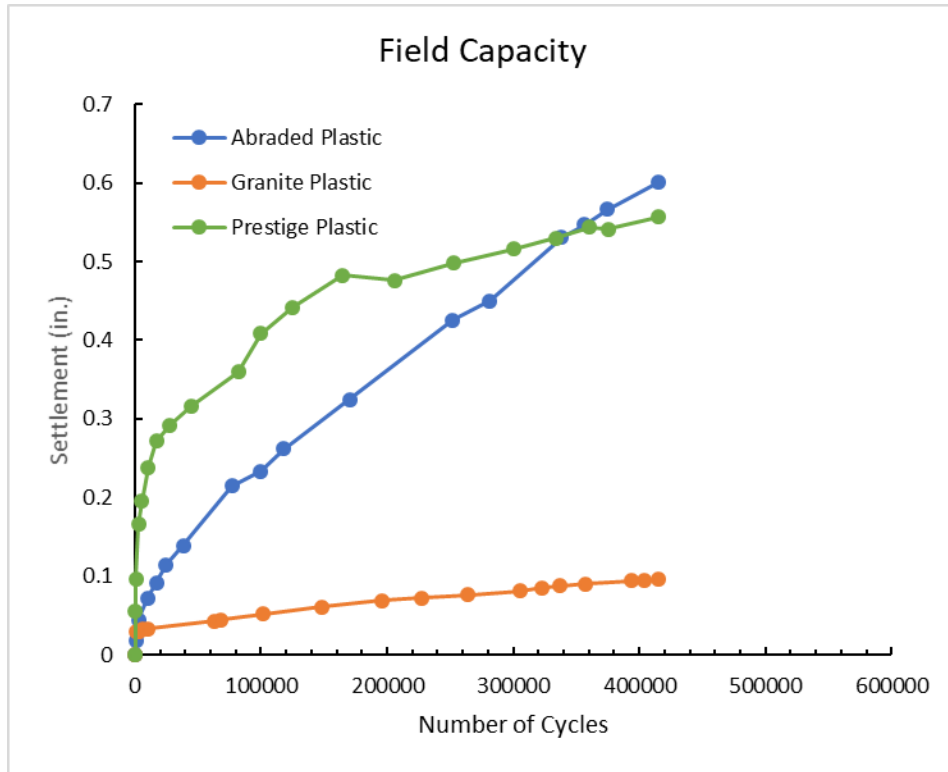


Figure 58 – 30 percent fouled tests, field capacity phase

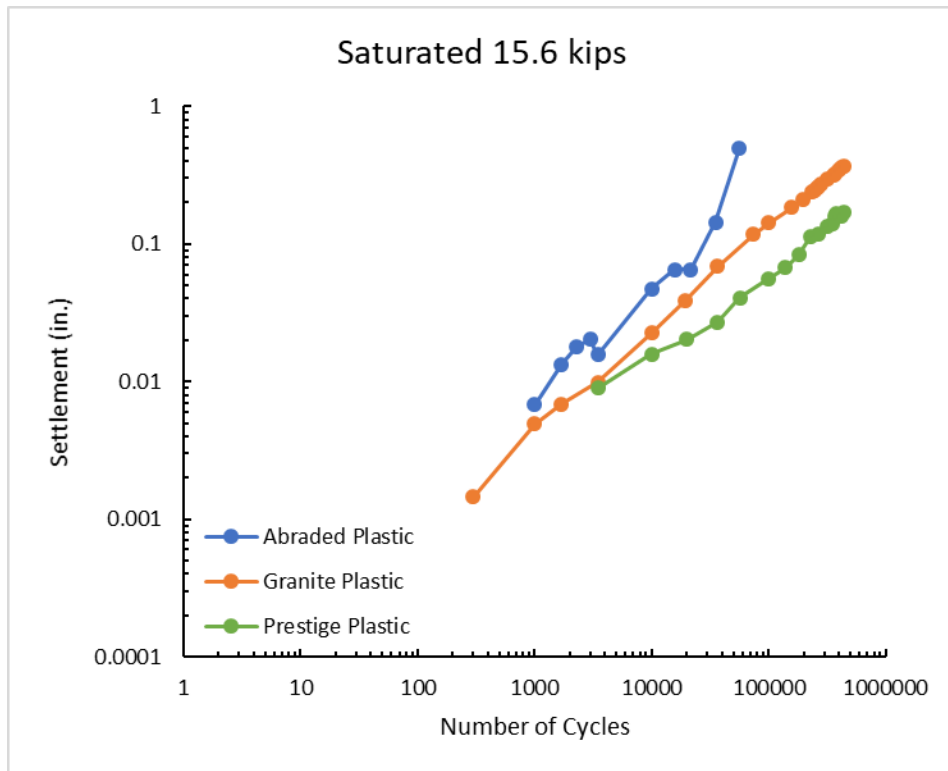
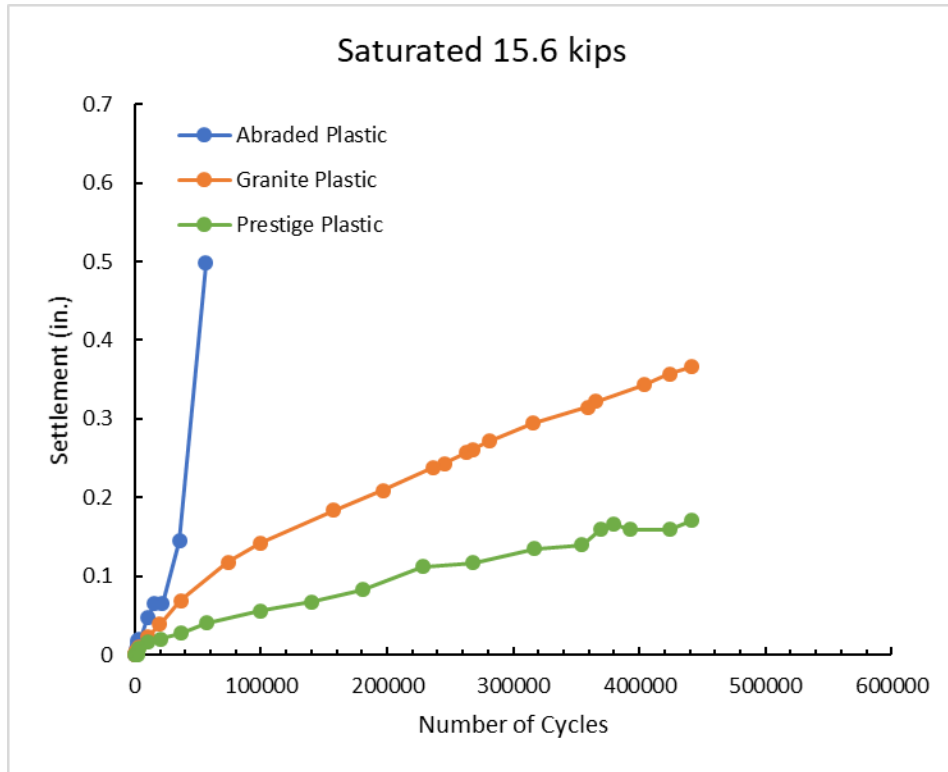


Figure 59 – 30 percent fouled tests, saturated phase, 15.6 kip loading

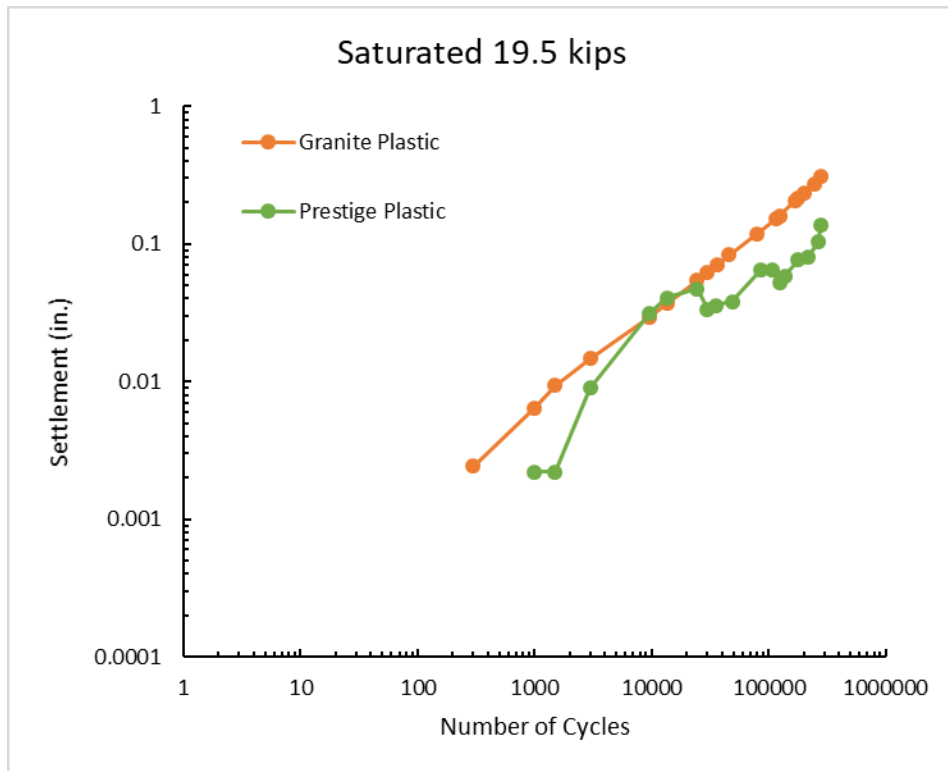
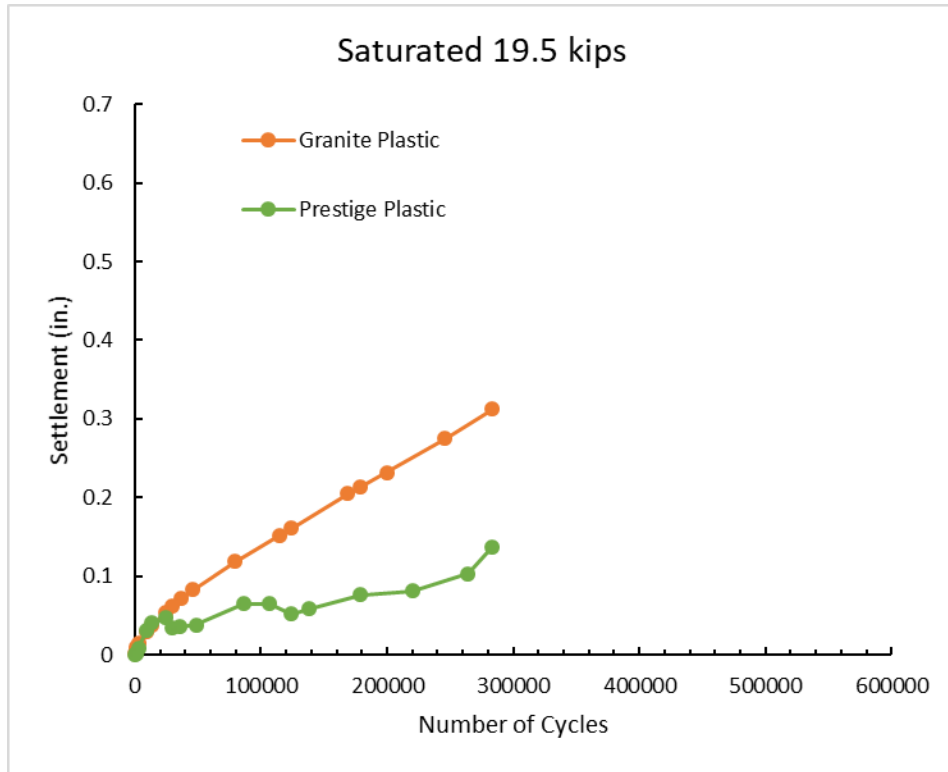


Figure 60 – 30 percent fouled tests, saturated phase, 19.5 kip loading

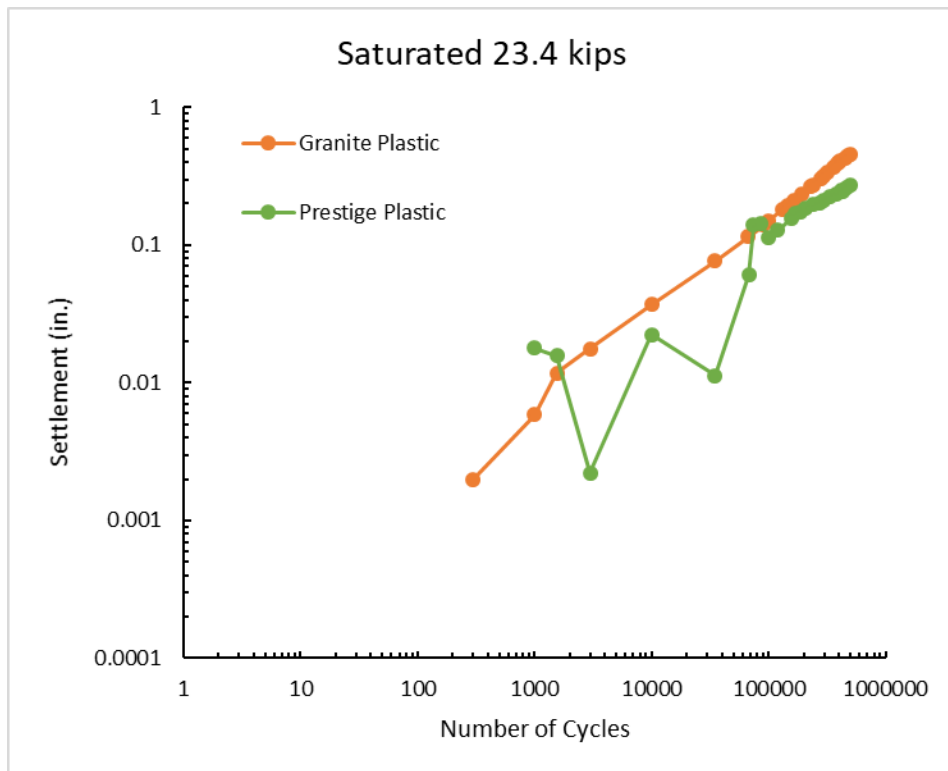
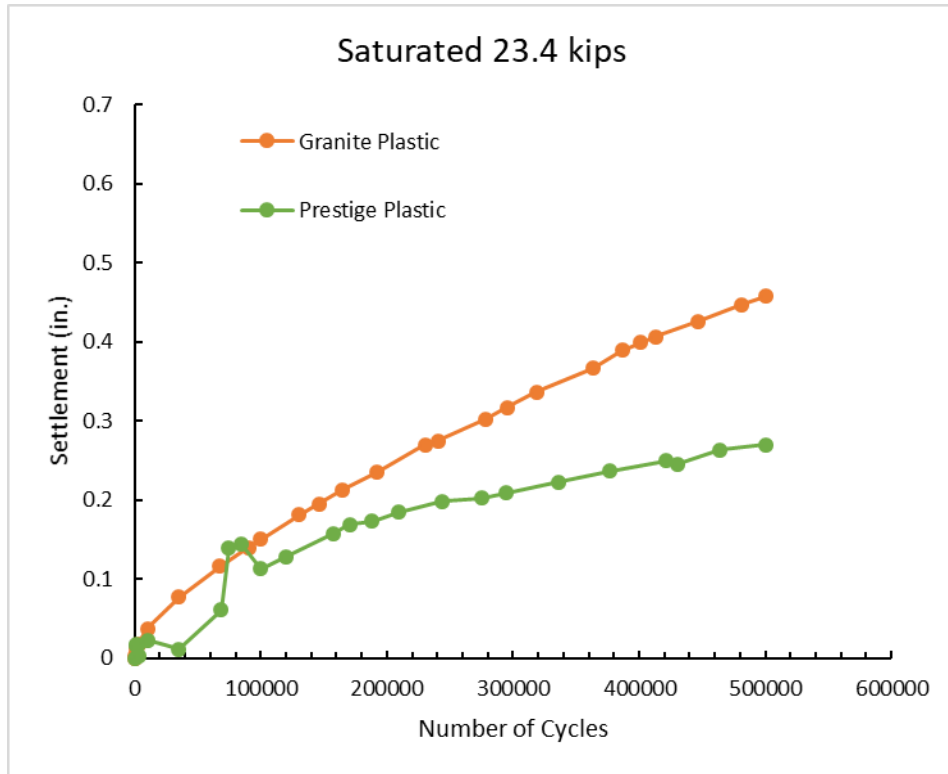


Figure 61 – 30 percent fouled tests, saturated phase, 23.4 kip loading

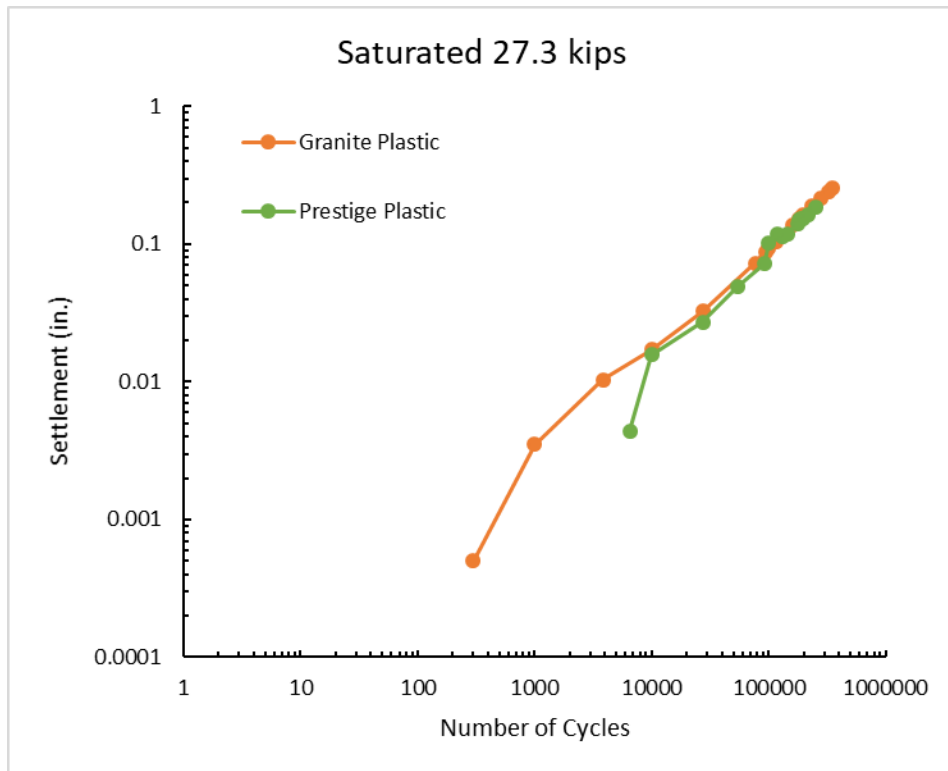
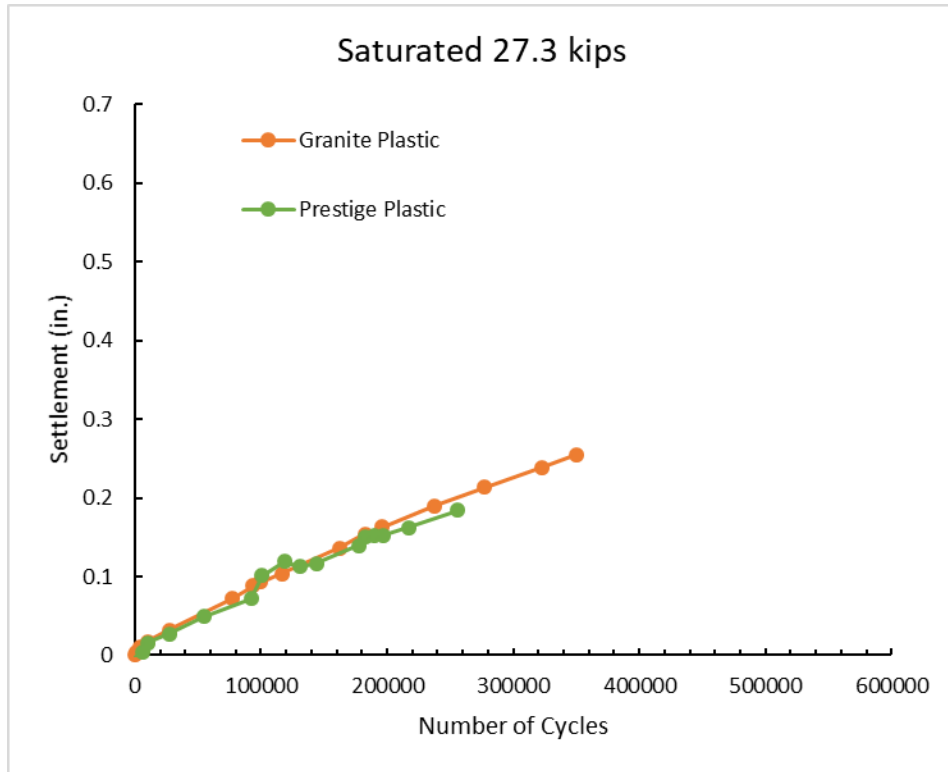


Figure 62 – 30 percent fouled tests, saturated phase, 27.3 kip loading

Abbreviations and Acronyms

| ACRONYMS | EXPLANATION |
|----------|---|
| AREMA | American Railway Engineering and Maintenance-of-Way Association |
| ASTM | American Society of Testing and Materials |
| CIDC | Consolidated Isotropic Drained Compression (Triaxial Test) |
| FRA | Federal Railroad Administration |
| FC | Field Capacity |
| LVDT | Linear Voltage Displacement Transducer |
| LA | Los Angeles |
| MGT | Million Gross Tons |
| PVC | Percent Void Contamination |
| V_1 | Void Volume of Compacted Ballast |
| V_2 | Volume of Compacted Fouling Material |